UNIVERSIDADE ESTADUAL DE CAMPINAS
Faculdade de Engenharia Mecânica

Flavio Nunes Pereira

Phononic Crystal Investigation using a Fluid-filled Cylindrical Shell Spectral Element

Investigação de Cristais Fonônicos usando um Elemento Espectral de Casca Cilíndrica Cheia de Fluido

CAMPINAS
2021

Flavio Nunes Pereira

Phononic Crystal Investigation using a Fluid-filled Cylindrical Shell Spectral Element

Investigação de Cristais Fonônicos usando um Elemento Espectral de Casca Cilíndrica Cheia de Fluido

Doctoral Thesis presented to the School of Mechanical Engineering of the University of Campinas in partial fulfillment of the requirements for the degree of Doctor in Mechanical Engineering, in the area of Solid Mechanics and Mechanical Design.

Tese de Doutorado apresentada à Faculdade de Engenharia Mecânica da Universidade Estadual de Campinas como parte dos requisitos exigidos para obtenção do título de Doutor em Engenharia Mecânica, na área de Mecânica dos Sólidos e Projeto Mecânico.

Orientador: Prof. Dr. José Maria Campos dos Santos

ESTE EXEMPLAR CORRESPONDE À VERSÃO FINAL DA TESE DEFENDIDA PELO ALUNO FLAVIO NUNES PEREIRA, E ORIENTADO PELO PROF. DR. JOSÉ MARIA CAMPOS DOS SANTOS.

CAMPINAS
2021

Ficha catalográfica
Universidade Estadual de Campinas
Biblioteca da Área de Engenharia e Arquitetura
Rose Meire da Silva - CRB 8/5974

P414p

Pereira, Flavio Nunes, 1981-
Phononic crystal investigation using a fluid-filled cylindrical shell spectral element / Flavio Nunes Pereira. – Campinas, SP : [s.n.], 2021.

Orientador: José Maria Campos dos Santos.
Tese (doutorado) – Universidade Estadual de Campinas, Faculdade de Engenharia Mecânica.

1. Cristais Fonônicos. 2. Metamateriais. 3. Estruturas periódicas. 4. Análise espectral. 5. Cascas (Engenharia). 6. Propagação de ondas. I. Santos, José Maria Campos dos, 1953-. II. Universidade Estadual de Campinas. Faculdade de Engenharia Mecânica. III. Título.

Informações para Biblioteca Digital

Título em outro idioma: Investigação de cristais fonônicos usando um elemento espectral de casca cilíndrica cheia de fluido
Palavras-chave em inglês:
Phononic Crystals
Metamaterials
Periodic structures
Spectral Element
Spectral analysis
Shells (Engineering)
Wave propagation
Área de concentração: Mecânica dos Sólidos e Projeto Mecânico
Titulação: Doutor em Engenharia Mecânica
Banca examinadora:
José Maria Campos dos Santos [Orientador]
José Roberto de França Arruda
Renato Pavanello
Domingos Alves Rade
Arcanjo Lenzi
Data de defesa: 26-07-2021
Programa de Pós-Graduação: Engenharia Mecânica

Identificação e informações acadêmicas do(a) aluno(a)
- ORCID do autor: https://orcid.org/0000-0002-8407-6672
- Currículo Lattes do autor: http://lattes.cnpq.br/3814942236166395

UNIVERSIDADE ESTADUAL DE CAMPINAS

FACULDADE DE ENGENHARIA MECÂNICA

TESE DE DOUTORADO

Phononic Crystal Investigation using a Fluid-filled Cylindrical Shell Spectral Element

Investigação de Cristais Fonônicos usando um Elemento Espectral de Casca Cilíndrica Cheia de Fluido

Autor: Flavio Nunes Pereira

Orientador: José Maria Campos dos Santos

A Banca Examinadora composta pelos membros abaixo aprovou esta Tese:

Prof. Dr. José Maria Campos dos Santos, Presidente
DMC - Faculdade de Engenharia Mecânica - UNICAMP

Prof. Dr. José Roberto de França Arruda
DMC - Faculdade de Engenharia Mecânica - UNICAMP

Prof. Dr. Renato Pavanello
DMC - Faculdade de Engenharia Mecânica - UNICAMP

Prof. Dr. Domingos Alves Rade
Instituto Tecnológico de Aeronáutica - ITA

Prof. Dr. Arcanjo Lenzi
LVA - Departamento de Engenharia Mecânica - UFSC

A Ata da defesa com as respectivas assinaturas dos membros encontra-se no processo de vida acadêmica do aluno.

Campinas, 26 de julho de 2021.

Dedication

I dedicate this thesis to my mother Elza, my wife Ilderlange and my children Nícolas Flael and Nicolli Flaelli.

Eu dedico esta tese a minha mãe Elza, à minha esposa Ilderlange e aos meus filhos Nícolas Flael e Nicolli Flaelli.

Acknowledgements

First of all, I thank God for giving me the gift of life.

I would like to thank my wife Ilderlange for their support, patience and motivation throughout the doctorate.

I would like to thank my family: my parents Gregório (*In Memorian*) and Elza, my brother Fábio for their unconditional support throughout this thesis. I am really thankful for their encouragement and effort to help whenever I need.

I would like to express my sincere thanks to my advisor Prof. Dr. José Maria Campos dos Santos for having believed in me, for having motivated me, for his total availability to assist me, and for his huge patience during this research.

I would like to thank the external members of the jury for coming to my defense and contribute with their experienced advice to improve this thesis. I also thank Prof. Dr. José Roberto de França Arruda and Prof. Dr. Renato Pavanello for countless contributions to the work, many of them informally proposed during a chat.

I also thank the Faculty of Mechanical Engineering at UNICAMP, in special, the Department of Computational Mechanics, for providing me the facilities necessary to develop this thesis.

I would also like to thank the State University of Maranhão - UEMA, for providing financial support for the development of this thesis. I would like also to thank the Department of Mechanical Engineering - DEMEC and my department friends for their support. I am also thankful to the Modeling and Simulation Laboratory - MSilab for providing me the facilities and also the good environment for the development of my research during the entire simulation step of the numerical results.

Thanks also to my friends at Dinter. All were important, in their own way, for the conclusion of my doctorate.

I am thankful to CAPES, through process Dinter UEMA-UNICAMP 23038.001802/2015-08, for providing me the financial support necessary to the development of this thesis.

Finally, I would like to thank all who in one way or another contributed to the completion of this thesis.

I am enough of an artist to draw freely upon my imagination. Imagination is more important than knowledge. Knowledge is limited. Imagination encircles the world.

Albert Einstein

"A vida é combate,
Que os fracos abate,
Que os fortes, os bravos
Só pode exaltar!".

Gonçalves Dias

Resumo

Os invólucros cilíndricos são frequentemente aplicados como elementos estruturais em engenharia e têm sido usados para muitas aplicações devido à sua favorável relação entre rigidez e peso. Mais recentemente, eles têm sido usados como novos materiais compostos periódicos conhecidos como Cristais Fonônicos, que são um arranjo periódico de células unitárias construídas como uma combinação de camadas com alta variação de impedância. A periodicidade gera espalhamento de onda de Bragg que produz bandas de parada ou bandas proibidas onde as ondas não se propagam. Este atributo nos permite buscar soluções novas e eficientes para o controle de ruídos e vibrações em estruturas. O objetivo desta tese é propor um novo elemento espectral baseado no modelo analítico de uma casca cilíndrica fechada com fluido interno, e aplicá-la ao cálculo da propagação de ondas em Cristais Fonônicos. Para atingir esse objetivo, o método do Elemento Espectral de Onda é aplicado para calcular as bandas proibidas em um Cristal Fonônico de casca cilíndrica cheia de fluido cujas propriedades elásticas variam periodicamente. A motivação é desenvolver uma nova formulação de um elemento espectral de casca cilíndrica preenchida com fluido é preciso e eficiente para modelar a interação fluido-estrutura em uma estrutura desse tipo. A formulação é verificada quanto ao seu desempenho e eficiência no cálculo de estruturas do tipo casca em geral, e em estruturas periódicas do tipo Cristais Ponônicos elásticos em particular. Nesse sentido, as bandas proibidas geradas pelo efeito de espalhamento de Bragg e as bandas de atenuação das respostas forçadas são calculadas para Cristais Fonônicos modelados com o elemento espectral de casca cilíndrica proposto. O modelo de elemento espectral envolve resolver as equações de movimento no domínio da frequência e usa as soluções para derivar a matriz de rigidez dinâmica formulada de forma análoga ao método dos elementos finitos. Respostas livres e forçadas para cascas cilíndricas homogêneas são investigadas e os resultados são verificados com o método dos elementos finitos. Exemplos simulados usando estruturas convencionais e Cristais Fonônicos modelados com o elemento espectral de casca cilíndrica proposto (com e sem fluido interno) são apresentados e os resultados mostrados como diagramas de dispersão e respostas de deslocamento, os quais demonstram mesma precisão dos métodos comparados, tais como o método dos elementos finitos, mas com eficiência computacional bem superior.

Palavras-chave: Cristais Fonônicos, Metamateriais, Bandas proibidas, Elemento espectral, Cascas Cilíndricas.

Abstract

Cylindrical shells are frequently applied as structural elements in engineering, and have been used for many applications due to their favorable stiffness to weight ratio. More recently they have been used as new periodic composite materials known as Phononic Crystals, which are a periodic arrangement of unit cells built as a combination of layers with high impedance variation. Periodicity generates Bragg wave scattering that produces stop bands or Band Gaps where waves do not propagate. This attribute allows us to search for new and efficient solutions to control noise and vibration in structures. The aim of this thesis is to propose a new spectral element based on the analytical model of a closed cylindrical shell with internal fluid, and apply it to calculate the wave propagation in Phononic Crystals. To reach this goal, the Wave Spectral Element method is applied to compute band gaps in a fluid-filled cylindrical shell phononic crystal whose elastic properties vary periodically. The motivation is to demonstrate that the Fluid-Filled Cylindrical Shell Spectral Element is accurate and efficient for modeling fluid-structure interaction in a cylindrical shell with internal fluid. The formulation is verified and its performance and efficiency in calculating periodic structures and elastic Phononic Crystals are evaluated. In this sense, the Band Gaps generated by the Bragg scattering effect and the attenuation bands of forced responses are calculated for Phononic Crystals modeled with the proposed cylindrical shell spectral element. The Spectral Element model involves solving the governing equations of motion in the frequency domain and uses the solutions to derive the dynamic stiffness matrix formulated in a way analogous to the Finite Element method. Free and forced responses for homogeneous cylindrical shells are investigated and the results are verified with the finite element method. Simulated examples using conventional structures and Phononic Crystals modeled with the proposed cylindrical shell spectral element (with and without internal fluid) are presented and the results are shown as dispersion diagrams and displacement responses, which demonstrate the same accuracy as compared methods, such as the finite element method, but with much higher computational efficiency.

Keywords: Phononic Crystals, Metamaterials, Band gaps, Spectral Element, Cylindrical shell.

List of Figures

List of Tables

List of Abbreviations and Acronyms

Matrices and Vectors

$\mathbf{C}_m$	-	Vector of integration constants
$\mathbf{D}_m$	-	coefficient matrix that relates the displacements
$\mathbf{F}_m$	-	coefficient matrix that relates loads
F_f	-	Fluid loading vector
$\mathbf{K}_{Fm}$	-	dynamic stiffness matrix of the Fluid-filled Cylindrical Shell Spectral Element - FCSSE
$\mathbf{K}_{Sm}$	-	dynamic stiffness matrix of the Cylindrical Shell Spectral Element - CSSE
$\mathbf{K}_{SEm}$	-	spectral dynamic stiffness element matrix as
$\mathscr{L}$	-	matrix differential operator
$\mathscr{L}_{D-M}$	-	matrix differential operator the Donnell-Mushtari
$\mathscr{L}_{MOD}$	-	matrix modifying operator
$\mathscr{L}_f$	-	matrix with the differential operators s
$\mathbf{p}_l$	-	left state vector
$\mathbf{p}_r$	-	right state vector
$\mathbf{q}$	-	displacement vector
$\mathbf{Q}$	-	force vector
$\mathbf{T}$	-	Transfer matrix
$\mathbf{u}$	-	Displacement vector

Subscripts

F	-	relative to Fluid
l	-	relative to left
m	-	relative to harmonic mode
r	-	relative to right
S	-	relative to structure

Latin Letters

a	-	radius
$A_{i,m}$, $B_{i,m}$, $C_{i,m}$	-	integration constants
c_F	-	fluid speed of sound
c_S	-	structure wave speed
$c_{i,m}$	-	coefficient of characteristic equation
d	-	unit cell length
D	-	stiffness in the mid surface of shell
E	-	Young's modulus
E_c	-	Complex Young's modulus
$E_{i,m}$	-	integration constants
f_v	-	volume forces
F	-	radial force
h	-	thickness
k	-	wavenumber
K	-	flexural stiffness
k_ϱ	-	nondimensional thickness parameter
$\bar{k}$	-	slice
L	-	length
m	-	harmonic
p	-	pressure
$\hat{p}$	-	spectral amplitude of pressure
$r_{i,m}$	-	characteristic equation roots
$s_{i,m}$	-	characteristic equation roots
s	-	nondimensional length
t	-	time
u, v, w	-	displacements components
$\hat{u}$,$\hat{v}$ $\hat{w}$	-	spectral amplitude of displacement components
x, φ, z	-	cylindrical coordinate
$\mathbb{Z}$	-	set of integer numbers

Greek Letters

$\alpha_{i,m}$	-	pressure amplitude ratio coefficients
$\gamma_{i,m}$	-	ratio of amplitudes of tangential-radial displacements
$\delta_{i,m}$	-	ratio of amplitudes of axial-radial displacements
η	-	loss factor
μ	-	attenuation constant
ν	-	Poisson's ratio
ρ	-	mass density
ρ_S	-	structure mass density
ρ_F	-	fluid mass density
φ	-	cylindrical coordinate - azimuth
ω	-	circular frequency

Acronyms

AS	-	Analytical Solution
CEM	-	Continuous Element Method
CSSE	-	Cylindrical Shell Spectral Element
DOF	-	Degree of Freedom
DSM	-	Dynamic Stiffness Method
FCSSE	-	Fluid-filled Cylindrical Shell Spectral Element
FE	-	Finite Element
FFT	-	Fast Fourier Transform
FSI	-	Boundary Element
IPWE	-	Improved Plane Wave Expansion
ODS	-	Operating Deflection Shape
PC	-	Phononic Crystal
PWE	-	Plane Wave Expansion
SE	-	Spectral Element
STMM	-	Spectral Transfer Matrix Method
WFE	-	Wave Finite Element
WSE	-	Wave Spectral Element
WSFEM	-	Wave Spectral Finite Element Method
FRF	-	Frequency Response Function

Other Notations

$\Re(\ )$	-	real part of a number
$\Im(\ )$	-	imaginary part of a number
$\lvert\ \rvert$	-	Absolute value of a number

Table of Contents

1 INTRODUCTION

1.1 Motivation

Understanding the dynamic behavior of a structure is fundamental. The interest may be either at the design stage or during operation. In the first case, understanding the dynamic response of a system is important for the purpose of design and optimization. In the second case, during operation, it can assist in monitoring and controlling structural integrity.

Regarding the type of analysis, analytical, numerical, or experimental studies can be performed. Although experimental tests may provide the best reproduction of the behavior of the system, they are usually expensive and can only be carried out in the final stages of the project, when the main characteristics of the equipment have already been defined. At the design stage of the development of real engineering systems, a fast and cheap numerical analysis is sought for predicting the dynamic behavior. This motivates the development of reliable and efficient numerical tools.

Due to their excellent structural and mechanical properties, cylindrical shells have been used frequently as structural elements in mechanical, civil, petrochemical, machinery, aerospace and naval engineering. This comes from the fact that shells can be used for large span structures with a good stiffness to weight ratio. Cylindrical shells are subjected to various complex loading and boundary conditions which can lead to structural failure; therefore, a good understanding of the dynamic behavior of shell elements is very important to guarantee a safe and inexpensive design.

In the context of structural dynamic analysis the thin are cylindrical shell is a complex fluid-structure interaction (FSI) problem. Therefore, the monitoring and detection of damage, vibratory and acoustic behavior of shells is very important. Current industrial equipment are usually under the FSI condition, such as pressure vessels (Fig.1.1a[1]), submarines (Fig.1.1b[2]), gas and oil pipelines (Fig.1.1c[3]), petrochemical containers (Fig.1.1d[4]), aircraft (Fig.1.1e[5]) and spacecraft shells (Fig.1.1f [6]).

Under certain loading conditions, vibration and even fracture of the shell can cause serious accidents. So it is critical to find an appropriate design method by studying the dynamic responses and vibration mechanism of thin cylindrical shells under the FSI condition.

---

[1]available on **https://en.wikipedia.org/wiki/Pressure_vessel** on may 2^{th}, 2021.

[2]available on **https://www.militaryaerospace.com/sensors/article/14072957/submarines-missiles-undersea-warfare** on may 2^{th}, 2021.

[3]available on **https://www.paint.org/coatingstech-magazine/articles/new-coating-could-prevent-gas-and-oil-pipeline-clogging/** on may 2^{th}, 2021.

[4]available on **https://www.istockphoto.com/br/fotos/fuel-storage-tank** on may 2^{th}, 2021.

[5]available on **https://moneyinc.com/embraer-190/** on may 2^{th}, 2021.

[6]available on **https://en.wikipedia.org/wiki/Apollo_command_and_service_module** on may 2^{th}, 2021.

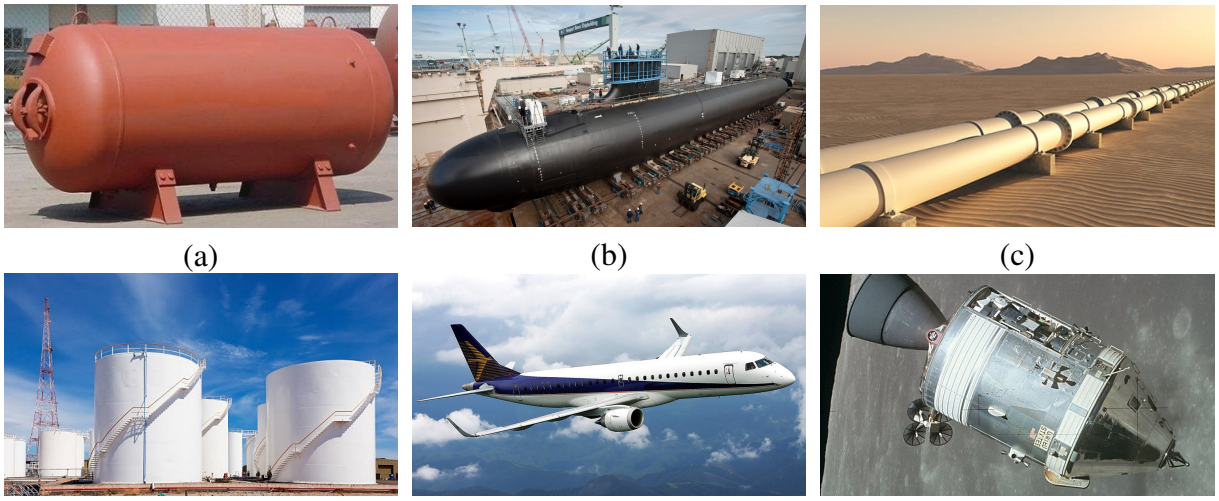

(a) (b) (c)

(d) (e) (f)

Figure 1.1: Industrial equipment and components that can be modeled as thin cylindrical shells: (a) pressure vessel, (b) submarine, (c) oil pipelines, (d) petrochemical containers, (e) aircraft, (f) service module of spacecraft.

When studying structural behaviors, the Finite Element (FE) method is one of the main tools for evaluating engineering problems. It has been implemented in several commercial computational packages. In general, this method is based on a domain discretization by finite elements that use approximated shape functions to describe the displacement field. Convergence is dictated by mesh refinement, which require many elements with smaller sizes (Zienkiewicz, 1977). It is well known that good, precise results using wave propagation analysis by FE require a discretization finer than six elements/wavelength. Thus, for analysis at high frequencies, complex computational models must become very large. DeLanghe and Sas (1996) affirm that although the FE method is effective at low frequencies for the prediction of structure-borne noise and structural vibration, it is less effective at high frequencies, even with the increased capacity of current computers and improvements in the FE method.

Presented by Doyle (1997), the Spectral Element (SE) method is the exact analytical solution in the frequency domain of the wave equation formulated in displacement. This solution is built in order to use the same matrix concept used in the assembly of the FE model. Because it is the exact solution of the differential equation in the frequency domain, a spectral element can be seen as an infinite number of finite elements. In this way, a geometrically uniform structural element can be represented using a single spectral element, which significantly reduces the total number of degrees of freedom when compared to other methods. Thus, the SE method is an interesting approach to evaluate the behavior of fluid-filled cylindrical shells.

Wave propagation in periodic structures has been studied by researchers for a long time. In the engineering field it started in the 1970s with Mead (1996), who authored many papers on this subject. Recently, works are directed towards trying to understand the behavior of propagation of elastic waves in periodic structures (Galán and Abascal, 2002; Castaings *et al.*, 2002; Lee and Staszewski, 2007; Santos *et al.*, 2008; Mencik and Ichchou, 2008; Rodrigues *et al.*, 2019;

Sales *et al.*, 2020; Gonçalves *et al.*, 2021).

In recent decades, a lot of research has been done about Metamaterials and Phononic Crystals (PCs). PC and band gap phenomena started to be analyzed in the 1990s, and one of the seminal works was written by Sigalas and Economou (1992). One of the first papers to name this type of periodic structure Phononic Crystals was published by Kushwaha *et al.* (1993), in which the authors presented the first full calculation of a PC band structure. Since then, new approaches have been appearing that use periodicity together with analytical and numerical modeling to calculate complex structures at low computational cost. This, as well as other methods, has been the focus of a large number of research papers on different types of periodic structures in the Vibroacoustic Laboratory of DMC-FEM-UNICAMP (Silva, 2015; Miranda Jr and Dos Santos, 2017; Goto *et al.*, 2020; Rosa *et al.*, 2019; Beli *et al.*, 2019; Dal Poggetto and Serpa, 2021; Pereira Flavio and Dos Santos, 2021).

As a new type of artificial material, metamaterials exhibit unusual properties and promising applications in the area of engineering when compared with natural materials. Acoustic metamaterials and PCs have some extraordinary physical properties, such as negative effective parameters, band gaps, negative refraction, etc., properties normally nonexistent in natural materials. These special properties have attracted the attention of researchers, and great progress has been made in engineering applications (Deymier, 2013; Liu *et al.*, 2020). In 1995, Francisco Meseguer and collaborators experimentally determined the aural filtering properties of a perfectly real but fortuitous phononic crystal in a minimalist sculpture by Eusebio Sempere (Fig.1.2a[7]), standing in a park in Madrid, Spain. Figure 1.2b[8] depicts a manufactured granular metamaterial in blue (a tailorable auxetic and vibration control metamaterial) and pantographic metamaterial in white (an ultra-light, ultra-deformable, ultra-resilient material).

(a) (b)

Figure 1.2: Examples of phononic crystals and metamaterials (a) Eusebio Sempere's sculpture (b) Auxetic metamaterials.

[7]available on **https://phys.org/news/2019-10-acoustic-insulation-enables-corners.html** on may 2^{th}, 2021.

[8]available on **https://www.eurekalert.org/multimedia/pub/183312.php** on may 2^{th}, 2021.

Phononic Crystals are artificial materials with a periodic arrangement of unit-cells built as a combination of layers with high impedance variation. Figure 1.3 shows an example of a closed circular cylindrical shell phononic crystal, made with five unit-cells comprising three layers of elastic materials ordered as steel-polyacetal-steel. The unit-cells are distributed periodically along its length, and a unit-cell detail is also shown in Fig. 1.3. As a consequence of periodicity, these structures may exhibit frequency band gaps where waves do not propagate. Based on this feature, PCs can be proposed as an efficient solution for noise and structural vibration control.

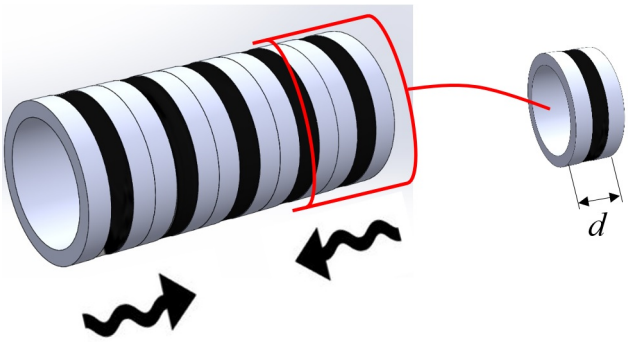

Figure 1.3: Circular cylindrical shell phononic crystal scheme and a three layers unit-cell [steel (*gray*)+polyacetal (*black*)+steel (*gray*)] detail.

The Wave Spectral Element (WSE) method considers the dynamic stiffness matrix obtained by the Spectral Element (SE) method to model a periodic structural member. Then, the spectral dynamic stiffness matrix is transformed in a transfer matrix, where the Floquet-Bloch theorem is applied to end up with a transfer matrix eigenproblem. The eigenvalues produce wavenumbers and the corresponding eigenvectors are the wave modes, which travel toward the right and left along the periodic structure. WSE and other analytical and numerical methods have been applied to different types of structural phononic crystals and periodic structures such as rods, beams, plates and shells (Silva and Arruda, 2012; Nobrega *et al.*, 2016; Pereira Flavio and Dos Santos, 2017; Sousa *et al.*, 2017).

In this thesis a new spectral element based on the analytical model of a closed circular cylindrical shell with internal fluid is proposed, and it is applied to calculate wave propagation in phononic crystals. To reach this goal, the WSE method is applied to compute band gaps in a fluid-filled cylindrical shell phononic crystal with elastic properties that vary periodically (Fig. 1.3). The motivation is to demonstrate that the Fluid-filled Cylindrical Shell Spectral Element (FCSSE) is accurate and efficient for modeling fluid-structure interaction (FSI) in a cylindrical shell with internal fluid. First, the dynamic stiffness matrix of a FCSSE is formulated by SE. Then, the governing equations time derivatives are transformed using spectral decomposition, while the circumferential coordinate is expanded in a Fourier series. A four degree of freedom (DOFs) fluid-filled cylindrical shell spectral element model is formulated and presented. The SE and WSE methods are computationally implemented and evaluated. A comparative study between the FCSSE and the analytical solution (AS) of a circular cylindrical shell as proposed

by Leissa (1973) is presented. Results show good agreement when compared with other methods and those from the literature.

1.2 Literature review

This section presents a review of the works found in the literature considered most relevant to the area of research addressed and to the development of the work.

1.2.1 Spectral element

The spectral element method is based on the analytical solution of the displacement wave equation, written in the frequency domain (Doyle, 1997; Lee, 2009). The element is tailored in the same concept as the finite element (FE) method, but the interpolation function is the exact (or approximated) solution of the wave equation. Built-up structures with geometrically uniform members can be modeled by a single spectral element, which significantly reduces the total number of DOFs as compared to approximated approaches.

Lee (2009) comments that the classic FE has been the most popular in many areas of engineering and science, as it is one of the most convenient and easy to use computational methods. Though the FEM is applicable to most geometries, boundary conditions and material variations, it can be extremely expensive and it is often impracticable to work out solutions to the large scale finite element models using a desktop computer. On the other hand, the spectral element method (SE) is a frequency domain solution method in which the spectral element equation is solved by using the fast Fourier Transform (FFT). In SE, the exact dynamic stiffness matrix, known as the spectral element matrix, is formulated in the frequency domain by using wave solutions for the governing differential equations. Accordingly, the SE will provide exact frequency domain solutions while using only one element. However, it is not always easy to derive the exact shape functions for any structure.

Many papers take advantage of the SE formulation to create other methods. For example, Lee (2000) introduces a general approach to spectral element formulation for one-dimensional structures, in which the spectral element matrix is computed numerically directly from the transfer matrix, which is formulated from the state vector equation of motion of a structure. Next, by combining the promising features of the SE (i.e., high accuracy) and the well-known transfer matrix method (i.e. high analysis efficiency for one-dimensional structures), a new solution approach named the Spectral Transfer Matrix Method (STMM) is created. As an application, a beam with periodic supports and a plane lattice structure with several beam-like periodic lattice substructures are simulated.

However, there are still some drawbacks, such as difficulties to model non-uniform members and models without closed-form solutions. For example, the vibration problem of a rectangular plate, can be solved in closed-form only for a few combinations of boundary conditions.

To overcome these problems, some spectral elements have been developed using approximations with superposition and Fourier series expansion.

Casimir *et al.* (2005) showed a procedure for building the dynamic stiffness matrix of a Kirchhoff rectangular plate element with free edge boundary conditions, while Gorman's method of boundary condition decomposition and Levy's series are both used to obtain the solution of the elementary problem. Later Casimir *et al.* (2007) demonstrated a procedure for calculating the dynamic stiffness matrix of tubular shells with free edge boundary conditions. The shell element takes rotatory inertia, transverse shear deformation and non-axisymmetric loadings into account. It is interesting to note that in his work, Casimir comments that the Dynamic Stiffness Method can also be called the Continuous Element Method (CEM).

Campos and Arruda (2008) presents a spectral element for thin plates that can be used to model beam-reinforced plates with arbitrary boundary conditions, as well as a detailed description on how to obtain all the terms needed to implement it. The results obtained proved to be appealing and its accuracy makes it a potential tool for structural analysis in mid and high-frequency ranges. The authors emphasize the need to use symbolic computation to obtain the expressions contained in the matrices of displacements and forces.

Nefovska-Danilovic and Petronijević (2015) describe the development of the dynamic stiffness matrix for an isotropic rectangular plate with arbitrary boundary conditions undergoing in-plane free vibration. Gorman's superposition method is exploited to obtain the solution of the governing equations of motion. The obtained results are in good agreement with the exact solutions for some special cases as well as with finite element solutions. As expected, modeling of plates undergoing in-plane vibration using the dynamic stiffness method demonstrates high precision, accuracy, and a low memory requirement in comparison with the finite element method.

Kolarevic *et al.* (2015) presented the dynamic stiffness matrix of the completely free rectangular Mindlin plate element. The system of three coupled equations of motion is transformed into two uncoupled equations which introduce a boundary layer function. The natural frequencies of individual plates and plate assemblies with arbitrary boundary conditions are calculated and validated. High efficiency and accuracy of the results are demonstrated.

The dynamic stiffness matrix for simple structural elements such as rods, beams and plates have been studied since the beginning of the past decade. However, more complex structures such as thin shells, thick shells and cylindrical shells have only recently received attention. Therefore, works that present the dynamic stiffness matrix of a shell are only found now. The main reason that postponed the formulation of the SE of these structures is the complexities of equations that describe these structures.

Thinh and Nguyen (2016) presented a theoretical investigation on the free vibration of circular cylindrical shells partially filled with fluid. A precise analytical model using the Dynamic Stiffness Method (DSM) or Continuous Elements (CEM) based on the Reissner–Mindlin theory and non-viscous incompressible fluid equations has been proposed for the structures.

A closed circular cylindrical shell spectral element was developed by Kolarević *et al.* (2016). The dynamic stiffness matrix is formulated on the base of exact solution for free vibration of a circular cylindrical shell according to the Flügge thin shell theory. The matrix is frequency-dependent and, besides the stiffness, includes inertia and damping effects. Only the natural frequencies and mode shapes of a circular cylindrical shell were calculated in the paper. This work is one of the main references of this thesis.

Harbaouia *et al.* (2018) present a spectral element based on the dynamic stiffness matrix of a prestressed cylindrical shell. The dynamic stiffness matrix is built using first-order shear deformation theory and natural frequencies are processed easily. Vibration analyses are performed with numerical examples to determine the performance of this approach and the effect prestressing has on frequency response functions.

1.2.2 Fluid-structure interaction

When a structural component vibrates in a viscous fluid, the presence of the fluid gives rise to a fluid reaction force which can be interpreted as an added mass and a damping contribution to the dynamic response of the component. Chen *et al.* (1976) presents an analytical and experimental study of a cylindrical rod vibrating in a viscous fluid that is enclosed by a rigid, concentric cylindrical shell. A closed-form solution for the added mass and damping coefficient is obtained and a series of experiments with cantilevered rods vibrating in various viscous fluids is performed.

One of the pioneer works considering fluid-structure coupling in a cylindrical shell was published in the 1980s by Fuller and Fahy (1982). The dispersion behaviour and energy distribution of free waves in thin walled cylindrical elastic shells filled with fluid are investigated. Dispersion curves are presented for a range of parameters and the behaviour of individual branches is explained. A non-dimensional equation which determines the distribution of vibrational energy between the shell wall and the contained fluid is derived and its variation with frequency and material parameters is studied. The work stands out for being one of the first to use the Bessel function to represent the fluid loading in the shell.

In the mid 1980s, Fahy and Gardonio consolidated many works about this subject in a book (Fahy and Gardonio, 1985). They investigated dispersion behavior and energy distribution of waves using the analytical model of a thin-walled elastic cylindrical shell filled with fluid, and included the fluid-structure coupling effects.

Another noteworthy work is the theoretical analysis developed by Gonçalves and Batista (1987) for the free vibration of simply-supported vertical cylindrical shells partially filled with or submerged in a fluid. The fluid is taken as non-viscous and compressible and the coupling between the deformable shell and this acoustic medium is taken into account. The Rayleigh-Ritz technique is used to obtain an approximate solution which coincides with the exact solution for the cases of an empty shell or a shell completely in contact with fluid.

Sinha *et al.* (1992) presented an analysis of axisymmetric waves propagating along fluid-loaded cylindrical shells within the framework of linear elasticity and classical perfect-slip boundary conditions at the solid-fluid interface. Numerical solutions are obtained for various axisymmetric eigenmodes for a cylindrical shell in vacuum. Numerical results are obtained for both the radiating and non-radiating eigenmodes. The results are presented for the dispersion curves as well as the displacement and stress amplitude component distributions along the radial direction for various propagating modes of the system.

Jeong and Lee (1996) presents an analytical method for free vibration of a partially liquid-filled circular cylindrical shell with various classical boundary conditions is developed by means of the Stokes' transformation and Fourier series expansion. The liquid-shell coupled system is divided into two regions for convenient formulation. One is the empty shell region in which the shell equations are formulated without the liquid effect, while the other is the wetted shell region in which the shell equations are formulated with consideration of the liquid dynamic effect.

Subsequently, Jeong and Lee (1998) presented an analytical method for hydroelastic vibration of a partially liquid-filled cylindrical shell with arbitrary classical boundary conditions using the Fast Fourier Transform (FFT). To demonstrate the validity and accuracy of the analytical method, the finite element analyses were performed for partially liquid-filled circular cylindrical shells with clamped—free and clamped—clamped boundary conditions.

In the early 2000s, Zhang (2002) presented an extension of the wave propagation approach to coupled frequency analysis of finite cylindrical shells submerged in a dense acoustic medium. A finite cylindrical shell enclosed with plate end-caps is modeled for coupled frequency analysis.

Qatu (2002) has presented a review of most of the recent research done in the field of dynamic response of homogeneous shells with special attention to free vibrations. The paper reviews the literature focusing on various aspects of research. The first aspect of research receiving interest here is the shell theory being used. Shell theories include thin and thick shell theories, shallow and deep theories, linear and nonlinear theories. Most theories are classified based on the thickness ratio of the shell being treated, the shallowness ratio, and the magnitude of displacement. It is reported that another aspect of research receiving interest are interactions between fluids, piezoelectric shells and acoustic radiation.

Chen *et al.* (2004) derived a state equation with variable coefficients in a unified matrix form based on the three-dimensional fundamental equations of anisotropic elasticity. The free vibration of simply supported, fluid-filled cylindrically orthotropic functionally graded cylindrical shells with arbitrary thickness was studied. Numerical examples are presented and compared with existing results in the literature.

Considering plane wave approximation, Gautier *et al.* (2007) investigated the interaction between the wall vibrations of a stretched elastic cylindrical membrane and the inner acoustic field. The first of these, called Korteweg's wave, propagates mainly within the fluid and corres-

ponds to the acoustic plane wave which is closely coupled to the wall vibrations. The two other waves mostly propagate within the structure and correspond to coupled longitudinal/flexural motions. One corresponds to predominant longitudinal motions in the membrane and the other exists only when tension is applied to the membrane and is similar to a string bending wave.

Using the Wave Finite Element (WFE) method, Mencik and Ichchou (2007) presented a general formulation which addresses the problem of wave propagation in elastodynamic cylindrical shells filled with acoustic fluid. The formulation is based on a finite element description of periodic systems. It leads to a general spectral problem, with eigenvalues and eigenvectors that are related to the free propagating wave properties. The formulation incorporates many simplified elastodynamic models of an analytical nature. Here, the formulation is stated for a fluid–structure-guided medium.

Many other works were published in this area. Larbi and Deü (2011) present a three-dimensional exact mixed state-space solution for the free vibration analysis of simply-supported arbitrarily thick laminated piezoceramic hollow cylinders completely filled with fluid.

Farshidianfar and Oliazadeh (2012) investigated the free vibration of circular cylindrical shells with simply supported boundary conditions which has been studied using different thin shell theories: Donnell-Mushtari, Love-Timoshenko, Amold-Warburton, Houghton-Johns, Flugge-Byme-Lur'ye, Reissner—Naghdi—Berry, Sanders, Vlasov, Kennard-Simplified and Soedel. Then, in order to check the accuracy of the theories, a comparison was carried out with experimental results.

1.2.3 Phononic crystals

A lot of research on phononic crystals and metamaterials has been done in recent decades. From an engineering point of view, analyzing and understanding these systems remains an open challenge. Hussein *et al.* (2014) defines a phononic medium as a material or structural system that usually exhibits some form of periodicity, which can be in constituent material phases, or internal geometry, or even boundary conditions.

Phononic crystals - PCs produce band gaps, which are generated by the Bragg scattering effect (destructive wave interference) along the structure. For a 1D periodic structure with a unit-cell length of d, band gaps would appear around frequencies governed by the Bragg condition, $d = n(\lambda/2), (n = 1,2,...)$ where λ is the wavelength.

In the early 1990s, one of the first papers to name this type of periodic structure as phononic crystals was published by Kushwaha *et al.* (1993). They present the first full band-structure calculations for periodic, elastic composites. For transverse polarization of the vibrations, we obtain a phononic band gap which extends throughout the Brillouin zone.

Research on forbidden bands in PCs and acoustic metamaterials mainly focuses on the calculation of elastic wave forbidden bands (Liu *et al.*, 2020). At present, there are several mature methods for calculating forbidden bands, such as the transfer matrix method (Munjal,

1993; Sigalas and Soukoulis, 1995), the plane wave expansion method (Kushwaha *et al.*, 1993, 1994; Wu *et al.*, 2002; Hsu and Wu, 2006), the finite difference time domain method (Sigalas and Garcıa, 2000; Shi *et al.*, 2004), and the multiple scattering method.

The transfer matrix method (Munjal, 1993; Sigalas and Soukoulis, 1995) is a method of converting the wave equation into the form of a transfer matrix equation and solving the eigenvalues. This method starts with the basic equations including state parameters to obtain the transfer equation of a flat solid medium, then obtains the boundary conditions according to the characteristics of the surrounding medium and the intermediate medium, and finally obtains the solution of the system. This method is mainly used for the calculation of band gaps of phononic crystal and acoustic metamaterials in a one-dimensional model. Because the transfer matrix is generally small and is an analytical solution, its calculation effort is small.

The plane wave expansion method (Kushwaha *et al.*, 1993, 1994; Wu *et al.*, 2002) is the earliest used method in the theoretical analysis of phononic crystals and acoustic metamaterials. In this method, the physical quantities such as displacements and elastic constants in the wave equation are expanded by a Fourier transform in the form of a superposition of plane waves in the inverse lattice space, and then the wave equation is solved to obtain the dispersion relationship between the characteristic frequency and the wave vector, that is, the band structure.

Phononic crystal studies have been focused on bulk waves and more recently have been extended to elastic waves in plates. They explore the plane wave expansion (PWE) method with the plate theory (Hsu and Wu, 2006). The main issue when using the PWE method is that the structural model is assumed to be infinite (no boundary conditions), which brings difficulties to its use in some applied engineering problems.

The finite difference time domain method (Sigalas and Garcıa, 2000; Shi *et al.*, 2004) discretizes partial differential equations by discretizing time and space, transforms the partial differential equations into differential equations. This method can simulate a variety of complex periodic structures, and can accurately simulate the non-uniformity, anisotropy, nonlinear problems, and dispersion characteristics of the medium. At the same time, the method can calculate the characteristics of the band structure in the periodic structure and the transmission and reflection in the finite structure.

Even with the existing methods for the study of PCs, researchers continue to develop new techniques with fast calculation and good convergence to lay the foundation for the follow-up research.

Nascimento (2009) combined SEM with FEM, resulting in a semi-analytical method called WSEM. This method was still restricted to simple structures, such that for modeling complex structures it required cumbersome analytical formulations. However, this problem was circumvented by Silva (2015), who built spectral finite elements from a finite element model of a slice of a structural waveguide with an arbitrary cross section and, potentially, of arbitrary order. This method was called the Wave Spectral Finite Element Method (WSFEM).

Within the WFE framework, the FE model of a small slice of a whole system is considered and a transfer matrix relation is expressed to link the kinematic quantities between the right and left boundaries of this slice. By considering Bloch's theorem, the so called wave modes of the periodic system can be computed, which involves assessing the eigenvalues and eigenvectors of the transfer matrix of the slice (Mencik and Ichchou, 2005). The proposed strategy considerably reduces the computational time when compared to the FE method.

1.3 Objectives

The main objective of this thesis is to propose new spectral elements based on the analytical model of a closed circular cylindrical shell with internal fluid, and to use these new spectral elements to investigate phononic crystals in cylindrical shells. In this sense, the specific objectives of this thesis are listed as the following.

- Formulate the Fluid-filled Cylindrical Shell Spectral Element - FCSSE.
- Implement SE for cylindrical shells and fluid-filled cylindrical shells.
- Evaluate the proposed SE by calculating the natural frequencies and comparing them with the FE.
- Calculate the forced responses for the cylindrical shell modeled by SE and validate the results found with those obtained by the FE model.
- Implement and validate the WSE method by calculating the dispersion diagrams and comparing the results found with the analytical results.
- Compute and investigate band gaps and attenuation effects in phononic crystal cylindrical shells with and without internal fluid.

1.4 Outline of the thesis

This thesis is organized as follows.

In Chapter 2, the formulations of closed circular Cylindrical Shell Spectral Element - CSSE, Fluid-filled Cylindrical Shell Spectral Element - FCSSE, and Wave Spectral Element - WSE are presented.

In Chapter 3, the numerical results obtained with the computational implementation of the cylindrical shell model are evaluated. The computational implementation of the CSSE is verified using the Analytical Solution and FE method. In addition, WSE is used to evaluate the dynamic behavior of the cylindrical shell phononic crystal. Simulated results are presented in the frequency domain as dispersion diagrams, displacement responses and operating deflection shapes (ODS).

In Chapter 4 the numerical results obtained with the computational implementation of the fluid-filled closed circular cylindrical shell models are evaluated. The computational implementation of the FCSSE is verified using the Analytical Solution and FE method. WSE is used to evaluate a fluid-filled spectral circular cylindrical PC. Simulated results are presented in the frequency domain as a dispersion diagram, displacement responses and ODS.

Finally, in Chapter 5, general conclusions regarding the work are drawn. Then, the original contributions of this work are highlighted. At the end, a list of publications that were developed throughout the thesis is presented.

2 THEORETICAL MODELS

In this chapter, the formulation of the closed circular Cylindrical Shell Spectral Element - CSSE, Fluid-filled Cylindrical Shell Spectral Element - FCSSE, and Wave Spectral Element - WSE are presented. the thin shell theory is shown in detail. Also, the equation for a single point excitation force of the structure is presented.

2.1 Cylindrical Shell Spectral Element - CSSE

This section is limited to the study of thin circular cylindrical shells, not including the effects of initial stress, anisotropy, variable thickness, shear deformation, rotary inertia, large deflections, or nonhomogeneity. Nevertheless, the standard or classical theories of thin shells are governed by eighth order systems of differential equations which take many forms, depending upon the assumptions made.

For this first SE the effect of an eventual filling of the cylindrical shell with an internal fluid is disregard, that is, the behavior of cylindrical shell is comparable *in vacuo*.

2.1.1 Thin Circular Cylindrical Shell Theory

The cylindrical geometry (thickness h, radius a, length L) and coordinate system (displacements u, v and w of the mid surface in x, φ and z directions, respectively) for a closed circular cylindrical shell are shown in Figure 2.1.

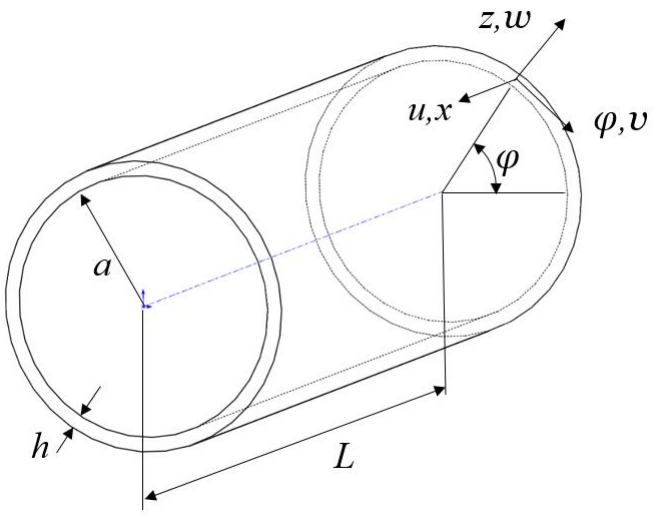

Figure 2.1: Geometry and coordinates system of a thin circular cylindrical shell.

Further, the length coordinate x is replaced by a nondimensional length s defined by.

$$s = \frac{x}{a}. \tag{2.1}$$

The homogeneous equations of motion for thin circular cylindrical shells can be written in matrix form as

$$\mathscr{L}\mathbf{u} = 0, \tag{2.2}$$

where **u** is the displacement vector

$$\mathbf{u} = \left\{ \begin{array}{c} u(x,\varphi,t) \\ v(x,\varphi,t) \\ w(x,\varphi,t) \end{array} \right\}, \tag{2.3}$$

where $u(x,\varphi,t)$, $v(x,\varphi,t)$ and $w(x,\varphi,t)$ denote displacement components in the position axial (x), angular position (φ) and time (t), respectively, and $\mathscr{L}$ is a matrix differential operator.

Differential eighth order systems of equations are commonly used to model the vibrational behavior of circular cylindrical shells. In this case the $\mathscr{L}$ operator in Equation (2.2) can be treated as the sum of two operators

$$\mathscr{L} = \mathscr{L}_{D-M} + k_{\varrho}\mathscr{L}_{MOD}, \tag{2.4}$$

where, $\mathscr{L}_{D-M}$ is the differential operator according to the Donnell-Mushtari theory, $\mathscr{L}_{MOD}$ is a "modifying" operator which alters the Donnell-Mushtari operator to yield another shell theory, and k_{ϱ} is the nondimensional thickness parameter defined by

$$k_{\varrho} = \frac{h^2}{12a^2}. \tag{2.5}$$

Thus, each eighth order shell theory for circular cylindrical shells differs from the Donnell-Mushtari theory by an operator $\mathscr{L}_{MOD}$ which is multiplied by the constant k_{ϱ}, which is very small for small h/a ratios.

Leissa (1973), presents the Donnell-Mushtari operator as

$$\mathscr{L}_{D-M} = \begin{bmatrix} \left[\frac{\partial^2}{\partial s^2} + \frac{(1-\nu)}{2}\frac{\partial^2}{\partial \varphi^2} - \rho\frac{(1-\nu^2)a^2}{E}\frac{\partial^2}{\partial t^2}\right] & \frac{(1+\nu)}{2}\frac{\partial^2}{\partial s \partial \varphi} & \nu\frac{\partial}{\partial s} \\ \frac{(1+\nu)}{2}\frac{\partial^2}{\partial s \partial \varphi} & \left[\frac{(1-\nu)}{2}\frac{\partial^2}{\partial s^2} + \frac{\partial s^2}{\partial \varphi^2} - \rho\frac{(1-\nu^2)a^2}{E}\frac{\partial^2}{\partial t^2}\right] & \frac{\partial}{\partial \varphi} \\ \nu\frac{\partial}{\partial s} & \frac{\partial}{\partial \varphi} & \left[1 + k\nabla^4 + \rho\frac{(1-\nu^2)a^2}{E}\frac{\partial^2}{\partial t^2}\right] \end{bmatrix}, \quad (2.6)$$

where, $\nabla^4 = \nabla^2\nabla^2$ and

$$\nabla^2 = \frac{\partial^2}{\partial s^2} + \frac{\partial^2}{\partial \varphi^2}. \quad (2.7)$$

Leissa (1973) also shows several shell models depending on the $\mathscr{L}_{MOD}$ operator. The model adopted in this thesis is the Flügge shell. The Flügge theory is based on Kirchhoff-Love hypothesis for thin elastic shells. The modification operator L_{MOD} for Flügge's circular cylindrical shell theory takes the form

$$\mathscr{L}_{MOD} = \begin{bmatrix} \frac{(1-\nu)}{2}\frac{\partial^2}{\partial \varphi^2} & 0 & -\frac{\partial^3}{\partial s^3} + \frac{(1-\nu)}{2}\frac{\partial^3}{\partial s \partial \varphi^2} \\ 0 & \frac{3(1-\nu)}{2}\frac{\partial^2}{\partial s^2} & -\frac{(3-\nu)}{2}\frac{\partial^3}{\partial s^2 \partial \varphi} \\ -\frac{\partial^3}{\partial s^3} + \frac{(1-\nu)}{2}\frac{\partial^3}{\partial s \partial \varphi^2} & -\frac{(3-\nu)}{2}\frac{\partial^3}{\partial s^2 \partial \varphi} & 1 + 2\frac{\partial^2}{\partial \varphi^2} \end{bmatrix}. \quad (2.8)$$

Therefore, to obtain the Flügge's cylindrical shell differential equation, Equation (2.7) and (2.8) must be replaced in Equation (2.4). Based on the Flügge thin shell theory (Leissa (1973), Kolarević *et al.* (2016)) the $\mathscr{L}$ operator equations for a closed circular cylindrical shell can be written in a matrix form as:

$$\mathscr{L} = \begin{bmatrix} \partial_x^2 + a_1\partial_\varphi^2 + a_2\partial_t^2 & a_3\partial_x\partial_\varphi & a_4\partial_x + a_5\partial_x^3 + a_6\partial_x\partial_\varphi^2 \\ a_3\partial_x\partial_\varphi & \mathrm{a}_7\partial_\varphi^2 + a_8\partial_x^2 + a_2\partial_t^2 & \mathrm{a}_7\partial_\varphi + a_9\partial_x^2\partial_\varphi \\ a_4\partial_x + a_5\partial_x^3 + a_6\partial_x\partial_\varphi^2 & \mathrm{a}_7\partial_\varphi + a_9\partial_x^2\partial_\varphi & \begin{array}{c} k\left(\partial_x^4 + 2a_7\partial_x^2\partial_\varphi^2 + {a_7}^2\partial_\varphi^4\right) \\ + a_7 - a_2\partial_t^2 + 2a_{10}\partial_\varphi^2 + a_{10} \end{array} \end{bmatrix}, \tag{2.9}$$

where, $\partial_x = \partial/\partial x$, $\partial_\varphi = \partial/\partial\varphi$, $\partial_t = \partial/\partial t$, $k = h^2/12$ and $a_i (i = 1 \ldots 10)$ coefficients are:

$$a_1 = \frac{1-\nu}{2a^2}\left(1 + \tfrac{K}{Da^2}\right), \quad a_2 = \frac{\rho h}{D}, \quad a_3 = \frac{1+\nu}{2a}, \quad a_4 = \frac{\nu}{a}, \quad a_5 = \frac{K}{Da},$$

$$a_6 = \frac{1-\nu}{2a^3}\frac{K}{D}, \quad a_7 = \frac{1}{a^2}, \quad a_8 = \frac{1-\nu}{2}\left(1 + \tfrac{3K}{Da^2}\right), \quad a_9 = \frac{3-\nu}{2}\frac{K}{Da^2}, \quad a_{10} = \frac{K}{Da^4},$$

where, ν is the Poisson's ratio, $K = Eh^3/12(1-\nu^2)$ is the flexural stiffness, $D = Eh/(1-\nu^2)$ is the stiffness in the mid surface of shell, ρ is the mass density and E is the Young's modulus.

2.1.2 General solution

By using the separation of variables, the general solution of Equation (2.2) can be obtained with:

$$u\,(x,\varphi,t) = \hat{u}\,(x,\varphi)\,e^{i\omega t}, \quad v\,(x,\varphi,t) = \hat{v}\,(x,\varphi)\,e^{i\omega t}, \quad w\,(x,\varphi,t) = \hat{w}\,(x,\varphi)\,e^{i\omega t}, \tag{2.10}$$

where, ω is the circular frequency and $\hat{u}$, $\hat{v}$, and $\hat{w}$ are the spectral amplitudes of displacement components. Substituting Equation (2.10) into Equation (2.2) the differential equation of circular cylindrical shell in the frequency domain is obtained as:

$$\begin{bmatrix} \partial_x^2 + a_1\partial_\varphi^2 - a_2\omega^2 & a_3\partial_x\partial_\varphi & a_4\partial_x + a_5\partial_x^3 + a_6\partial_x\partial_\varphi^2 \\ a_3\partial_x\partial_\varphi & \mathrm{a}_7\partial_\varphi^2 + a_8\partial_x^2 - a_2\omega^2 & \mathrm{a}_7\partial_\varphi + a_9\partial_x^2\partial_\varphi \\ a_4\partial_x + a_5\partial_x^3 + a_6\partial_x\partial_\varphi^2 & \mathrm{a}_7\partial_\varphi + a_9\partial_x^2\partial_\varphi & k\left(\partial_x^4 + 2a_7\partial_x^2\partial_\varphi^2 + {a_7}^2\partial_\varphi^4\right) \\ & & + a_7 + a_2\omega^2 + 2a_{10}\partial_\varphi^2 + a_{10} \end{bmatrix} \begin{Bmatrix} \hat{u}\,(x,\varphi) \\ \hat{v}\,(x,\varphi) \\ \hat{w}\,(x,\varphi) \end{Bmatrix} = \begin{Bmatrix} 0 \\ 0 \\ 0 \end{Bmatrix}. \tag{2.11}$$

For a closed circular cylindrical shell, the displacement components $\hat{u}$, $\hat{v}$ and $\hat{w}$ should satisfy periodicity in the circumferential direction. Therefore, the solution of Equation (2.11) can be expanded in an infinite Fourier series as:

$$\begin{aligned} \hat{u}(x,\varphi) &= \sum_{m=0}^{\infty} U_m(x)\cos(m\varphi) + \sum_{m=1}^{\infty} \bar{U}_m(x)\sin(m\varphi), \\ \hat{v}(x,\varphi) &= \sum_{m=0}^{\infty} V_m(x)\sin(m\varphi) + \sum_{m=1}^{\infty} \bar{V}_m(x)\cos(m\varphi), \\ \hat{w}(x,\varphi) &= \sum_{m=0}^{\infty} W_m(x)\cos(m\varphi) + \sum_{m=1}^{\infty} \bar{W}_m(x)\sin(m\varphi), \end{aligned} \tag{2.12}$$

where, $m \in \mathbb{Z}$. Let's consider the case where the boundary conditions do not depend on φ. Then, the solutions for the different harmonics are uncoupled and instead of taking the solution in the form of summations, only the solutions for the m-th harmonic will be considered. The solution for the asymmetric vibration $(m \geq 1)$ will be presented, while the solution for the axisymmetric vibration $(m = 0)$ will not be considered. The solution procedure for the 1st terms of Equation (2.12) will be presented, while the solution for the 2nd terms can be obtained in the same way. Notice that the natural frequencies obtained with the 1st and 2nd terms of Equation (2.12) are the same, which means that for the closed circular cylindrical shell all the natural frequencies are duplicated. By substituting the 1st terms of Equation (2.12) in the Equation (2.11) it has:

$$\begin{bmatrix} C_1\partial_x^2 + C_2 & C_3\partial_x & C_4\partial_x^3 + C_5\partial_x \\ -C_3\partial_x & C_6\partial_x^2 + C_7 & C_8\partial_x^2 + C_9 \\ C_4\partial_x^3 + C_5\partial_x & -C_8\partial_x^2 - C_9 & C_{10}\partial_x^4 + C_{11}\partial_x^2 + C_{12} \end{bmatrix} \begin{Bmatrix} \hat{u}\,(x) \\ \hat{v}\,(x) \\ \hat{w}\,(x) \end{Bmatrix} = \begin{Bmatrix} 0 \\ 0 \\ 0 \end{Bmatrix}, \tag{2.13}$$

where,

$$\begin{array}{lll} C_{1,m}=1, & C_{2,m}=-m^2a_1-w^2a_2, & C_{3,m}=-ma_3, \\ C_{4,m}=-a_5, & C_{5,m}=a_4-m^2a_6, & C_{6,m}=a_8, \\ C_{7,m}=-m^2a_7-w^2a_2, & C_{8,m}=-ma_9, & C_{9,m}=-ma_7, \\ C_{10,m}=k, & C_{11,m}=-2km^2a_7, & \begin{array}{l} C_{12,m}=-a_7+w^2a_2 \\ +k(m^4a_7^2-2m^2a_7+a_7^4) \end{array} \end{array} . \quad (2.14)$$

By expanding the determinant of the matrix of Equation (2.13), an 8-th order differential equation is obtained as:

$$(\partial_x^8+a_{1,m}\partial_x^6+a_{2,m}\partial_x^4+a_{3,m}\partial_x^2+a_{4,m}\partial_x)\Psi=0, \quad (2.15)$$

where, $\Psi=U_m$ or V_m or W_m, and:

$$a_{1,m}=\frac{c_{10}c_3^2+2c_3c_4c_8-c_7c_4^2-2c_5c_6c_4+c_1c_8^2+c_1c_6c_{11}+c_1c_7c_{10}+c_2c_6c_{10}}{c_1c_6c_{10}-c_6c_4^2},$$

$$a_{2,m}=\frac{c_6(c_1c_{12}-c_5^2)+c_{11}(c_3^2+c_1c_7+c_2c_6)+2(c_8(c_3c_5+c_1c_9)+c_4(c_9c_3-c_7c_5))+c_2(c_8^2+c_7c_{10})}{c_1c_6c_{10}-c_6c_4^2},$$

$$a_{3m}=\frac{c_{12}c_3^2+2c_3c_5c_9-c_7c_5^2+c_1c_9^2+2c_2c_8c_9+c_1c_7c_{12}+c_2c_6c_{12}+c_2c_7c_{11}}{c_1c_6c_{10}-c_6c_4^2},$$

$$a_{4,m}=\frac{c_2c_9^2+c_2c_7c_{12}}{c_1c_6c_{10}-c_6c_4^2}.$$

Assuming the solution of the Equation (2.15) in the form $\Psi=e^{rx}$ the corresponding characteristic equation is obtained as:

$$r^8+a_{1,m}r^6+a_{2,m}rx^4+a_{3,m}r^2+a_{4,m}r=0, \quad (2.16)$$

whose roots are $r_{i,m}(i=1,\ldots,8)$. The solutions for unknown functions can be written as:

$$U_m(x)=\sum_{i=1}^{\infty}A_{i,m}e^{r_{i,m}x}, \quad V_m(x)=\sum_{i=1}^{\infty}B_{i,m}e^{r_{i,m}x}, \quad W_m(x)=\sum_{i=1}^{\infty}C_{i,m}e^{r_{i,m}x}. \quad (2.17)$$

where, from a total of 24 integration constants only 8 are independent. The integration constants $A_{i,m}$, and $B_{i,m}$, can be expressed in terms of $C_{i,m}$ by doing

$$A_{i,m} = \delta_{i,m} C_{i,m} \quad \text{and} \quad B_{i,m} = \gamma_{i,m} C_{i,m}. \tag{2.18}$$

where $\delta_{i,m}$, and $\gamma_{i,m}$, are coefficients that represent the ratio of amplitudes of axial-radial and tangential-radial displacements, respectively, given by:

$$\delta_{i,m} = \frac{(c_9 + c_8 r_i^2)^2 + (c_7 + c_6 r_i^2)(c_{12} + c_{11} r_i^2 + c_{10} r_i^4)}{r_i(c_5 + c_4 r_i^2)(c_7 + c_6 r_i^2) - c_3 r_i (c_9 + c_8 r_i^2)}, \tag{2.19}$$

$$\gamma_{i,m} = \frac{(c_{12} c_3 + c_5 c_9 + (c_{11} c_3 + c_5 c_8 + c_4 c_9)(r_i^2) + (c_1 0 c_3 + c_4 c_8) r_i^4)}{(c_5 c_7 - c_3 c_9 + (c_5 c_6 + c_4 c_7 - c_3 c_8)(r_i^2) + c_4 c_6 r_i^4)}. \tag{2.20}$$

Substituting Equations (2.17) and (2.18) in Equations (2.12), keeping only the 1st terms and truncating the summation index as $m = 1, \ldots, M$ the displacement components can be written as:

$$\begin{aligned}
\hat{u}(x,\varphi) &= \sum_{m=1}^{M} \left(\sum_{i=1}^{8} \delta_{i,m} C_{i,m} e^{r_{i,m} x} \right) \cos(m\varphi), \\
\hat{v}(x,\varphi) &= \sum_{m=1}^{M} \left(\sum_{i=1}^{8} \gamma_{i,m} C_{i,m} e^{r_{i,m} x} \right) \sin(m\varphi), \\
\hat{w}(x,\varphi) &= \sum_{m=1}^{M} \left(\sum_{i=1}^{8} C_{i,m} e^{r_{i,m} x} \right) \cos(m\varphi).
\end{aligned} \tag{2.21}$$

2.1.3 Spectral Dynamic Stiffness Matrix

Figure 2.2 shows the schemes of two-edge circular cylindrical shell spectral element of length L including the displacements (*left*) and loads (*right*).

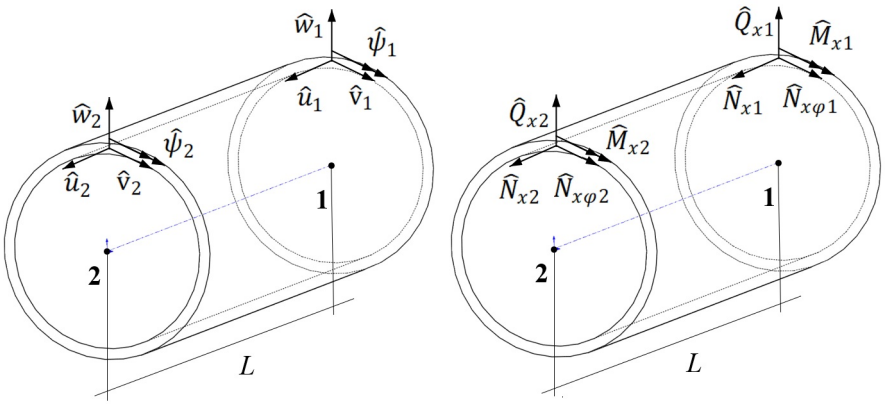

Figure 2.2: Two-edge circular cylindrical shell spectral element with components of the displacement (*left*) and the load (*right*) vectors.

The internal forces and moments in terms of displacements can be written as (Leissa, 1973):

$$N_x = D\left[\frac{\partial u}{\partial x} + \frac{\nu}{a}\left(w + \frac{\partial v}{\partial \varphi}\right)\right] - \frac{K}{a}\frac{\partial^2 w}{\partial x^2}, \tag{2.22}$$

$$N_\varphi = D\left[\frac{1}{a}\left(w + \frac{\partial v}{\partial \varphi}\right) + \nu\frac{\partial u}{\partial x}\right] + \frac{K}{a^3}\left(\frac{\partial^2 w}{\partial \varphi^2} + w\right), \tag{2.23}$$

$$N_{x\varphi} = \frac{D(1-\nu)}{2}\left(\frac{1}{a}\frac{\partial u}{\partial \varphi} + \frac{\partial v}{\partial x}\right) + K\frac{(1-\nu)}{2a^2}\left(\frac{\partial v}{\partial x} - \frac{\partial^2 w}{\partial x \partial \varphi}\right), \tag{2.24}$$

$$N_{\varphi x} = \frac{D(1-\nu)}{2}\left(\frac{1}{a}\frac{\partial u}{\partial \varphi} + \frac{\partial v}{\partial x}\right) + K\frac{(1-\nu)}{2a^2}\left(\frac{1}{a}\frac{\partial u}{\partial \varphi} + \frac{\partial^2 w}{\partial x \partial \varphi}\right), \tag{2.25}$$

$$M_x = -K\left[\frac{\partial^2 w}{\partial x^2} + \frac{\nu}{a^2}\left(\frac{\partial^2 w}{\partial \varphi^2} - \frac{\partial v}{\partial \varphi}\right) - \frac{1}{a}\frac{\partial u}{\partial x}\right], \tag{2.26}$$

$$M_\varphi = -K\left[\frac{1}{a^2}\left(\frac{\partial^2 w}{\partial \varphi^2} + w\right) + \nu\frac{\partial^2 w}{\partial x^2}\right], \tag{2.27}$$

$$M_{x\varphi} = -\frac{K(1-\nu)}{a}\left(\frac{\partial^2 w}{\partial x \partial \varphi} - \frac{\partial v}{\partial x}\right), \tag{2.28}$$

$$M_{\varphi x} = -\frac{K(1-\nu)}{2a}\left(2\frac{\partial^2 w}{\partial x \partial \varphi} - \frac{\partial v}{\partial x} + \frac{1}{a}\frac{\partial^2 u}{\partial \varphi}\right), \tag{2.29}$$

$$Q_x = \frac{\partial M_x}{\partial x} + \frac{1}{a}\frac{\partial M_{\varphi x}}{\partial \varphi}, \tag{2.30}$$

$$Q_\varphi = \frac{1}{a}\frac{\partial M_\varphi}{\partial \varphi} + \frac{\partial M_{x\varphi}}{\partial x}. \tag{2.31}$$

By defining the displacement vector $\hat{q}$ containing the displacements and rotations at the element edge $x = 0$ and $x = L$ it has:

$$\hat{\mathbf{q}} = [\hat{u}_1\ \hat{v}_1\ \hat{w}_1\ \hat{\psi}_{\varphi 1}\ \hat{u}_2\ \hat{v}_2\ \hat{w}_2\ \hat{\psi}_{\varphi 2}]^T, \tag{2.32}$$

where,

$$\begin{aligned}
&\hat{u}_1 = \hat{u}(0,\varphi) = U_m(0)\cos(m\varphi), && \hat{u}_2 = \hat{u}(L,\varphi) = U_m(L)\cos(m\varphi),\\
&\hat{v}_1 = \hat{v}(0,\varphi) = \hat{v}(0,\varphi) = V_m(0)\sin(m\varphi), && \hat{v}_2 = \hat{v}(L,\varphi) = \hat{v}(L,\varphi) = V_m(L)\sin(m\varphi),\\
&\hat{w}_1 = \hat{w}(0,\varphi) = \hat{w}(0,\varphi) = W_m(0)\cos(m\varphi), && \hat{w}(L,\varphi) = \hat{w}(L,\varphi) = W_m(L)\cos(m\varphi),\\
&\hat{\psi}_{\varphi 1} = \hat{\psi}_{\varphi}(0,\varphi) = \hat{\psi}_{\varphi}(0,\varphi) = \Psi_m(0)\cos(m\varphi), && \hat{\psi}_{\varphi 2}(L,\varphi) = \hat{\psi}_{\varphi}(L,\varphi) = \Psi_m(L)\cos(m\varphi),\\
&\hat{\psi}_{\varphi}(x,\varphi) = \frac{\partial \hat{w}(x,\varphi)}{\partial x}.
\end{aligned} \tag{2.33}$$

Similarly for the load vector,

$$\hat{\mathbf{Q}} = [\hat{N}_{x1}\ \hat{N}_{x\varphi 1}\ \hat{Q}_{x1}\ \hat{M}_{x1}\ \hat{N}_{x2}\ \hat{N}_{x\varphi 2}\ \hat{Q}_{x2}\ \hat{M}_{x2}]^T, \tag{2.34}$$

where, $\hat{N}_{x1} = -\hat{N}_x(0,\varphi)$, $\hat{N}_{x\varphi 1} = -\hat{N}_{x\varphi}(0,\varphi)$, $\hat{Q}_{x1} = -\hat{Q}_x(0,\varphi)$, $\hat{M}_{x1} = -\hat{M}_x(0,\varphi)$, $\hat{N}_{x2} = \hat{N}_x(L,\varphi)$, $\hat{N}_{x\varphi 2} = \hat{N}_{x\varphi}(L,\varphi)$, $\hat{Q}_{x2} = \hat{Q}_x(L,\varphi)$ and $\hat{M}_{x2} = \hat{M}_x(L,\varphi)$, with the nodal forces and moments given by Equations (2.22) to (2.31)

$$\hat{N}_{x(i,m)}(x,\varphi) = \frac{(D\nu(1+m\gamma_{i,m}) + aDr_{i,m}\delta_{i,m} - Kr_{i,m}^2}{a} \tag{2.35}$$

$$\hat{N}_{x\varphi(i,m)}(x,\varphi) = \frac{(1-\nu)[-aD\delta_{i,m}m + a^2D\gamma_{i,m}r_{i,m} + 3Kr_{i,m}(\gamma_{i,m}+m)]}{2a^2} \tag{2.36}$$

$$\begin{aligned}
\hat{Q}_{x(i,m)}(x,\varphi) = \frac{K[(1-\nu)\delta_{i,m}m^2 + 2a^2r_{i,m}^2(\delta_{i,m} - ar_{i,m})]}{2a^3} + \\
\frac{Kmr_{i,m}[(3-\nu)\gamma_{i,m} + 2m(2-\nu)]}{2a^2}
\end{aligned} \tag{2.37}$$

$$\hat{M}_{x(i,m)}(x,\varphi) = \frac{K[m\nu(\gamma_{i,m}+m) + ar_{i,m}\delta_{i,m} - a^2r_{i,m}^2]}{a^2} \tag{2.38}$$

The new displacement and load vector, namely $\hat{\mathbf{q}}_m$, that contain the amplitudes of displacements, and $\hat{\mathbf{Q}}_m$ that include the amplitudes of forces and moments, both on the element edges 1 ($x = 0$) and 2 ($x = L$) for the m-th harmonic are:

$$\hat{\mathbf{q}}_m = [U_m(0)\ V_m(0)\ W_m(0)\ \Psi_{\varphi m}(0)\ U_m(L)\ V_m(L)\ W_m(L)\ \Psi_{\varphi m}(L)]^T, \tag{2.39}$$

$$\begin{aligned}
\hat{\mathbf{Q}}_m = [&-\hat{N}_{xm}(0)\ -\hat{N}_{x\varphi m}(0)\ -\hat{Q}_{xm}(0)\ -\hat{M}_{xm}(0)\\
&+\hat{N}_{xm}(L)\ +\hat{N}_{x\varphi m}(L)\ +\hat{Q}_{xm}(L)\ +\hat{M}_{xm}(L)]^T.
\end{aligned} \tag{2.40}$$

The vector $\hat{\mathbf{q}}_m$ is related to the vector of integration constants $\mathbf{C}_m$ by the matrix $\mathbf{D}_m$,

while the vectors $\hat{\mathbf{Q}}_m$ and $\mathbf{C}_m$ are related through the matrix $\mathbf{F}_m$, as follows:

$$\hat{\mathbf{q}}_m = \mathbf{D}_m \mathbf{C}_m, \tag{2.41}$$

$$\hat{\mathbf{Q}}_m = \mathbf{F}_m \mathbf{C}_m, \tag{2.42}$$

where, the vector of integration constants $\mathbf{C}_m$ and the matrices $\mathbf{D}_m$ and $\mathbf{F}_m$ are:

$$\mathbf{C}_m = \left[C_{1,m}\ C_{2,m}\ C_{3,m}\ C_{4,m}\ C_{5,m}\ C_{6,m}\ C_{7,m}\ C_{8,m}\right]^T, \tag{2.43}$$

$$\mathbf{D}_m = \begin{bmatrix} \delta_{1,m} & \cdots & \delta_{8,m} \\ \gamma_{i,m} & \cdots & \gamma_{i,m} \\ 1 & \cdots & 1 \\ -r_{1,m} & \cdots & -r_{8,m} \\ \delta_{1,m}e^{r_{i,m}L} & \cdots & \delta_{8,m}e^{r_{8,m}L} \\ \gamma_{i,m}e^{r_{i,m}L} & \cdots & \gamma_{i,m}e^{r_{i,m}L} \\ e^{r_{i,m}L} & \cdots & e^{r_{i,m}L} \\ -r_{1,m}e^{r_{i,m}L} & \cdots & -r_{8,m}e^{r_{i,m}L} \end{bmatrix}, \tag{2.44}$$

$$\mathbf{F}_m = \begin{bmatrix} -\hat{N}_{x(1,m)} & \cdots & -\hat{N}_{x(8,m)} \\ -\hat{N}_{x\varphi(1,m)} & \cdots & -\hat{N}_{x\varphi(8,m)} \\ -\hat{Q}_{x(1,m)} & \cdots & -\hat{Q}_{x(8,m)} \\ -\hat{M}_{x(1,m)} & \cdots & -\hat{M}_{x(8\mathrm{m})} \\ \hat{N}_{x(1,m)}e^{r_{i,m}L} & \cdots & \hat{N}_{x(8,m)}e^{r_{8,m}L} \\ \hat{N}_{x\varphi(1,m)}e^{r_{i,m}L} & \cdots & \hat{N}_{x\varphi(8,m)}e^{r_{8,m}L} \\ \hat{Q}_{x(1,m)}e^{r_{i,m}L} & \cdots & \hat{Q}_{x(8,m)}e^{r_{8,m}L} \\ \hat{M}_{x(1,m)}e^{r_{i,m}L} & \cdots & \hat{M}_{x(8\mathrm{m})}e^{r_{8,m}L} \end{bmatrix}. \tag{2.45}$$

If vector $\mathbf{C}_m$ is expressed from the Equation (2.41) as a function of $\hat{\mathbf{q}}_m$ and replaced in the Equation (2.42), the relation between vectors $\hat{\mathbf{Q}}_m$ and $\hat{\mathbf{q}}_m$ is obtained as:

$$\hat{\mathbf{Q}}_m = \mathbf{K}_{Sm}\hat{\mathbf{q}}_m, \tag{2.46}$$

where, $\mathbf{K}_{Sm} = \mathbf{F}_m(\mathbf{D}_m)^{-1}$ is the dynamic stiffness matrix of the Cylindrical Shell Spectral Element - CSSE for the m-th harmonic.

2.2 Point load

In an attempt to apply point load on a shell element care must be taken due the fact that the DOFs of SE model are distributed along the entire edge of the element. Figure 2.3 shows a CSSE scheme, where the shell is modeled with a single element with two edges and at each edge the degrees of freedom u , v, w and ψ. A force is projected in the radial direction at point A (x = 0 and $\varphi = \varphi_1$) with amplitude F. Thus, the focus is to evaluate the displacement caused by loading F at any position of the cylindrical shell, for example at point B ($x = L$ and $\varphi = \varphi_2$).

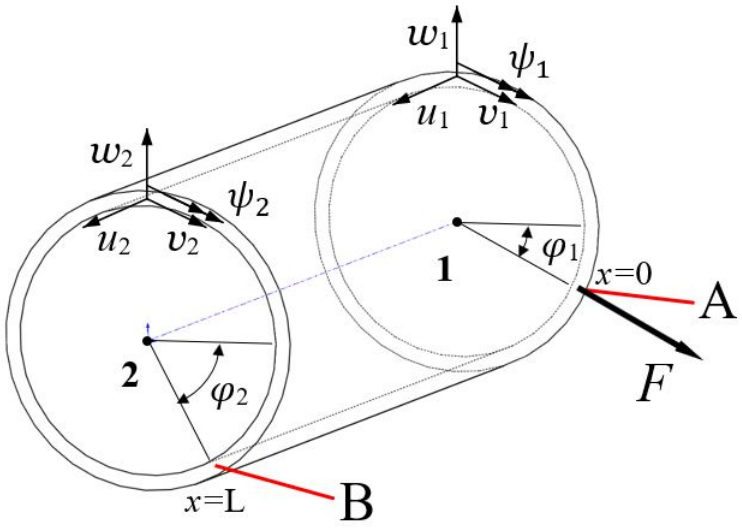

Figure 2.3: CSSE with the point load.

The problem presented is written in the spectral form as:

$$\mathbf{K}_{Sm} \begin{bmatrix} \hat{u}_{1m}(0,\varphi) \\ \hat{v}_{1m}(0,\varphi) \\ \hat{w}_{1m}(0,\varphi) \\ \hat{\psi}_{1m}(0,\varphi) \\ \hat{u}_{2m}(L,\varphi) \\ \hat{v}_{2m}(L,\varphi) \\ \hat{w}_{2m}(L,\varphi) \\ \hat{\psi}_{2m}(L,\varphi) \end{bmatrix} = \begin{bmatrix} 0 \\ 0 \\ F_m(0,\varphi) \\ 0 \\ 0 \\ 0 \\ 0 \\ 0 \end{bmatrix} \tag{2.47}$$

where $\mathbf{K}_{Sm}$ is the dynamic stiffness matrix (Eq. 2.46) and $F_m(0,\varphi)$ is a loading vector projected in the radial direction along the entire edge of the cylindrical shell.

Lee and Lee (1999) showed a point force loading for a spectral plate element. The force must be projected on the basis of cosine function in terms of the harmonic m related to the w direction. This representation takes into account the position of the concentrated driving force, φ_1. Adapting for the case of a CSSE developed in this thesis the form of $F_m(0,\varphi)$ is given by,

$$F_m(0,\varphi) = 2\frac{F}{L_x}\cos(m\varphi_1) \tag{2.48}$$

where, F is magnitude of the point load in the direction w, $L_x = 2\pi$, circumference of cylindrical shell.

Finally, as the load is projected across the edge, the displacement represents the behavior of the entire edge. Therefore, to find the displacement at point B is necessary to use Eq. 2.21, thus the radial displacement in $\hat{w}_2(L,\varphi_2)$ is

$$\hat{w}_2(L,\varphi_2) = \sum_{m=1}^{M} \hat{w}_{2m}(L,\varphi)\cos(m\varphi_2) \tag{2.49}$$

To evaluate the behavior of the fluid-filled closed cylindrical shell when subjected to a point force, follows the same strategy presented in this section.

2.3 Fluid-filled Cylindrical Shell Spectral Element - FCSSE

In this section, a thin circular cylindrical shell filled with a compressible fluid is formulated. The vibroacoustic coupling between the inner fluid and the closed cylindrical shell is the main focus of the work. The effect of external fluid is disregarded. The structure is assumed to be linear and elastic-dissipative, while the fluid is assumed to be homogeneous, barotropic, compressible and inviscid.

2.3.1 Fluid-Structure Theory

The cylindrical geometry (thickness h, radius a, length L) and coordinate system (displacements u, v and w of the mid surface in x, φ and z directions, respectively) for a closed circular cylindrical shell are shown in Figure 2.2.

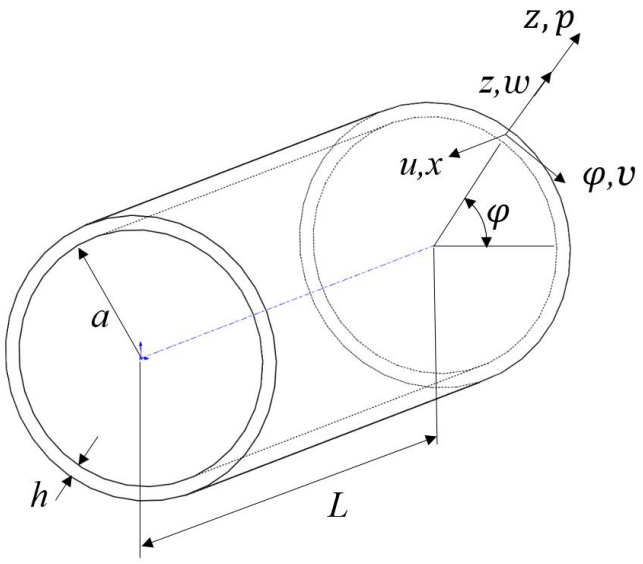

Figure 2.4: Geometry and coordinates system of a fluid-filled circular cylindrical thin shell.

Based on the Flügge thin shell theory Leissa (1973), the governing differential equations a fluid-filled closed circular cylindrical shell can be written in matrix form as (Gautier *et al.*, 2007):

$$\mathscr{L}\mathbf{u} = F_f, \tag{2.50}$$

where, $\mathscr{L}$ is operator equations for a closed circular cylindrical shell (Eq. 2.9), $\mathbf{u}$ is the displacement vector (Eq. 2.3) and the force vector is:

$$F_f = \left\{ 0 \quad 0 \quad -\frac{p}{\rho_S c_S^2 h} \right\}^T , \tag{2.51}$$

where, p is the internal pressure, $c_S = \sqrt{E/\rho_S(1-\nu^2)}$ is the structure wave speed, E is the Young's modulus, ρ_S is the structure mass density, ν is the Poisson's rate.

The governing wave propagation equation for the fluid may be written as (Fahy and Gardonio, 1985):

$$\nabla^2 p = \frac{1}{c_F^2}\frac{\partial^2 p}{\partial t^2} + f_v \ , \tag{2.52}$$

where c_F is the fluid speed of sound, p is the acoustic pressure and f_v are the volume forces that is proportional to the acceleration and mass of the fluid inside the cylindrical shell. Equation (2.52) may be written in cylindrical coordinates (r,φ, x) as (Zhang, 2002),

$$\frac{1}{r}\frac{\partial}{\partial r}\left(r\frac{\partial p}{\partial r}\right) + \frac{1}{r^2}\frac{\partial^2 p}{\partial \varphi^2} + \frac{\partial^2 p}{\partial x^2} = \frac{1}{c_F^2}\frac{\partial^2 p}{\partial t^2} + f_v \ , \tag{2.53}$$

where, r represents the radial distance, φ the azimuth angle and z is the length. For the cyl-

indrical shell, the radial distance is constant($r = a$), then one has,

$$\frac{1}{a^2}\frac{\partial^2 p}{\partial \varphi^2} + \frac{\partial^2 p}{\partial x^2} = \frac{1}{c_F^2}\frac{\partial^2 p}{\partial t^2} + f_v \ , \tag{2.54}$$

Assuming linear approximations and wave propagation, the pressure p inside the shell satisfies the wave equation (Fahy and Gardonio, 1985; Gautier *et al.*, 2005),

$$\frac{1}{a^2}\frac{\partial^2 p}{\partial \varphi^2} + \frac{\partial^2 p}{\partial x^2} - \frac{1}{c_F^2}\frac{\partial^2 p}{\partial t^2} = \frac{2\rho_F}{a}\frac{\partial^2 w}{\partial t^2}, \tag{2.55}$$

where, ρ_F is the fluid mass density. In Equation (2.55) the right hand-side represents an acoustic source describing the vibration of shell wall effect on the internal pressure field.

Equations (2.50) and (2.55) give a set of four linear second order differential coupled equations, as a function of four variables p, u, v, and w , which can be written in a matrix form as:

$$\begin{bmatrix} \left(\frac{1}{a^2}\partial_\varphi^2 + \partial_x^2 - \frac{1}{c_F^2}\partial_t^2\right) & 0 & 0 & \frac{2\rho_F}{a}\partial_t^2 \\ 0 & & & \\ 0 & & \mathscr{L}_{[3\times 3]} & \\ \frac{1}{\rho_S c_S^2 h} & & & \end{bmatrix} \begin{Bmatrix} p(x,\varphi,t) \\ u(x,\varphi,t) \\ v(x,\varphi,t) \\ w(x,\varphi,t) \end{Bmatrix} = \begin{Bmatrix} 0 \\ 0 \\ 0 \\ 0 \end{Bmatrix} \tag{2.56}$$

2.3.2 General solution

By using the separation of variables, the general solution can be considered as:

$$\begin{aligned} p\,(x,\varphi,t) &= \hat{p}\,(x,\varphi)\,e^{i\omega t}, \quad u\,(x,\varphi,t) = \hat{u}\,(x,\varphi)\,e^{i\omega t}, \\ v\,(x,\varphi,t) &= \hat{v}\,(x,\varphi)\,e^{i\omega t}, \quad w\,(x,\varphi,t) = \hat{w}\,(x,\varphi)\,e^{i\omega t}, \end{aligned} \tag{2.57}$$

where, ω is the circular frequency and $\hat{p}$, $\hat{u}$, $\hat{v}$, and $\hat{w}$ are the spectral amplitude of pressure and displacement components. For a closed circular cylindrical shell, displacement and pressure needs to satisfy periodicity in the circumferential direction.

Then, the solution of Eq. (2.56) is assumed as an infinite Fourier series as:

$$\begin{aligned}
\hat{p}(x,\varphi) &= \sum_{m=0}^{\infty} P_m(x)\cos(m\varphi) + \sum_{m=1}^{\infty} \bar{P}_m(x)\sin(m\varphi),\\
\hat{u}(x,\varphi) &= \sum_{m=0}^{\infty} U_m(x)\cos(m\varphi) + \sum_{m=1}^{\infty} \bar{U}_m(x)\sin(m\varphi),\\
\hat{v}(x,\varphi) &= \sum_{m=1}^{\infty} V_m(x)\sin(m\varphi) + \sum_{m=0}^{\infty} \bar{V}_m(x)\cos(m\varphi),\\
\hat{w}(x,\varphi) &= \sum_{m=0}^{\infty} W_m(x)\cos(m\varphi) + \sum_{m=1}^{\infty} \bar{W}_m(x)\sin(m\varphi),
\end{aligned} \tag{2.58}$$

where $m \in \mathbb{Z}$. Considering that boundary conditions are independent of φ, the solutions for different harmonics are uncoupled and only the m-th harmonic can be considered. Here only the solution for the asymmetric vibration $(m \geq 1)$ is presented, while the axisymmetric vibration solution $(m = 0)$ will not be considered. The solution procedure for the 1st terms of Eq.(2.58) is presented, while for the 2nd terms it can be obtained in a similar way. Natural frequencies obtained with the 1st and 2nd terms of Eq. (2.58) are the same, which means that for the closed circular cylindrical shell all the natural frequencies are duplicated. By substituting the 1st terms of Eq.(2.58) in the Eq.(2.56) it has:

$$\mathscr{L}_f \bar{\mathbf{u}} = \{\mathbf{0}\}\,, \tag{2.59}$$

where

$$\mathscr{L}_f = \begin{bmatrix}
c_{13,m} + \partial_x^2 & 0 & 0 & c_{14,m} \\
0 & c_{1,m}\partial_x^2 + c_{2,m} & c_{3,m}\partial_x & c_{4,m}\partial_x^3 + c_{5,m}\partial_x \\
0 & -c_{3,m}\partial_x & c_{6,m}\partial_x^2 + c_{7,m} & c_{8,m}\partial_x^2 + c_{9,m} \\
c_{15,m} & c_{4,m}\partial_x^3 + c_{5,m}\partial_x & -c_{8,m}\partial_x^2 - c_{9,m} & c_{10,m}\partial_x^4 + c_{11,m}\partial_x^2 \\
 & & & + c_{12,m}
\end{bmatrix}, \tag{2.60}$$

$$\bar{\mathbf{u}}(x) = \{P_m(x) \quad U_m(x) \quad V_m(x) \quad W_m(x)\}^T, \tag{2.61}$$

where, $\mathscr{L}_f$ is a matrix with the differential operators and coefficients $c_{i,m}(i = 1 \ldots 15)$. For the sake of conciseness, the coefficients are

$$
\begin{array}{lll}
c_{1,m} = 1, & c_{2,m} = -m^2 a_1 - w^2 a_2, & c_{3,m} = -m a_3, \\
c_{4,m} = -a_5, & c_{5,m} = a_4 - m^2 a_6, & c_{6,m} = a_8, \\
c_{7,m} = -m^2 a_7 - w^2 a_2, & c_{8,m} = -m a_9, & c_{9,m} = -m a_7, \\
c_{10,m} = k, & c_{11,m} = -2km^2 a_7, & c_{12,m} = -a_7 + w^2 a_2 \\
 & & \quad + k(m^4 a_7^2 - 2m^2 a_7 + a_7^4), \\
c_{13,m} = m^2/a^2 - \omega^2/c_F^2, & c_{14,m} = 2\rho_F \omega^2 / a, & c_{15,m} = 1/\rho_S c_S^2 h.
\end{array}
\tag{2.62}
$$

By expanding the determinant of $\mathscr{L}_f$ (Eq. 2.60), a 10-th order differential equation is obtained as:

$$
(\mathtt{b}_{1,m}\partial_x^{10} + \mathtt{b}_{2,m}\partial_x^8 + \mathtt{b}_{3,m}\partial_x^6 + \mathtt{b}_{4,m}\partial_x^4 + \mathtt{b}_{5,m}\partial_x^2 + \mathtt{b}_{6,m}\partial_x)\Psi = 0, \tag{2.63}
$$

where, $\Psi = U_m$ or V_m or W_m or P_m, and the coefficients $\mathtt{b}_{i,m}(i = 1, \ldots, 6)$ are shown in 2.64.

$$
\begin{aligned}
&\mathtt{b}_{1,m} = -c_{6,m}(-c_{4,m}^2 + c_{1,m}c_{10,m}),\\[2ex]
&\mathtt{b}_{2,m} = (c_{7,m} - c_{6,m}c_{13,m})c_{4,m}^2 + (2c_{5,m}c_{6,m} - 2c_{3,m}c_{8,m})c_{4,m}\\
&-c_{10,m}(c_{3,m}^2 + c_{2,m}c_{6,m}) - c_{1,m}(c_{8,m}^2 + c_{6,m}c_{11,m} + c_{10,m}(c_{7,m} - c_{6,m}c_{13,m})),\\[2ex]
&\mathtt{b}_{3,m} = c_{5,m}^2c_{6,m} - c_{2,m}c_{8,m}^2 - c_{3,m}^2c_{11,m} - c_{1,m}(-c_{13,m}c_{8,m}^2 + 2c_{9,m}c_{8,m}\\
&+c_{6,m}c_{12,m} + c_{7,m}c_{11,m} - c_{6,m}c_{11,m}c_{13,m}) + c_{10,m}(c_{13,m}c_{3,m}^2 - c_{2,m}c_{7,m}\\
&+c_{1,m}c_{7,m}c_{13,m} + c_{2,m}c_{6,m}c_{13,m}) - 2c_{3,m}c_{4,m}c_{9,m} - 2c_{3,m}c_{5,m}c_{8,m}\\
&+2c_{4,m}c_{5,m}c_{7,m} - c_{2,m}c_{6,m}c_{11,m} - c_{4,m}^2c_{7,m}c_{13,m} + 2c_{3,m}c_{4,m}c_{8,m}c_{13,m}\\
&-2c_{4,m}c_{5,m}c_{6,m}c_{13,m},\\[2ex]
&\mathtt{b}_{4,m} = c_{5,m}^2c_{7,m} - c_{3,m}^2c_{12,m} - c_{1,m}(c_{9,m}^2 - 2c_{8,m}c_{13,m}c_{9,m} + c_{7,m}c_{12,m}\\
&-c_{6,m}c_{12,m}c_{13,m} + c_{6,m}c_{14,m}c_{15,m}) + c_{11,m}(c_{13,m}c_{3,m}^2 - c_{2,m}c_{7,m}\\
&+c_{1,m}c_{7,m}c_{13,m} + c_{2,m}c_{6,m}c_{13,m}) - 2c_{3,m}c_{5,m}c_{9,m} - 2c_{2,m}c_{8,m}c_{9,m}\\
&-c_{2,m}c_{6,m}c_{12,m} + c_{2,m}c_{8,m}^2c_{13,m} - c_{5,m}^2c_{6,m}c_{13,m} + 2c_{3,m}c_{4,m}c_{9,m}c_{13,m}\\
&+2c_{3,m}c_{5,m}c_{8,m}c_{13,m} - 2c_{4,m}c_{5,m}c_{7,m}c_{13,m} + c_{2,m}c_{7,m}c_{10,m}c_{13,m},\\[2ex]
&\mathtt{b}_{5,m} = c_{12,m}(c_{13,m}c_{3,m}^2 - c_{2,m}c_{7,m} + c_{1,m}c_{7,m}c_{13,m} + c_{2,m}c_{6,m}c_{13,m})\\
&-c_{2,m}c_{9,m}^2 + c_{1,m}c_{9,m}^2c_{13,m} - c_{5,m}^2c_{7,m}c_{13,m} - c_{3,m}^2c_{14,m}c_{15,m}\\
&+2c_{3,m}c_{5,m}c_{9,m}c_{13,m} + 2c_{2,m}c_{8,m}c_{9,m}c_{13,m} + c_{2,m}c_{7,m}c_{11,m}c_{13,m}\\
&-c_{1,m}c_{7,m}c_{14,m}c_{15,m} - c_{2,m}c_{6,m}c_{14,m}c_{15,m},\\[2ex]
&\mathtt{b}_{6,m} = c_{2,m}(c_{13,m}c_{9,m}^2 + c_{7,m}c_{12,m}c_{13,m} - c_{7,m}c_{14,m}c_{15,m}).
\end{aligned}
\tag{2.64}
$$

By assuming the solution of Equation (2.71) in the form $\Psi = e^{sx}$ the corresponding characteristic equation is obtained as:

$$
\mathtt{b}_{1,m}s^{10} + \mathtt{b}_{2,m}s^8 + \mathtt{b}_{3,m}s^6 + \mathtt{b}_{4,m}s^4 + \mathtt{b}_{5,m}s^2 + \mathtt{b}_{6,m} = 0, \tag{2.65}
$$

whose roots, $s_{i,m}(i = 1,\ldots,10)$, are obtained using `roots` function of MATLAB software. The solutions for unknown functions can be written as:

$$
\begin{aligned}
P_m(x) &= \sum_{i=1}^{10} E_{i,m}e^{s_{i,m}x}, \quad U_m(x) = \sum_{i=1}^{10} A_{i,m}e^{s_{i,m}x},\\
V_m(x) &= \sum_{i=1}^{10} B_{i,m}e^{s_{i,m}x}, \quad W_m(x) = \sum_{i=1}^{10} C_{i,m}e^{s_{i,m}x},
\end{aligned}
\tag{2.66}
$$

where from a total of 40 integration constants only 10 are independent. The integration constants

$E_{i,m}$, $A_{i,m}$, and $B_{i,m}$, can be expressed in terms of $C_{i,m}$ by doing

$$E_{i,m} = \alpha_{i,m} C_{i,m}, \quad A_{i,m} = \delta_{i,m} C_{i,m}; \quad B_{i,m} = \gamma_{i,m} C_{i,m}, \tag{2.67}$$

where $\alpha_{i,m}$, is the pressure amplitude ratio coefficients, and $\delta_{i,m}$, and $\gamma_{i,m}$, are the amplitude ratios of axial-radial and tangential-radial displacement, respectively. The amplitude ratio coefficients are shown in 2.68 to 2.70.

$$\alpha_{i,m} = -\frac{c_{14,m}}{-s_i^2 + c_{13,m}}, \tag{2.68}$$

$$\delta_{i,m} = \frac{c_{9,m} + c_{8,m} s_i^2 + \left[\frac{(c_{6,m} s_i^2 + c_{7,m}) \left(k_{c1} - \frac{c_{14,m} c_{15,m}}{-s_i^2 + c_{13,m}} \right)}{k_{c2}} \right]}{c_{3,m} s_i - \frac{(c_{4,m} s_i^3 + c_{5,m} s_i)(c_{6,m} s_i^2 + c_{7,m})}{k_{c2}}}, \tag{2.69}$$

$$\gamma_{i,m} = \frac{\left[k_{c1} + \frac{(c_{4,m} s_i^3 + c_{5,m} s_i)(k_{c2} + \frac{(c_{6,m} s_i^2 + c_{7,m}) \left(k_{c1} - \frac{c_{14,m} c_{15,m}}{-s_i^2 + c_{13,m}} \right)}{k_{c2}})}{c_{3,m} s_i - \frac{(c_{4,m} s_i^3 + c_{5,m} s_i)(c_{6,m} s_i^2 + c_{7,m})}{k_{c2}}} - \frac{c_{14,m} c_{15,m}}{-s_i^2 + c_{13,m}} \right]}{k_{c2}}, \tag{2.70}$$

where $k_{c1} = c_{12,m} + c_{11,m} s_i^2 + c_{10,m} s_i^4, \quad k_{c2} = c_{8,m} s_i^2 + c_{9,m}$.

Substituting Equations (2.66) and (2.67) in Equation (2.58), keeping only the 1st terms and truncating the summation index as $m = 1, \ldots, M$ the displacement components can be written as:

$$\begin{aligned}
\hat{p}(x,\varphi) &= \sum_{m=1}^{M} \left(\sum_{i=1}^{10} \alpha_{i,m} C_{i,m} e^{s_{i,m} x} \right) \cos(m\varphi), \\
\hat{u}(x,\varphi) &= \sum_{m=1}^{M} \left(\sum_{i=1}^{10} \delta_{i,m} C_{i,m} e^{s_{i,m} x} \right) \cos(m\varphi), \\
\hat{v}(x,\varphi) &= \sum_{m=1}^{M} \left(\sum_{i=1}^{10} \gamma_{i,m} C_{i,m} e^{s_{i,m} x} \right) \sin(m\varphi), \\
\hat{w}(x,\varphi) &= \sum_{m=1}^{M} \left(\sum_{i=1}^{10} C_{i,m} e^{s_{i,m} x} \right) \cos(m\varphi).
\end{aligned} \tag{2.71}$$

2.3.3 Spectral Dynamic Stiffness Matrix

Figure 2.5 shows the schemes of two-edge fluid-filled circular cylindrical shell spectral element of length L including the displacements and pressure (*left*), and loads (*right*).

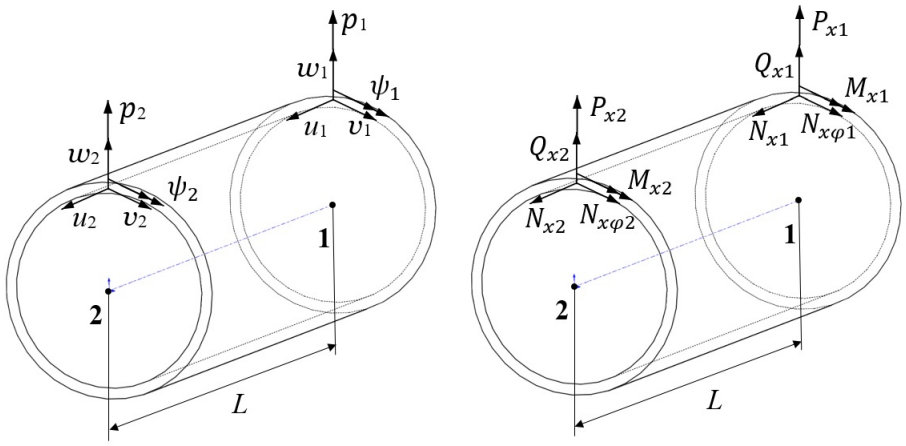

Figure 2.5: two-edge fluid-filled cylindrical shell spectral element with components of displacement and pressure (*left*), and the load (*right*) vectors.

The displacements and pressure at the element ends $x = 0$ and $x = L$ is defined by:

$$\mathbf{q} = \{p_1\ u_1\ v_1\ w_1\ \psi_{\varphi 1}\ p_2\ u_2\ v_2\ w_2\ \psi_{\varphi 2}\}^T, \tag{2.72}$$

where

$$\begin{aligned}
&p_1 = p(0,\varphi) = P_m(0)\cos(m\varphi), && p_2 = p(L,\varphi) = P_m(L)\cos(m\varphi),\\
&u_1 = u(0,\varphi) = U_m(0)\cos(m\varphi), && u_2 = u(L,\varphi) = U_m(L)\cos(m\varphi),\\
&v_1 = v(0,\varphi) = V_m(0)\sin(m\varphi), && v_2 = v(L,\varphi) = V_m(L)\sin(m\varphi),\\
&w_1 = w(0,\varphi) = W_m(0)\cos(m\varphi), && w_2 = w(L,\varphi) = W_m(L)\cos(m\varphi),\\
&\psi_{\varphi 1} = \psi_\varphi(0,\varphi) = \Psi_m(0)\cos(m\varphi), && \psi_{\varphi 2} = \psi_{\varphi 2}(L,\varphi) = \Psi_m(L)\cos(m\varphi),
\end{aligned} \tag{2.73}$$

and $\psi_\varphi(x,\varphi) = \partial w(x,\varphi)/\partial x$. Similarly, the load vector is given by,

$$\mathbf{Q} = \{P_{x1}\ N_{x1}\ N_{x\varphi 1}\ Q_{x1}\ M_{x1}\ P_{x2}\ N_{x2}\ N_{x\varphi 2}\ Q_{x2}\ M_{x2}\}^T, \tag{2.74}$$

with $P_{x1} = P_x(0,\varphi)$, $N_{x1} = -N_x(0,\varphi)$, $N_{x\varphi 1} = -N_{x\varphi}(0,\varphi)$, $Q_{x1} = -Q_x(0,\varphi)$, $M_{x1} = -M_x(0,\varphi)$, $P_{x2} = P_x(L,\varphi)$, $N_{x2} = N_x(L,\varphi)$, $N_{x\varphi 2} = N_{x\varphi}(L,\varphi)$, $Q_{x2} = Q_x(L,\varphi)$, and $M_{x2} = M_x(L,\varphi)$ where the load amplitudes are given by:

$$N_{x(i,m)}(x,\varphi) = \frac{(D\nu(1+m\gamma_{i,m}) + aDs_{i,m}\delta_{i,m} - Ks_{i,m}^2}{a}, \tag{2.75}$$

$$N_{x\varphi(i,m)}(x,\varphi) = \frac{(1-\nu)[-aD\delta_{i,m}m + a^2D\gamma_{i,m}s_{i,m} + 3Ks_{i,m}(\gamma_{i,m}+m)]}{2a^2}, \tag{2.76}$$

$$Q_{x(i,m)}(x,\varphi) = \frac{K[(1-\nu)\delta_{i,m}m^2 + 2a^2 s_{i,m}^2(\delta_{i,m} - a s_{i,m})]}{2a^3} + \frac{K m s_{i,m}[(3-\nu)\gamma_{i,m} + 2m(2-\nu)]}{2a^2}, \tag{2.77}$$

$$M_{x(i,m)}(x,\varphi) = \frac{K[m\nu(\gamma_{i,m} + m) + a s_{i,m}\delta_{i,m} - a^2 s_{i,m}^2]}{a^2}, \tag{2.78}$$

$$P_{x(i,m)}(x,\varphi) = \alpha_{i,m} s_{i,m}. \tag{2.79}$$

The new displacements and pressure amplitudes vector, and the load vector that include the load amplitudes, both on the boundaries $x = 0$ and $x = L$ for the m-th harmonic are:

$$\begin{aligned}\mathbf{q}_m = \{&P_m(0)\ U_m(0)\ V_m(0)\ W_m(0)\ \Psi_{\varphi m}(0)\\ &P_m(L)\ U_m(L)\ V_m(L)\ W_m(L)\ \Psi_{\varphi m}(L)\}^T,\end{aligned} \tag{2.80}$$

$$\begin{aligned}\mathbf{Q}_m = \{&-P_{xm}(0)\ -N_{xm}(0)\ -N_{x\varphi m}(0)\ -Q_{xm}(0)\ -M_{xm}(0)\\ &+P_{xm}(L)\ +N_{xm}(L)\ +N_{x\varphi m}(L)\ +Q_{xm}(L)\ +M_{xm}(L)\}^T,\end{aligned} \tag{2.81}$$

By arranging the vectors $\mathbf{q}_m$ and $\mathbf{Q}_m$ in a matrix form it has:

$$\mathbf{q}_m = \mathbf{D}_m \mathbf{C}_m, \tag{2.82}$$

$$\mathbf{Q}_m = \mathbf{F}_m \mathbf{C}_m, \tag{2.83}$$

where, $\mathbf{C}_m = C_{i,m}, i = 1, \ldots, 10$ is the integration constant vector and $\mathbf{D}_m$ is the coefficient matrix that relates the displacements and pressure with the integration constant vector, while $\mathbf{F}_m$ is the coefficient matrix that relates loads with the integration constant vector. Matrices $\mathbf{D}_m$ and $\mathbf{F}_m$ are shown in Eqs. (2.84) and (2.85).

$$\mathbf{D}_m = \begin{bmatrix} \alpha_{1,m} & \cdots & \alpha_{10,m} \\ \delta_{1,m} & \cdots & \delta_{10,m} \\ \gamma_{i,m} & \cdots & \gamma_{10,m} \\ 1 & \cdots & 1 \\ -s_{1,m} & \cdots & -s_{10,m} \\ \alpha_{1,m}e^{s_{1,m}L} & \cdots & \alpha_{10,m}e^{s_{10,m}L} \\ \delta_{1,m}e^{s_{1,m}L} & \cdots & \delta_{10,m}e^{s_{10,m}L} \\ \gamma_{1,m}e^{s_{1,m}L} & \cdots & \gamma_{10,m}e^{s_{10,m}L} \\ e^{s_{1,m}L} & \cdots & e^{s_{10,m}L} \\ -s_{1,m}e^{s_{1,m}L} & \cdots & -s_{10,m}e^{s_{10,m}L} \end{bmatrix}, \tag{2.84}$$

$$\mathbf{F}_m = \begin{bmatrix} -\hat{P}_{x(1,m)} & \cdots & -\hat{P}_{x(10,m)} \\ -\hat{N}_{x(1,m)} & \cdots & -\hat{N}_{x(10,m)} \\ -\hat{N}_{x\varphi(1,m)} & \cdots & -\hat{N}_{x\varphi(10,m)} \\ -\hat{Q}_{x(1,m)} & \cdots & -\hat{Q}_{x(10,m)} \\ -\hat{M}_{x(1,m)} & \cdots & -\hat{M}_{x(10\mathrm{m})} \\ \hat{P}_{x(1,m)}e^{s_{1,m}L} & \cdots & \hat{P}_{x(10,m)}e^{s_{10,m}L} \\ \hat{N}_{x(1,m)}e^{s_{1,m}L} & \cdots & \hat{N}_{x(10,m)}e^{s_{10,m}L} \\ \hat{N}_{x\varphi(1,m)}e^{s_{1,m}L} & \cdots & \hat{N}_{x\varphi(10,m)}e^{s_{8,m}L} \\ \hat{Q}_{x(1,m)}e^{s_{1,m}L} & \cdots & \hat{Q}_{x(10,m)}e^{s_{10,m}L} \\ \hat{M}_{x(1,\mathrm{m})}e^{s_{1,m}L} & \cdots & \hat{M}_{x(10\mathrm{m})}e^{s_{10,m}L} \end{bmatrix}. \tag{2.85}$$

By rewriting Eq. (2.82) as $\mathbf{C}_m = \mathbf{D}_m^{-1}\mathbf{q}_m$ and substituting in the Eq.(2.83) one has,

$$\mathbf{Q}_m = \underbrace{\mathbf{F}_m\mathbf{D}_m^{-1}}_{\mathbf{K}_{Fm}}\mathbf{q}_m, \tag{2.86}$$

where, $\mathbf{K}_{Fm}$ is the dynamic stiffness matrix of the Fluid-filled Cylindrical Shell Spectral Element - FCSSE for the m-th harmonic.

2.4 Wave Spectral Element - WSE

In this section, the Wave Spectral Element - WSE method is presented to study wave propagation and phononic crystal in periodic cylindrical shells. In WSE, the dynamic stiffness matrix of a small slice of the structure modeled by the spectral element method is used for the application of periodicity conditions in the propagation of a wave through the shell.

Periodicity conditions results in an eigenproblem, from where the dispersion diagram (wavenumber x frequency) and forced responses (FRF's) can be obtained. In Goto *et al.* (2020) work is used WSE to evaluate band gap in bars, in Mencik and Ichchou (2007) work is used WFE to evaluate the cylindrical shell. This thesis stands out because it is the first one that uses the WSE for cylindrical shell with and without filling of internal fluid.

2.4.1 Periodic Structure Modelling

Consider an elastic circular cylindrical shell in which the structure is discretized into several slices of length d , consider a slice $\bar{k}$ ($\bar{k}$ = 1,..., N) , as sketched in Fig. 2.6.

The circular cylindrical shell model is formulated with the SE method, presented in section 2.1, the equilibrium equation for the finite circular cylindrical shell by SE is given by Eq. (2.46). For the case Fluid-filled Cylindrical Shell Spectral Element, presented in section 2.3 the equilibrium equation by SE is given by Eq. (2.86). Renaming the spectral dynamic stiffness

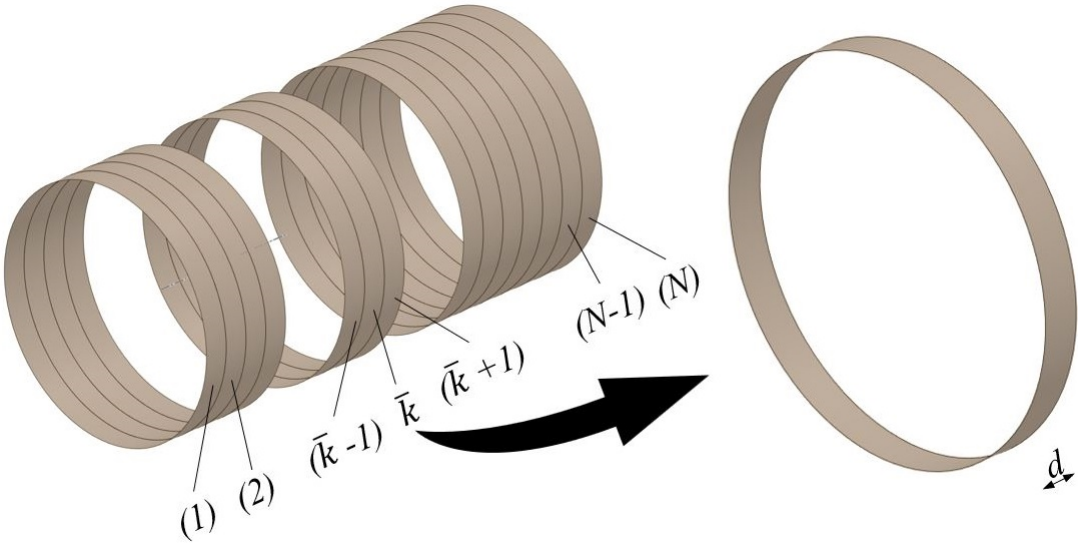

Figure 2.6: Circular cylindrical shell discretized in N slices.

element matrix as $\mathbf{K}_{SEm}$.

Within the framework of the WSE method, only one substructure is modeled by means of spectral elements (see Figure 2.7). Here, the left and right boundaries of the substructure are built in the same way, i.e., by means of the same number of degrees of freedom (DOFs)

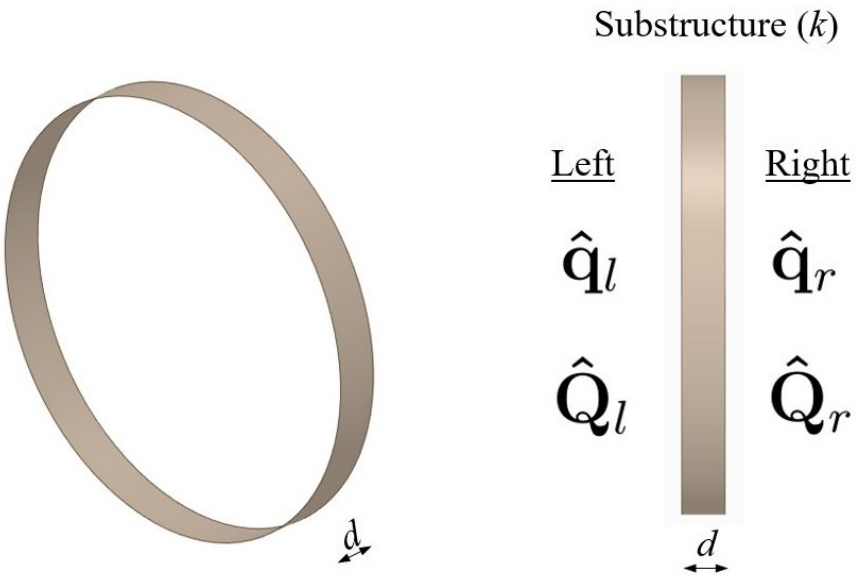

Figure 2.7: Substructure ($\bar{k}$) slices.

From a slice ($\bar{k}$), the dynamic stiffness matrix D is obtained through the matrices of that slice calculated by SE, such as:

$$\mathbf{D}\hat{\mathbf{q}} = \hat{\mathbf{Q}}, \tag{2.87}$$

where, $\mathbf{D} = \mathbf{K}_{SEm}$, $\hat{\mathbf{q}}$ is the displacement vector, $\hat{\mathbf{Q}}$ is the force vector. Eq. (2.87) can be expressed in terms of the state vectors on the left (l) and right (r) sides of the slice as:

$$\begin{bmatrix} \mathbf{D}_{ll} & \mathbf{D}_{lr} \\ \mathbf{D}_{rl} & \mathbf{D}_{rr} \end{bmatrix} \begin{Bmatrix} \hat{\mathbf{q}}_l \\ \hat{\mathbf{q}}_r \end{Bmatrix} = \begin{Bmatrix} \hat{\mathbf{Q}}_l \\ \hat{\mathbf{Q}}_r \end{Bmatrix}, \tag{2.88}$$

which can be rearranged in a state-space formulation to give:

$$\underbrace{\begin{Bmatrix} \hat{\mathbf{q}}_r \\ -\hat{\mathbf{Q}}_r \end{Bmatrix}}_{\mathbf{p}_r} = \underbrace{\begin{Bmatrix} -\mathbf{D}_{lr}^{-1}\mathbf{D}_{ll} & -\mathbf{D}_{lr}^{-1} \\ \mathbf{D}_{rl} - \mathbf{D}_{rr}\mathbf{D}_{lr}^{-1}\mathbf{D}_{ll} & -\mathbf{D}_{rr}^{-1}\mathbf{D}_{lr} \end{Bmatrix}}_{\mathbf{T}} \underbrace{\begin{Bmatrix} \hat{\mathbf{q}}_l \\ \hat{\mathbf{Q}}_l \end{Bmatrix}}_{\mathbf{p}_l}, \tag{2.89}$$

where, $\mathbf{T}$ is the transfer matrix that relates the left state vector $\mathbf{p}_l$ with the right state vector $\mathbf{p}_r$ of the circular cylindrical shell. Which can be written in compact form as, for every slice ($\bar{k}$):

$$\mathbf{p}_r^{(\bar{k})} = \mathbf{T}\mathbf{p}_l^{(\bar{k})}. \tag{2.90}$$

The continuity conditions between two subsequent slices, ($\bar{k}$) and ($\bar{k}$+1), it is known that $\hat{\mathbf{p}}_r^{(\bar{k})} = \hat{\mathbf{p}}_l^{(\bar{k}+1)}$ and $\hat{\mathbf{Q}}_r^{(\bar{k})} = \hat{\mathbf{Q}}_l^{(\bar{k}+1)}$, matricially, is:

$$\underbrace{\begin{Bmatrix} \hat{\mathbf{q}}_r^{(\bar{k})} \\ -\hat{\mathbf{Q}}_r^{(\bar{k})} \end{Bmatrix}}_{\mathbf{p}_r^{(\bar{k})}} = \underbrace{\begin{Bmatrix} \hat{\mathbf{q}}_l^{(\bar{k}+1)} \\ \hat{\mathbf{Q}}_l^{(\bar{k}+1)} \end{Bmatrix}}_{\mathbf{p}_l^{(\bar{k}+1)}}, \tag{2.91}$$

and replacing Eq. (2.91) in Eq. (2.90), results in:

$$\mathbf{p}_l^{(\bar{k}+1)} = \mathbf{T}\mathbf{p}_l^{(\bar{k})}. \tag{2.92}$$

From the Bloch-Floquet Theorem (Mead, 1970), one can write the periodicity relationships between consecutive slices:

$$\begin{aligned} \mathbf{q}_l^{(\bar{k}+1)} &= e^{\mu}\mathbf{q}_l^{(\bar{k})}, \\ \mathbf{Q}_l^{(\bar{k}+1)} &= -e^{\mu}\mathbf{Q}_l^{(\bar{k})}, \end{aligned} \tag{2.93}$$

replacing Eq. (2.93) in Eq. (2.92) and rearranging, it is found

$$\mathbf{T}\begin{Bmatrix} \hat{\mathbf{q}}_l^{(\bar{k})} \\ \hat{\mathbf{Q}}_l^{(\bar{k})} \end{Bmatrix} = e^{\mu} \begin{Bmatrix} \hat{\mathbf{q}}_l^{(\bar{k})} \\ \hat{\mathbf{Q}}_l^{(\bar{k})} \end{Bmatrix}. \tag{2.94}$$

For wave propagation in an infinite periodic system, Floquet-Bloch's theorem produces

an eigenvalue problem given by

$$\mathbf{T}\mathbf{p}_l = e^{\mu}\mathbf{p}_l, \tag{2.95}$$

where, e^{μ} is the eigenvalue, $\mathbf{p}_l$ is the eigenvector, $\mu = -ikd$ is the attenuation constant, where d is the unit-cell length, k is the wavenumber and i is the imaginary unit. This solution provides the wavenumbers and corresponding wave modes propagating inside the structure.

3 CYLINDRICAL SHELL SIMULATED RESULTS

In this chapter, the numerical results obtained with the computational implementation of the cylindrical shell model shown in Section 2.1 are evaluated. The computational implementation of the in vacuo closed circular Cylindrical Shell Spectral Element - CSSE is verified using some numerical examples. In addition, WSE is used to evaluate the dynamic behavior of the cylindrical shell phononic crystal. Simulated results are presented in the frequency domain as dispersion diagrams and displacement responses and displacement interpolated over the entire cylindrical shell .

3.1 Spectral element verification

To verify the implementation of the SE method, an in vacuo circular cylindrical shell is evaluated. First, the natural frequencies analysis using the SE method, implemented in MATLAB code. Then, forced response for the cylindrical shell with a single point and two opposite point excitation are evaluated. A comparison between the two types of loads is performed. Finally, an interpolation is performed between the edges of the CSSE, thus obtaining the Operating Deflection Shapes (ODS) throughout the structure. These results are compared with those calculated by the FE method with the commercial software ANSYS.

3.1.1 Natural frequencies

In this example, a simple circular cylindrical shell of radius $a = 1.0$ m, thickness $h = 0.01$ m and length $L = 20.0$ m under Clamped-Clamped (C-C) and Free-Free (F-F) boundary conditions is calculated using the proposed SE element model and verified by the FE model. The natural frequencies are calculated over a frequency band of $DC - 50.0$ Hz. It is included a structural damping as a complex Young's modulus, $E_c = E(1 + i\eta)$. Table 3.1 shows the material properties used.

Table 3.1: Cylindrical Shell Material Properties.

Material Properties	Value
Young's modulus (E)	210 GPa
Density (ρ_S)	7850 kg/m^3
Poisson's ratio (ν)	0.30
Loss factor (η)	0.005

Since the dynamic stiffness matrix K_{Sm} (from Eq. (2.46)) is a transcendent matrix the natural frequencies are obtained from the peaks of its inverse given by κ_m = 1/log(|K_{Sm}|) are sought (Kolarević *et al.* (2016)).

Figure 3.1 shows the plots of κ_m versus frequency with m = 1,...,5, for cases F-F and C-C.

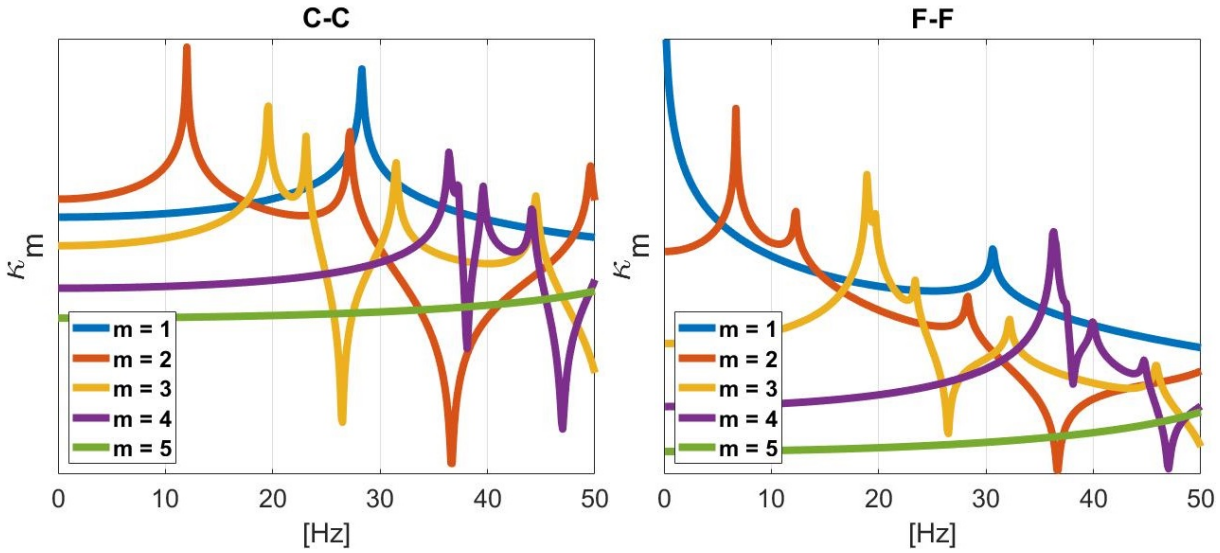

(*a*) C-C (*b*) F-F

Figure 3.1: Plot κ_m versus frequency using in vacuo CSSE model with m = 1,...,5, under CC and FF boundary conditions.

Each peak in the Figure 3.1 indicates a natural frequency and is associated with a mode shape (m,n), where m and n are integer number that indicate the number of half waves in the radial and longitudinal directions, respectively. For example, in the Figure 3.1*(a)*, the C-C case is shown where the first natural frequency appears at the value of 12.03 Hz and is associated with mode m = 2, thus this mode of vibration is called (m, n) = (2,1). The natural frequencies related to m = 5 do not appear in this frequency range. The results for the F-F case (Fig. 3.1*(b)*) are similar to the C-C case.

These results of the CSSE are compared with those calculated by the FE method in the commercial software ANSYS, using element type SHELL63 (6 DOFs/node) which is discretized with 12,400 elements and 12,462 nodes. Meanwhile, the proposed CSSE model is discretized with 2 elements and 3 edges. Figure 3.2 shows the cylindrical shell meshed by FE and SE methods.

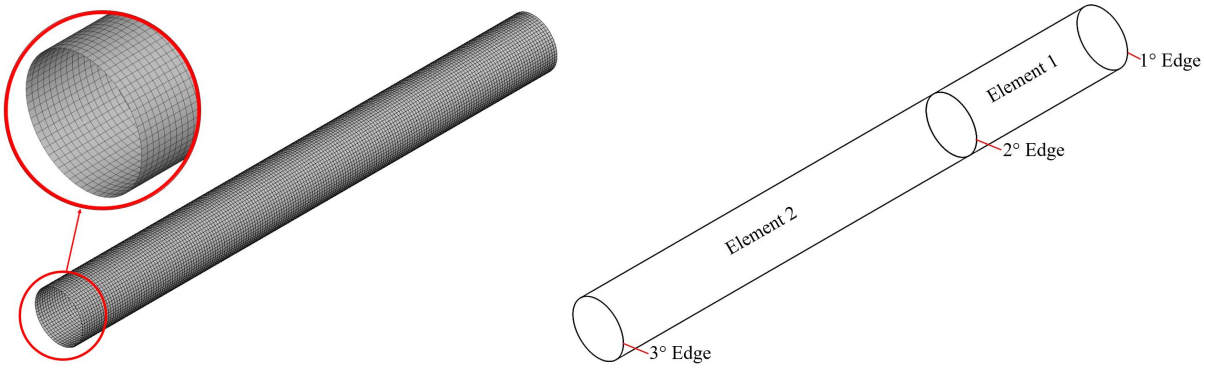

(*a*) FE Mesh (*b*) SE Mesh

Figure 3.2: In vacuo cylindrical shell example meshed by: (a) FE method with a mesh detail zoom and (b) SE method.

The FE modal analyses are performed using C-C and F-F boundary conditions. The results are shown in Table 3.2 and 3.3, including the mode number, natural frequencies calculated by FE and SE and percent error between SE and FE. It can be seen that for both boundary conditions, the natural frequency relative errors between FE and SE are very small, with the highest value of 0.11 % for C-C and 0.73 % for F-F. Of course, these values are dependent on the FE model discretization, and errors even lower can be reached by using finer meshing.

Table 3.2: Natural Frequency of a Clamped-Clamped cylindrical shell

n	***m* = 1**			***m* = 2**			***m* = 3**			***m* = 4**		
	FE [Hz]	SE [Hz]	Error [%]	FE [Hz]	SE [Hz]	Error [%]	FE [Hz]	SE [Hz]	Error [%]	FE [Hz]	SE [Hz]	Error [%]
1	28.27	28.30	0.11	11.99	12.00	0.08	19.57	19.56	0.05	36.44	36.42	0.05
2	-	-	-	27.14	27.16	0.07	23.09	23.09	0.00	37.29	37.25	0.11
3	-	-	-	49.57	49.59	0.04	31.46	31.47	0.03	39.59	39.59	0.00
4	-	-	-	-	-	-	44.48	44.49	0.02	44.14	44.14	0.00

Table 3.3: Natural Frequency of a Free-Free cylindrical shell

n	***m* = 1**			***m* = 2**			***m* = 3**			***m* = 4**		
	FE [Hz]	SE [Hz]	Error [%]	FE [Hz]	SE [Hz]	Error [%]	FE [Hz]	SE [Hz]	Error [%]	FE [Hz]	SE [Hz]	Error [%]
0	-	-	-	6.69	6.69	0.00	18.91	18.91	0.00	36.26	36.26	0.00
1	30.64	30.62	0.07	12.25	12.26	0.00	19.69	19.67	0.10	37.51	37.40	0.29
2	-	-	-	28.24	28.26	0.07	23.40	23,40	0.00	39.65	39.94	0.73
3	-	-	-	-	-	-	32.16	32.17	0.03	44.73	44.71	0.04
4	-	-	-	-	-	-	45.83	45.85	0.04	-	-	-

3.1.2 Dynamic responses to a single point excitation force

Forced responses for the in vacuo cylindrical shell modeled by SE are performed and the results are compared with those obtained by the FE model. A C-C homogeneous cylindrical shell with same material property as in the former case (Table 3.1), but with geometry, $L = 14$ m, $h = 0.005$ m, $a = 0.5$ m.

The FE model is calcualted by ANSYS, meshed using SHELL63 element type (6 DOFs/node) with 47,161 elements and 47,059 nodes. As compared with the example of Section 3.1.1, the mesh is refined to minimize the difference between FE and SE results. Figure 3.3*(a)* shows the cylindrical shell FE mesh with the excitation and response points. Figure 3.3*(b)* shows the CSSE mesh with 4 elements and 5 edges.

One radial point force of magnitude $F = 100$ N is applied at point A, which is located 4.2 m from the right-end of the cylindrical shell. The total displacements are obtained at points A, B and C, which are located from the right-end of the shell at $4.2, 7.0$ and 12.6 m, respectively.

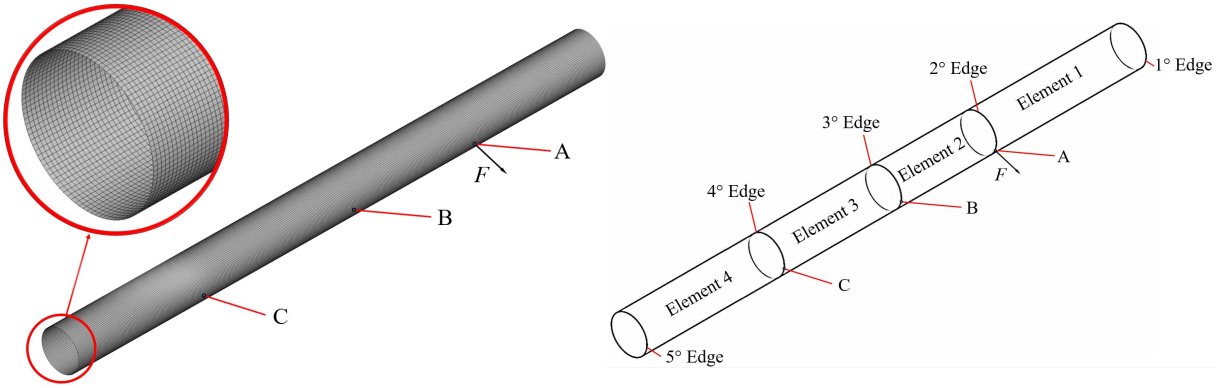

(*a*) FE Mesh

(*b*) SE Mesh

Figure 3.3: In vacuo cylindrical shell FE and SE mesh including the one-point loading (point A) and response (points A, B and C).

Figure 3.4 shows the displacement responses at points A, B and C for a frequency range from 0 up to 100 Hz. For all the response points, it can be seen good agreement between the total displacement curves calculated by SE and FE.

In terms of CPU time, the SE method (MATLAB) takes around 350 s and the FE method (ANSYS) 14,400 s to compute the forced responses of the cylindrical shell. This yields CPU time savings around 97.6 % regarding FE solution. The results made to evidence the relevance of the proposed method in terms of accuracy and CPU time saving. Highlight, neither method is optimized to maximize performance. Simulations were made using a processor Intel Core^{TM} i7-6700.

3.1.3 Dynamic responses to two opposite point excitation forces

Forced response for the cylindrical shell with two opposite point excitation forces is evaluated using the same C-C boundary conditions, geometry and material properties as the example of Section 3.1.2. The comparison is made between the results obtained by the FE and SE. Two radial point forces of magnitude $F = 100$ N in opposite directions are applied at point A, which is located 4.2 m from the right-end of the shell. The total displacements are obtained at points A, B and C, which are located from the right-end of the shell at $4.2, 7.0$ and 12.6 m, respectively. The FE model is meshed using SHELL63 element type (6 DOFs/node) with 47,161 elements and 47,059 nodes. The SE mesh using with 4 elements and 5 edges. Figure 3.5 shows the cylindrical shell FE and SE with the excitation and response points.

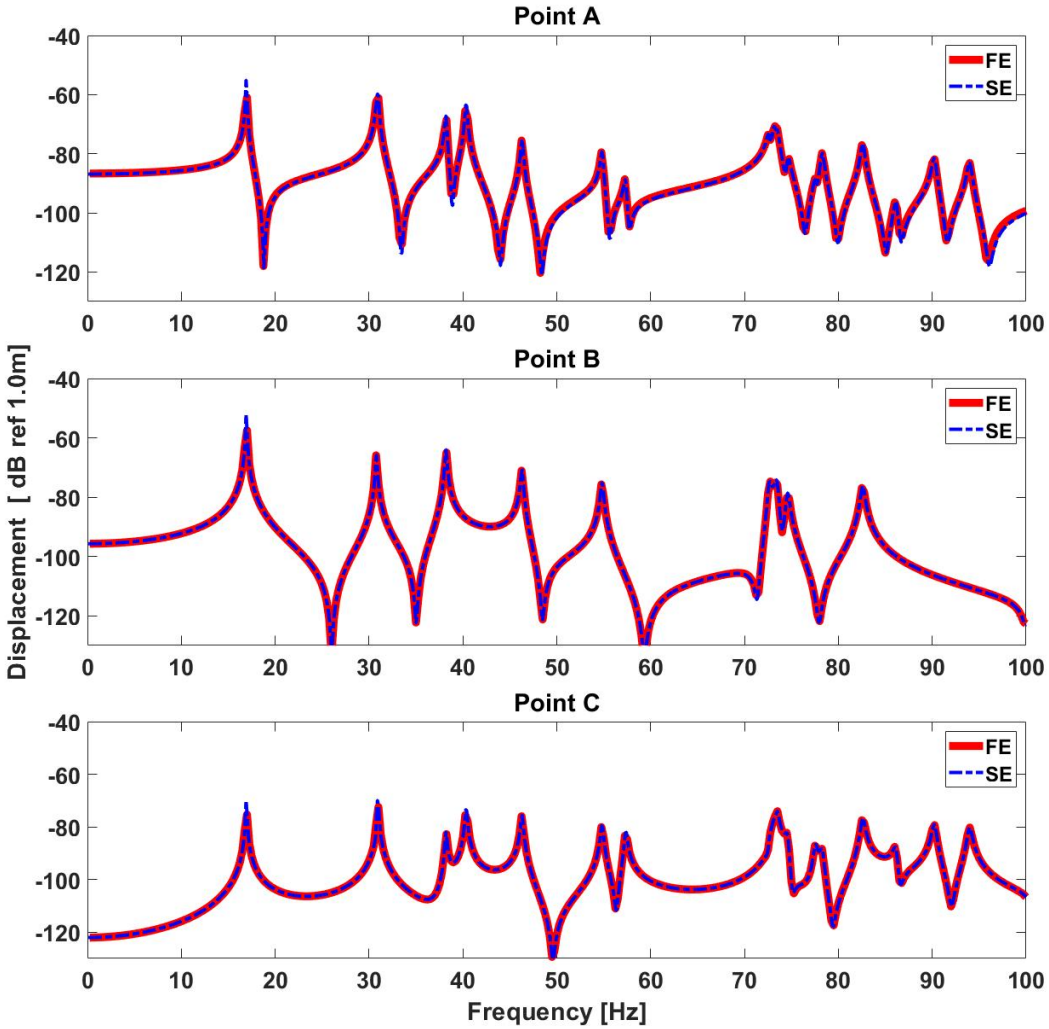

Figure 3.4: Forced responses of an cylindrical shell by FE and SE with excitation force at point A and total displacement responses at points A, B and C.

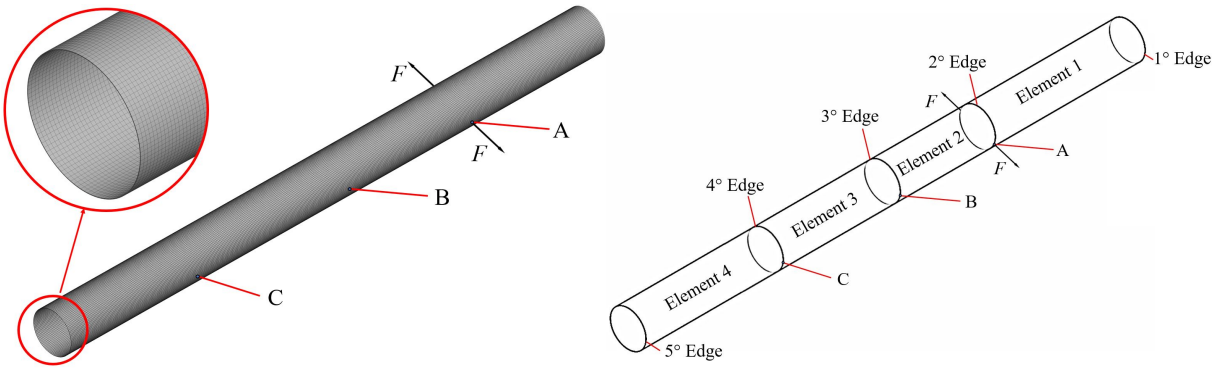

(*a*) FE Mesh

(*b*) SE Mesh

Figure 3.5: In vacuo cylindrical shell FE and SE mesh including the two opposite point forces (point A) and response (points A, B and C).

Due to the DOFs of CSSE are distributed along the element edges, the forced response is not possible to obtain straight away for all types of excitation. Therefore, for the two opposite

point excitation forces the superposition approach must be used. In order to obtain it, first the response for one force is calculated, next the response for the other force is calculated, and both responses are added to obtain the two excitation forces response. This approach allows any amount of point excitation to be evaluated with the cylindrical shell model presented in this thesis.

Figure 3.6 shows the displacement responses at points A, B and C for a frequency range from 0 up to 100 Hz. For all the response points, it can be seen good agreement between the total displacement curves calculated by SE and FE, thus validating the CSSE model proposed in this thesis. In terms of CPU time, the SE method (MATLAB) takes around 392 s and the FE method (ANSYS) 14,400 s to compute the forced responses of the cylindrical shell. This yields CPU time savings around 97.3 % regarding FE solution. The results made to highlight the relevance of the proposed method in terms of accuracy and CPU time saving. Simulations were made using a processor Intel Core^{TM} i7-6700.

!htb

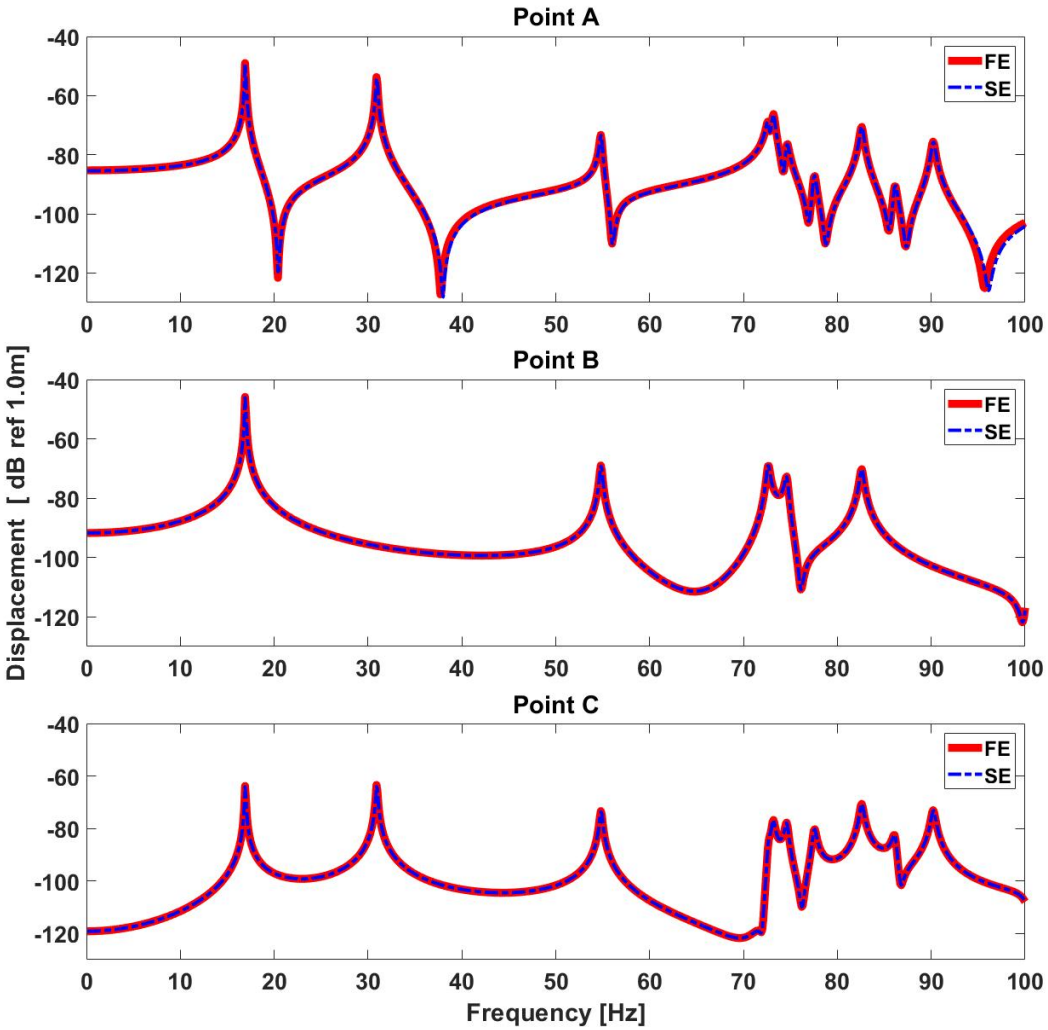

Figure 3.6: Forced responses of an in vacuo cylindrical shell by FE and SE an with excitation Two-point loading at A and total displacement responses at points A, B and C.

3.1.4 Single and two point excitation force comparison

Figure 3.7 shows the forced response of CSSE for with a single and two opposite point excitation forces.

For all displacement responses (points A, B and C) it can be seen that there are more resonance peaks with single than the two point excitation.

These behaviors can be explained by observing that two point excitation works as a filter that does not stimulate the cylindrical shell for odd vibrating modes (m = 1 and 3), therefore, only the even vibration modes have their natural frequencies stimulated in this type of loads.

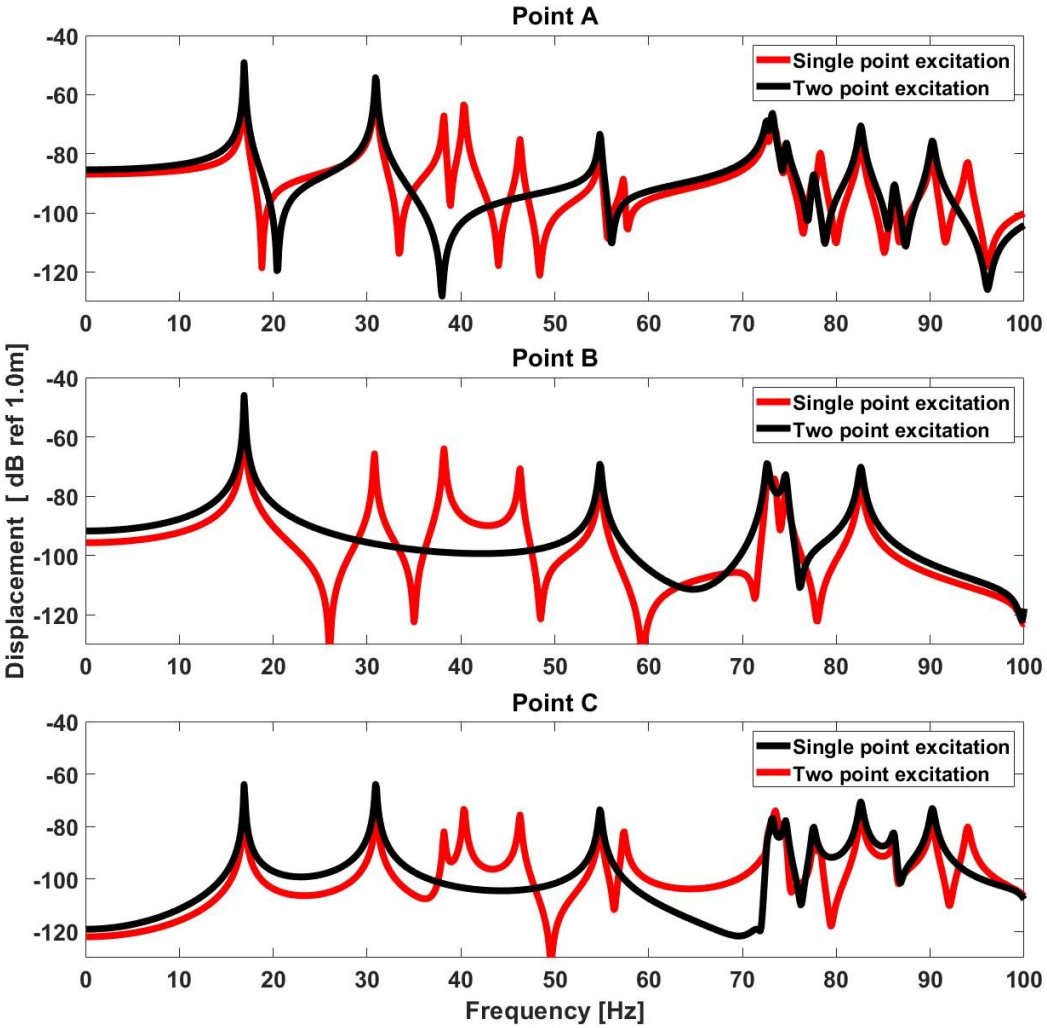

Figure 3.7: Forced responses of an in vacuo cylindrical shell by SE with One-point and Two-point loading at point A and total displacement responses at points A, B and C.

The strategy of applying two radial forces is an interesting tool since the cylindrical shell is a structure with many wave propagation modes. Thus, later in this work, when the band gap phenomenon will be studied, filtering some propagation modes will be relevant for the observation of the phenomenon of vibration attenuation.

3.1.5 CSSE interpolated results

In order to obtain the displacement results along the whole structure, an interpolation between de edges of CSSE must be performed. By taken the displacement results calculated in the edges, and substituting them in the Eq. (2.21), the integration constants $A_{i,m}$, $B_{i,m}$, and $C_{i,m}$ are found. Thus, the spectral amplitude of displacement components $\hat{u}(x,\varphi)$, $\hat{v}(x,\varphi)$, and $\hat{w}(x,\varphi)$ can be calculated for any special position in the cylindrical shell between the edges.

To evaluate the interpolated results cylindrical shell of the Section 3.1.3, case excitation and response at point A, is used to calculate by FE and SE, the interpolated displacements at the angle φ = 0°, along the entire length of the structure ($L = 14$ m) (Fig. 3.8) with a discretization of $\Delta x = 0.1$ m.

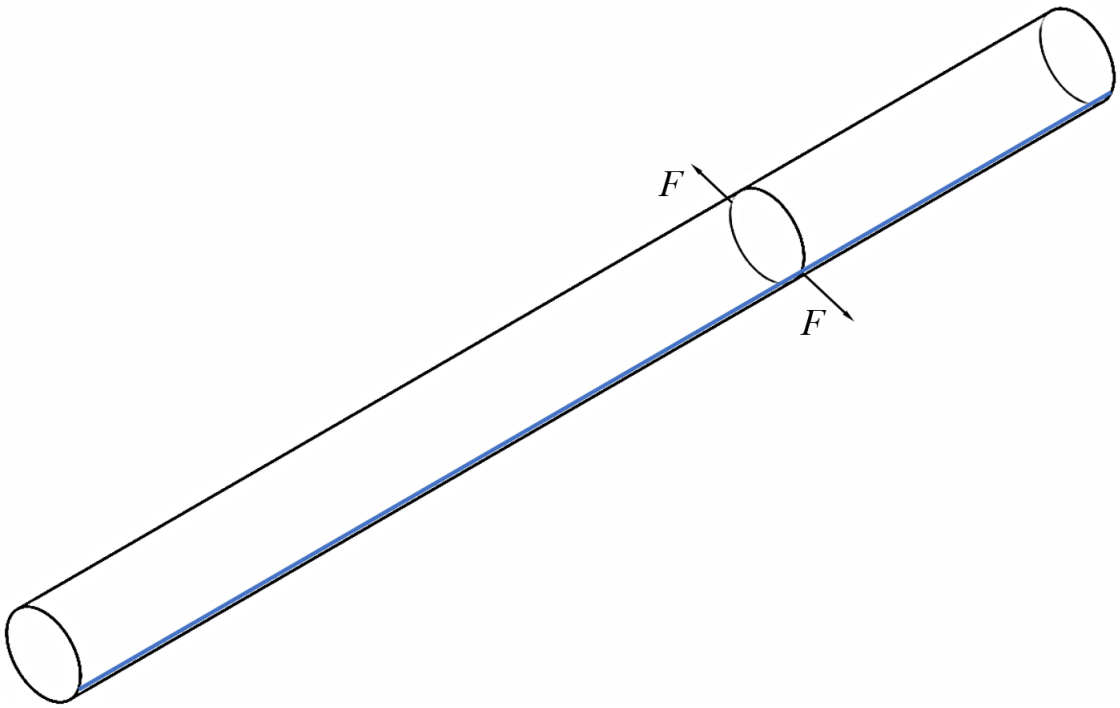

Figure 3.8: Spatial position of the interpolation line (blue line) in the cylindrical shell model.

Figures 3.9 to 3.14 show the interpolated dimensionless displacement amplitude versus cylindrical shell length, for several frequency values with F-F and C-C boundary condition. For all results, a good agreement between FE and SE methods are observed.

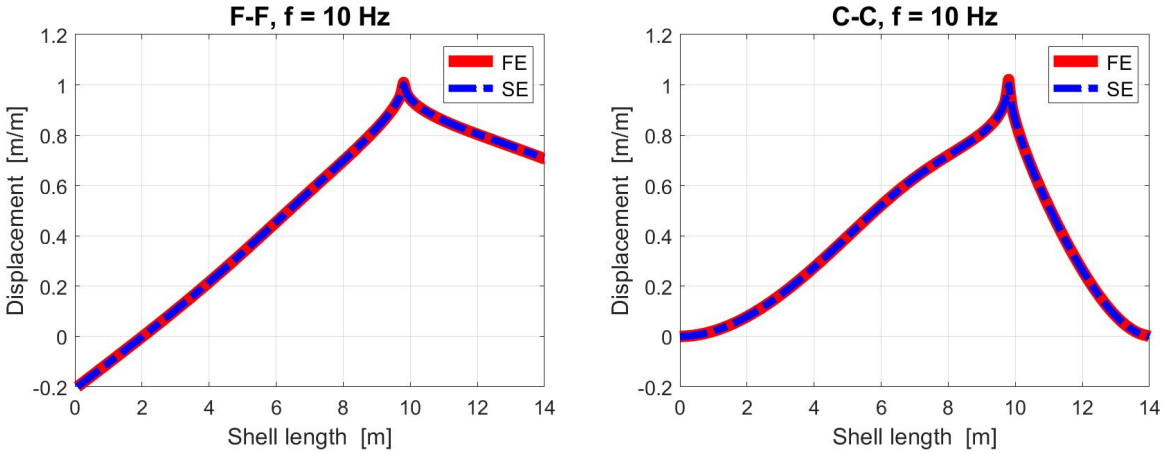

Figure 3.9: Cylindrical shell interpolated dimensionless displacement amplitude at f = 10 Hz with F-F and C-C boundary conditions.

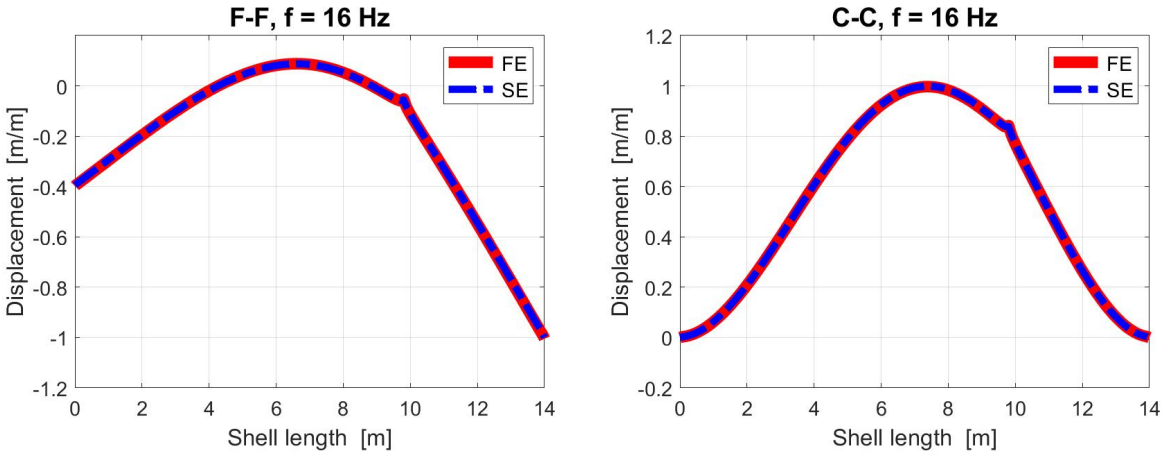

Figure 3.10: Cylindrical shell interpolated dimensionless displacement amplitude at f = 16 Hz with F-F and C-C boundary conditions.

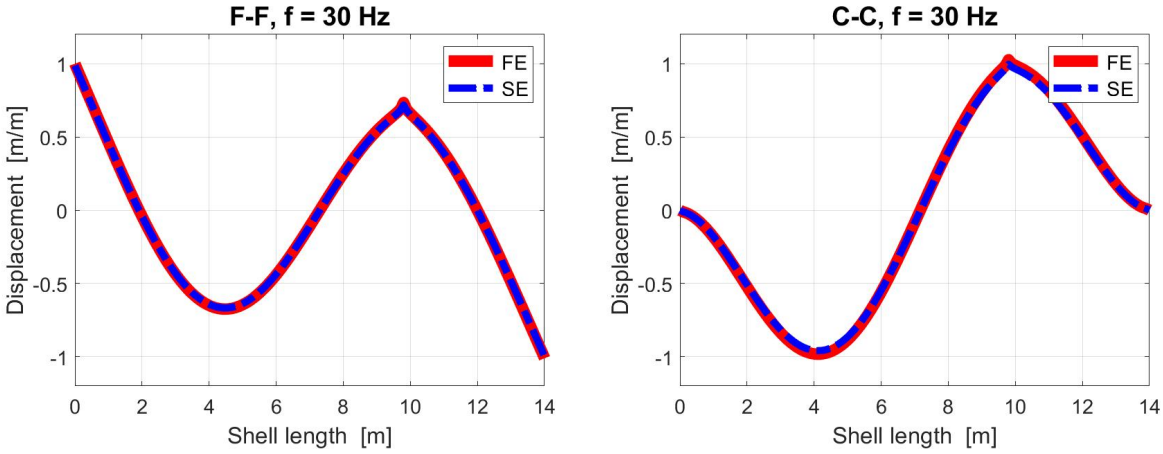

Figure 3.11: Cylindrical shell interpolated dimensionless displacement amplitude at f = 30 Hz with F-F and C-C boundary conditions.

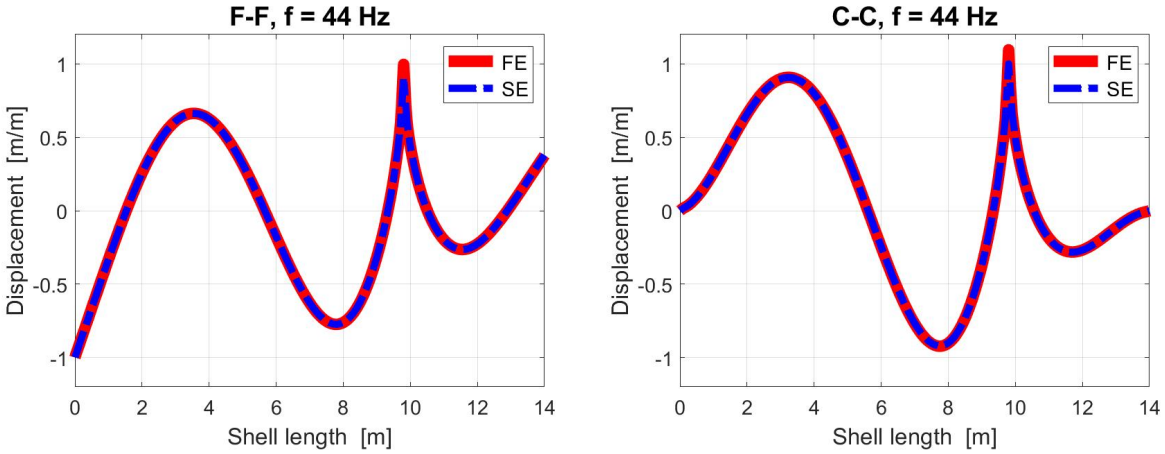

Figure 3.12: Cylindrical shell interpolated dimensionless displacement amplitude at f = 44 Hz with F-F and C-C boundary conditions.

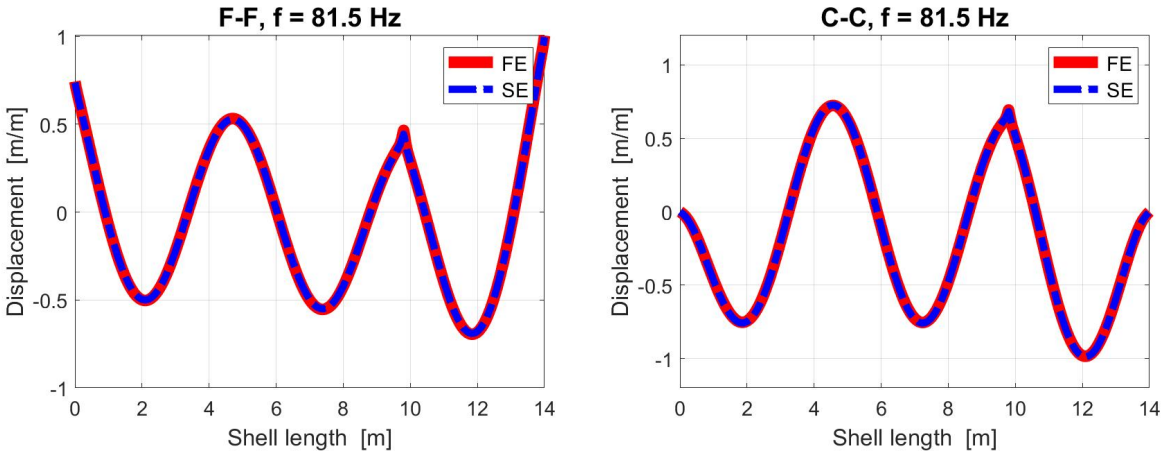

Figure 3.13: Cylindrical shell interpolated dimensionless displacement amplitude at f = 81.5 Hz with F-F and C-C boundary conditions.

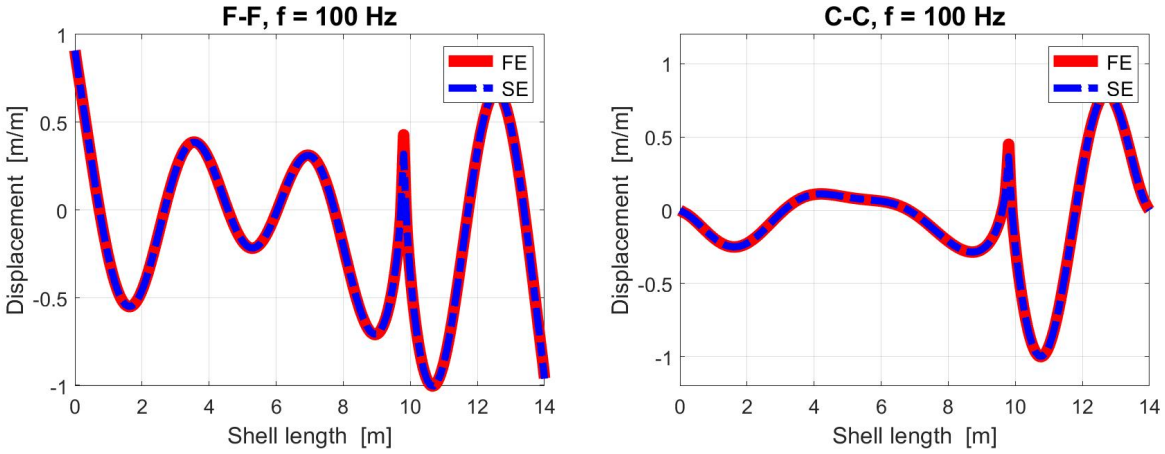

Figure 3.14: Cylindrical shell interpolated dimensionless displacement amplitude at f = 100 Hz with F-F and C-C boundary conditions.

In order to obtain the Operating Deflection Shapes (ODS) for the cylindrical shell, the procedure applied for one line ($L = 14$ m at $\varphi = 0°$ with $\Delta x = 0.1$ m discretization at x direction) is extended to several lines around the cylindrical shell circle (with discretization $\Delta x = 0.1$ m at x direction and $\Delta\varphi = \pi/20$ at the circle direction).

Figures 3.15 to 3.18 show the cylindrical shell ODS's with C-C boundary conditions calculated by FE and SE method at the frequencies f = 30, 44, 85.1 and 100 Hz. It can be emphasized the zero displacement at the structure ends due to the C-C boundary conditions.

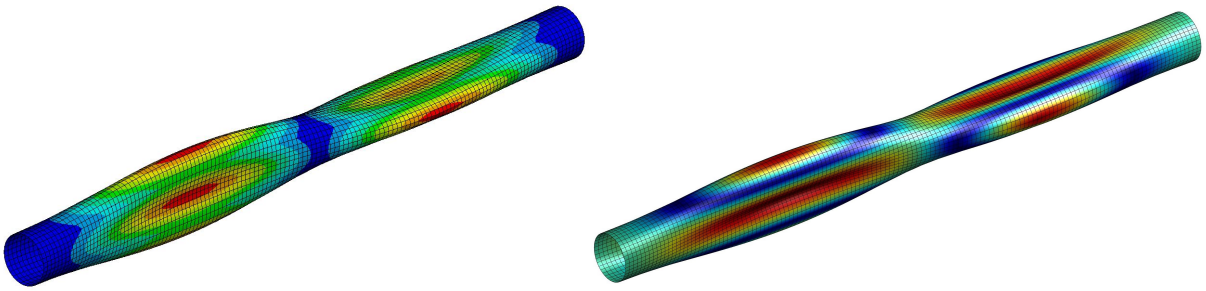

(*a*) FE model (*b*) SE model

Figure 3.15: Cylindrical shell ODS at frequency 30 Hz with C-C boundary conditions.

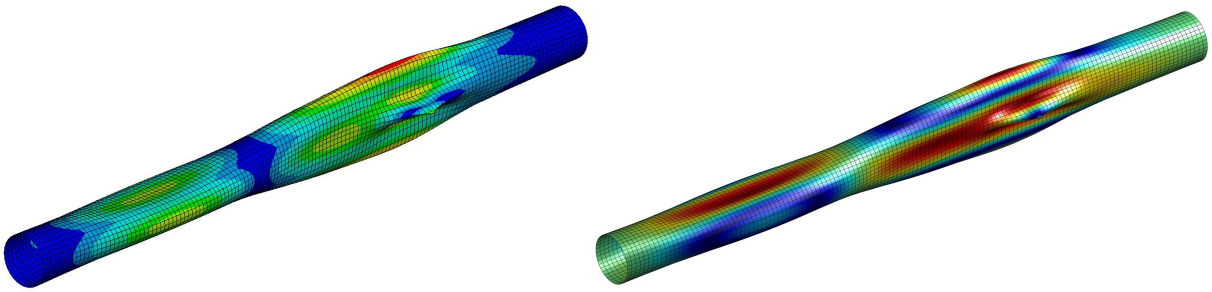

(*a*) FE model (*b*) SE model

Figure 3.16: Cylindrical shell ODS at frequency 44 Hz with C-C boundary conditions.

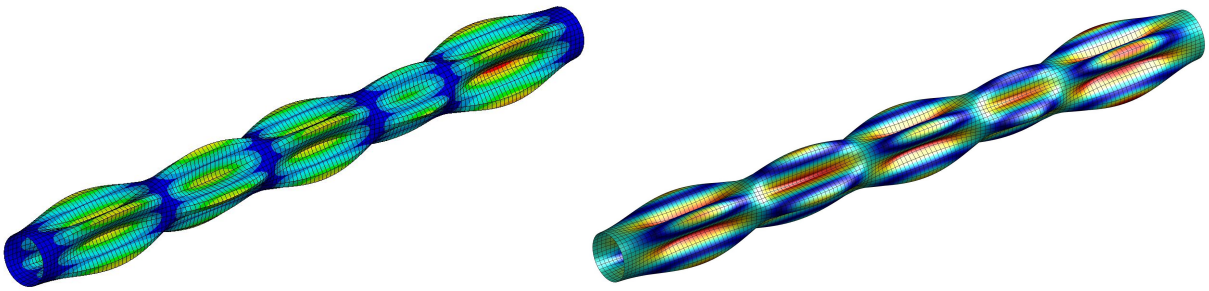

(*a*) FE model (*b*) SE model

Figure 3.17: Cylindrical shell ODS at frequency 81.5 Hz with C-C boundary conditions.

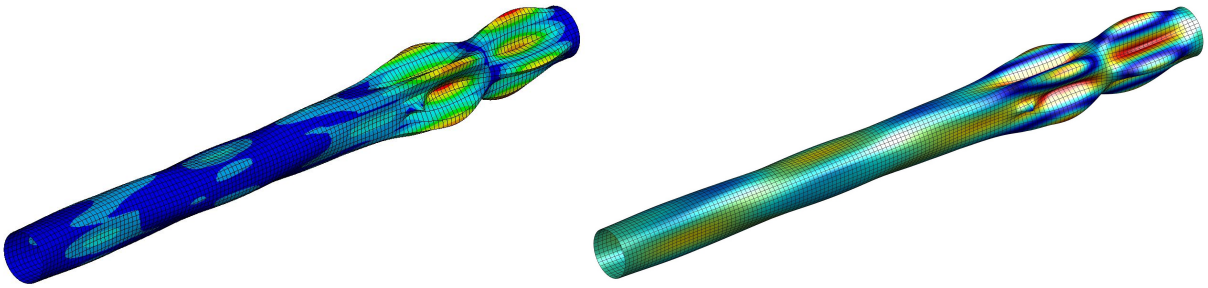

(*a*) FE model (*b*) SE model

Figure 3.18: Cylindrical shell ODS at frequency 100 Hz with C-C boundary conditions.

Figures 3.19 to 3.22 show the cylindrical shell ODS's with F-F boundary conditions calculated by FE and SE method at the frequencies f = 30, 44, 85.1 and 100 Hz. However, for this case, due the F-F boundary conditions, displacements at the structure ends are noticed.

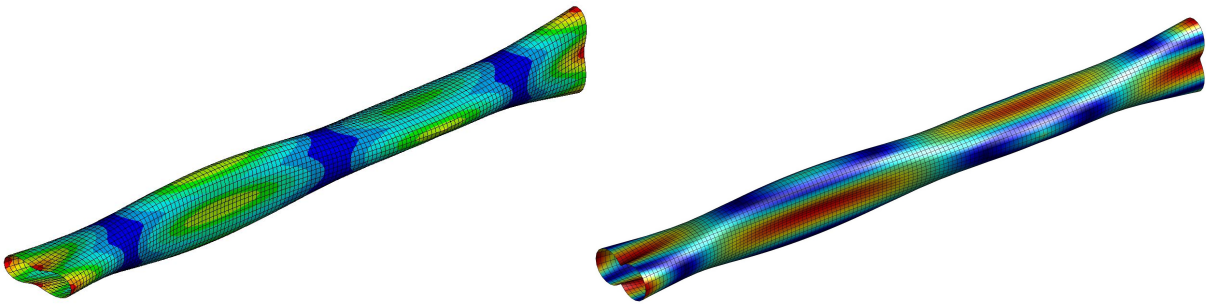

(*a*) FE model (*b*) SE model

Figure 3.19: Cylindrical shell ODS at frequency 30 Hz with F-F boundary conditions.

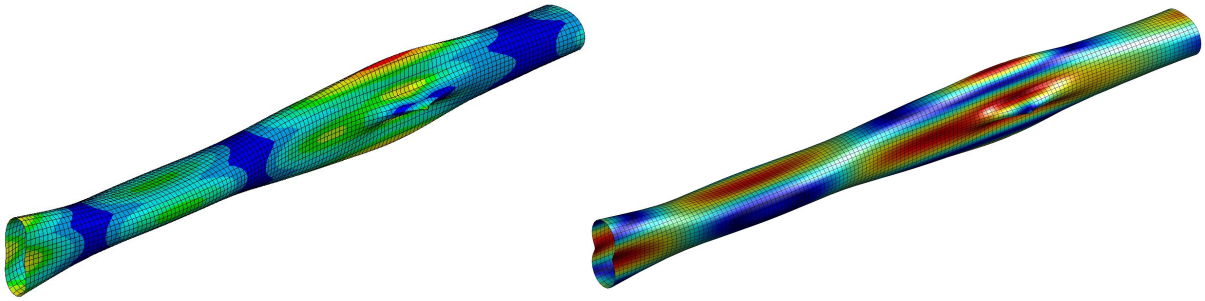

(*a*) FE model (*b*) SE model

Figure 3.20: Cylindrical shell ODS at frequency 44 Hz with F-F boundary conditions.

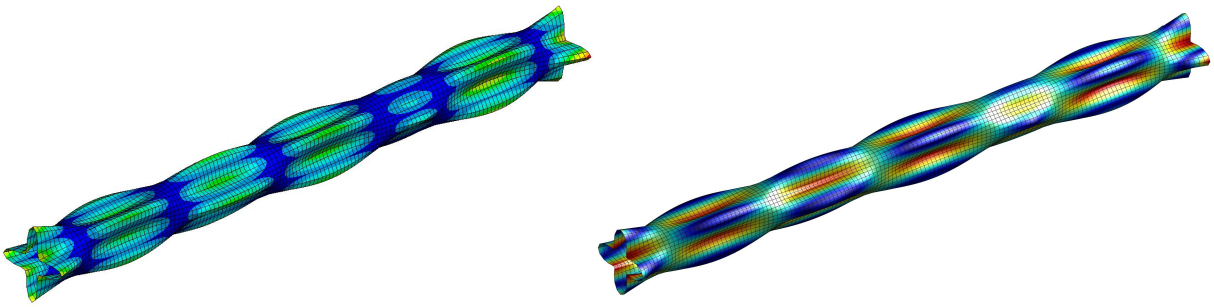

(*a*) FE model (*b*) SE model

Figure 3.21: Cylindrical shell ODS at frequency 81.5 Hz with F-F boundary conditions.

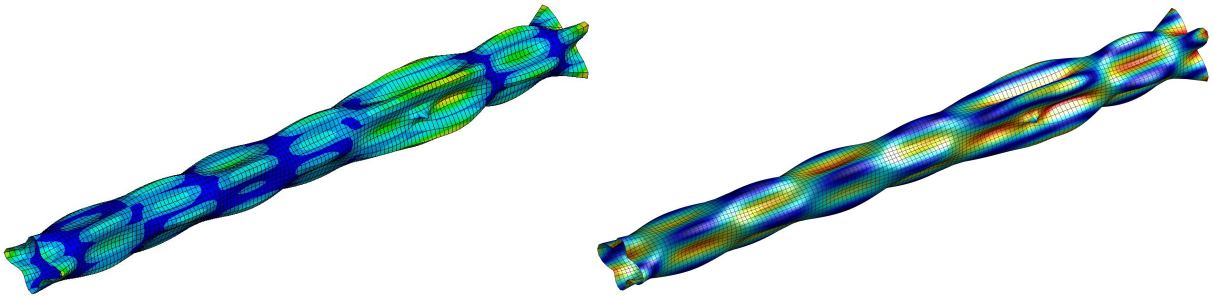

(*a*) FE model (*b*) SE model

Figure 3.22: Cylindrical shell ODS at frequency 100 Hz with F-F boundary conditions.

3.2 Wave Spectral Element verification

An evaluation of the Wave Spectral Element-WSE method is made for a periodic structure using a slice of length $d = 0.2$ m of an in vacuo homogeneous circular cylindrical shell, with the same geometry and material properties as in the section 3.1.1. Dispersion diagrams are calculated and compared with those obtained by Analytical Solution (AS) as reported by Fuller and Fahy (1982). The dispersion curves for the cylindrical shell are obtained from de Equation (2.95) by plotting a set of functions $k(\Omega)$, where $\Omega = \omega a/c_S$ is the non-dimensional frequency.

Figure 3.23 shows the dispersion diagrams calculated by WSE and AS for $m = 0, \ldots, 3$ harmonic modes, each including four wave propagation mode branches ($b = 1, \ldots, 4$). At low frequency, both diagrams present the branch $b = 1$, which are purely real wavenumbers and correspond to a beam type shell motion or the longitudinal elastic mode.

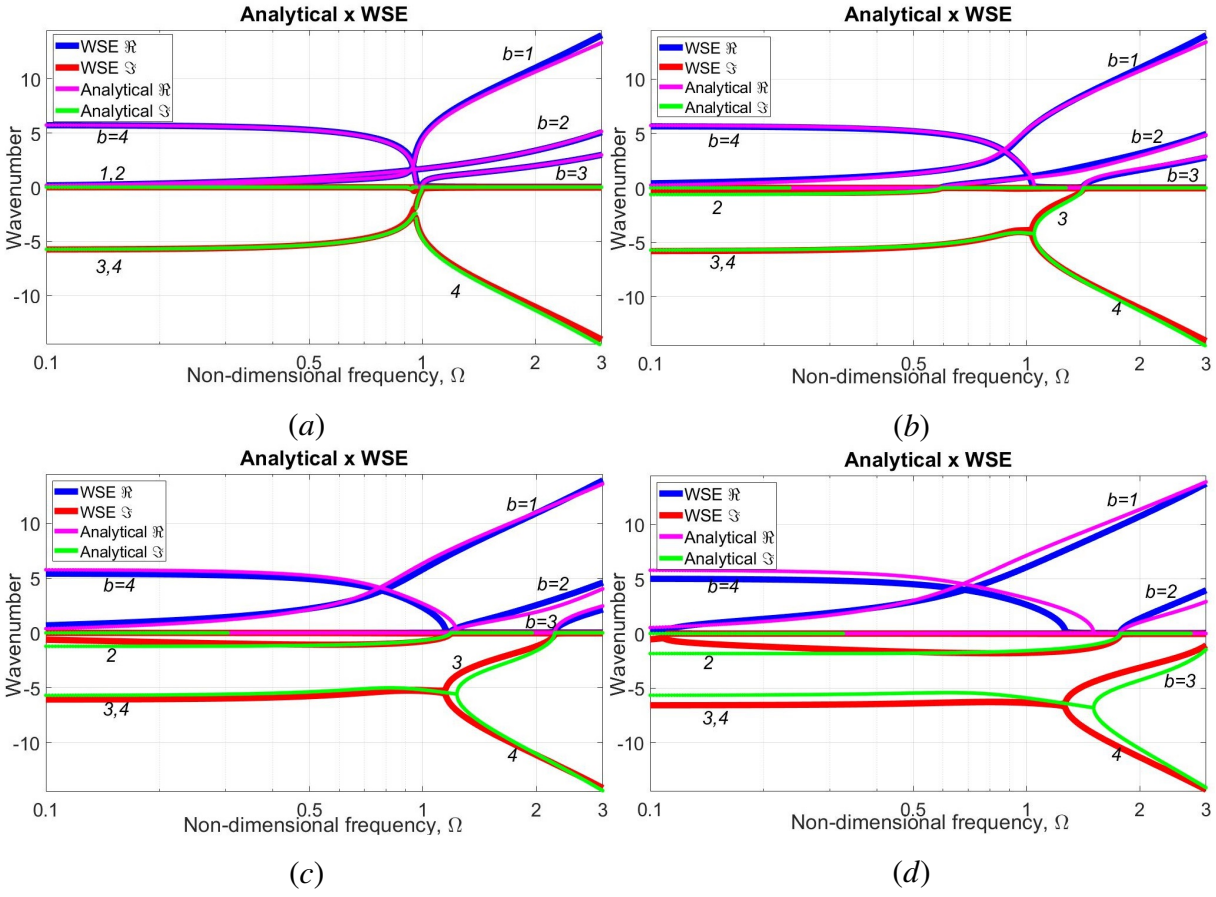

Figure 3.23: Dispersion diagram calculated by AS and WSE methods for the harmonic modes: (*a*) $m = 0$; (*b*) $m = 1$; (*c*) $m = 2$ and (*d*) $m = 3$.

The branch $b = 2$ corresponds to the ring elastic mode, for $m = 0$ (Figure 3.23*a*) the branch is purely real, for the other cases, $m = 1$, 2 and 3, it presents cut on frequencies $\Omega_2 \approx 0.6$ (Figure 3.23*b*) and $\Omega_2 \approx 1.4$ (Figure 3.23*c*) and $\Omega_2 \approx 1.8$ (Figure 3.23*d*).

The branch $b = 3$ is predominantly a torsional shell motion. At low frequency it is a non-propagating mode (k is pure imaginary) with cut on frequencies,$\Omega_3 \approx 1.0$ (Figure 3.23*a*) and $\Omega_3 \approx 1.3$ (Figure 3.23*b*) and $\Omega_3 \approx 2.2$ (Figure 3.23*c*) and $\Omega_3 \approx 3.2$ (Figure 3.23*d*), and after these the waves become propagating (k is pure real).

Finally, at low frequencies the branch $b = 4$ presents complex wavenumbers where real and imaginary parts have the same absolute magnitude until before the cut on frequencies $\Omega_4 \approx 1.0$ (Figure 3.23*a*) and $\Omega_4 \approx 1.1$ (Figure 3.23*b*). $\Omega_4 \approx 1.2$ (Figure 3.23*c*) and $\Omega_4 \approx 1.3$ (Figure 3.23*d*). After these, the real part goes to zero and the imaginary part decreases as the frequency increases. Complex wave modes occur in combinations of $\pm(\Re \pm i\Im)$, and the pair that represents wave motion in the shell axial direction produces an attenuated standing wave. Then, the complex branches would represent evanescent motion.

Relate to the methods (WSE and AS), a very good agreement between both at low frequency bands can be seen, but as the frequency bands increase they start to become discordant. This comes from differences in the shell models, where the WSE cylindrical shell model is based on Flügge's shell theory, while the AS model is formulated using the Donnell-Musthari model.

3.3 Phononic crystal example

An example of an in vacuo closed circular cylindrical shell phononic crystal (PC) is evaluated (Fig. 3.24). The WSE is applied to calculate the dispersion diagrams and the SE is used to obtain the forced responses. The unit-cell is made with three layers of two elastic materials combined as: steel(20%)-polyacetal(60%)-steel(20%). Table 3.4 shows the PC material properties and geometric parameters.

Table 3.4: Phononic Crystal Material Properties & Geometry

Property/Geometry	Steel	Polyacetal
Young's modulus (E)	193 GPa	3.3 GPa
Density (ρ_S)	8030 kg/m^3	1418 kg/m^3
Poisson's ratio (ν)	0.27	0.35
Loss factor (η)	0.001	0.001
Radius (a)	0.05 m	0.05 m
Thickness (h)	0.0025 m	0.0025 m
Unit-cell length (d)	0.01 m	0.03

The total displacement response is calculated over a frequency band of $DC - 16.0$ kHz, for a Clamped-Clamped cylindrical shell PC build up with $N = 20$ unit-cells as shown in Figure 3.24. The PC is excited by two opposite radial point forces of magnitude $F = 100$ N at point A and the displacement response is obtained at point C.

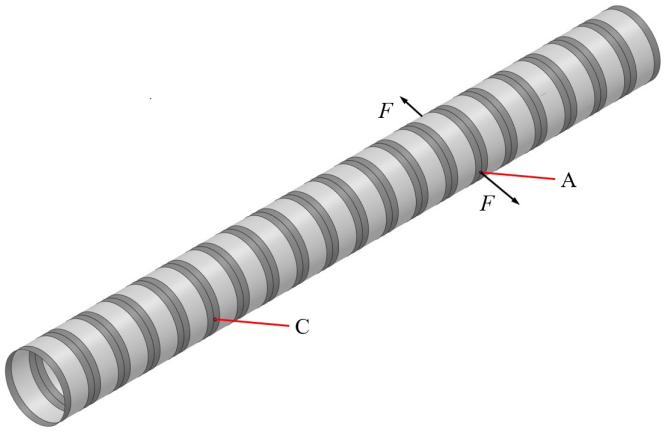

Figure 3.24: Cylindrical shell phononic crystal including $N = 20$ unit-cells, with force excitation (point A) and response (point C) positions.

The wavenumbers are calculated and the dispersion diagrams are obtained for the wave modes $m = 2, 4, 6$ and 8. The total displacement response at point C and dispersion diagrams are shown in Figure 3.25.

In the dispersion curve $k(\omega)$, band gaps are identified as a frequency bands where the real part of the wavenumber is the Bragg limit or zero ($\Re\{k\} = \pi/d = 62.83$ m^{-1} or $\Re\{k\} = 0$), and the imaginary part is different from zero ($\Im\{k\} \neq 0$). Under these conditions, the waves become evanescent (non-propagating) and a band gap is identified. Otherwise, the wave is propagating

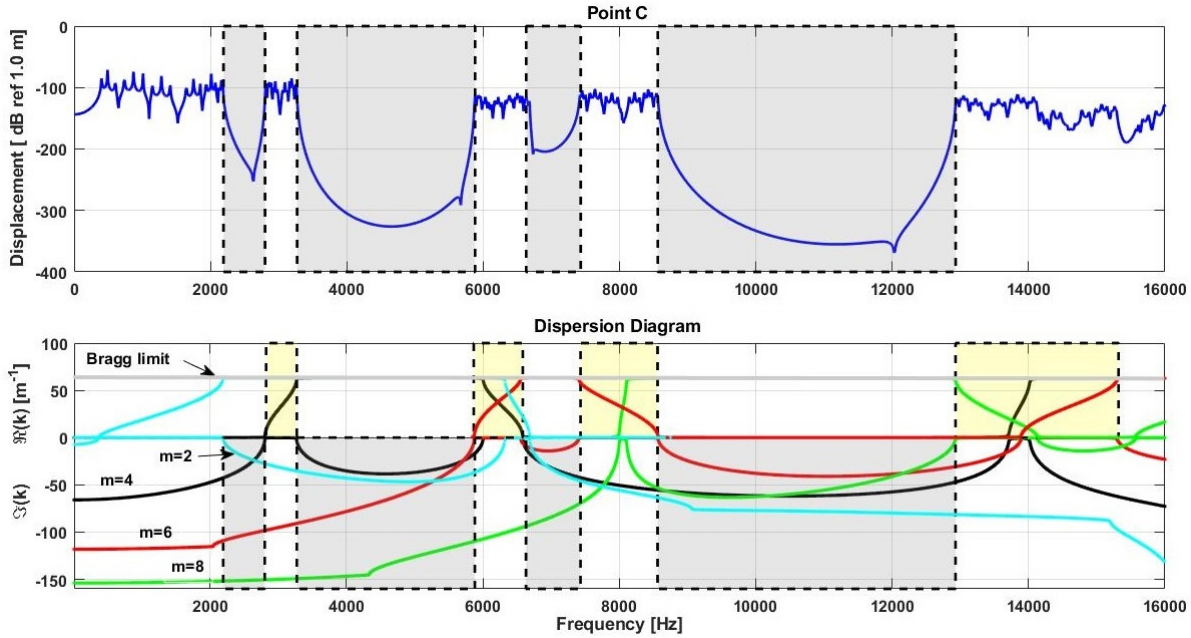

Figure 3.25: Total displacement response at point C and excitation at point A (*top*), and dispersion diagram for the wave modes m =2(■), 4(■), 6(■) and 8(■) (*bottom*), for the in vacuo cylindrical shell phononic crystal.

and a pass band is obtained. Figure 3.25 (*bottom*) shows that at least one or two complete band gaps can be easily identified for each wave modes in the analyzed frequency band. For example, the dispersion curve of mode $m = 4$ (*black* curve) two complete band gaps 3.2-6.0 kHz and 6.6-13.7 kHz can be identified in the analyzed frequency band. Note that the complete band gap 6.6-13.7 kHz in the dispersion curve $m = 4$ (Figs. 3.25 *bottom*), does not necessarily mean attenuation in the PC displacement response over this entire band (Figs. 3.25 *top*). Actually the attenuation occurs in the bands 6.6-7.4 kHz and 8.5-12.9 kHz (gray shaded), while very low or unnoticeable attenuation is observed in the band 7.4-8.5 kHz. Such behavior comes from the contribution of other wave modes in the analyzed frequency band. The frequency band 7.4-8.5 kHz in the displacement response (Fig. 3.25 (*top*)) corresponds to a pass band (yellow shade) in the dispersion diagram (Fig 3.25 (*bottom*)), where it can be seen that in addition to the evanescent mode ($m = 4$) there is another evanescent mode ($m = 2$), and two propagating modes ($m = 6$ and 8). The presence of propagating modes reduce the destructive interference effect (Bragg effect), and consequently reduces the PC response attenuation.

Based on the previous evaluation, gray shaded areas in the imaginary part of dispersion diagram emphasize the frequency bands (2.1-2.8 kHz; 3.2-5.9 kHz; 6.6-7.4 kHz; 8.5-12.9 kHz) that contains only evanescent waves (complete or partial band gaps), which will be named hereafter as *effective band gaps*, and correspond to the frequency bands attenuated in the PC displacement response. Otherwise, yellow shaded areas in the real part of the dispersion diagram indicate the frequency bands (2.8-3.2, 5.8-6.6, 7.4-8.5 kHz and 12.9-15.5 kHz) where evanescent and propagating waves coexist, are called pass bands, and correspond tho the frequency

bands with low or unnoticeable attenuation in the PC displacement response.

It must be noticed that for complex structures, like cylindrical shell, which may contain many propagation wave modes, the number of wave modes included in the calculation of the dispersion diagrams and forced responses is an important design parameter to predict the PC performance.

Therefore, in order to promote the understanding, the curves are presented mode by mode revealing the mechanism of band gaps formation shown in Figures 3.26 to 3.29. Thus Figure 3.26 shows dispersion curve only for the $m = 2$ mode, thus illustrating the appearance of band gaps, the first from 2.2 kHz to 6.3 kHz and the second from 6.7 kHz to over 16 kHz.

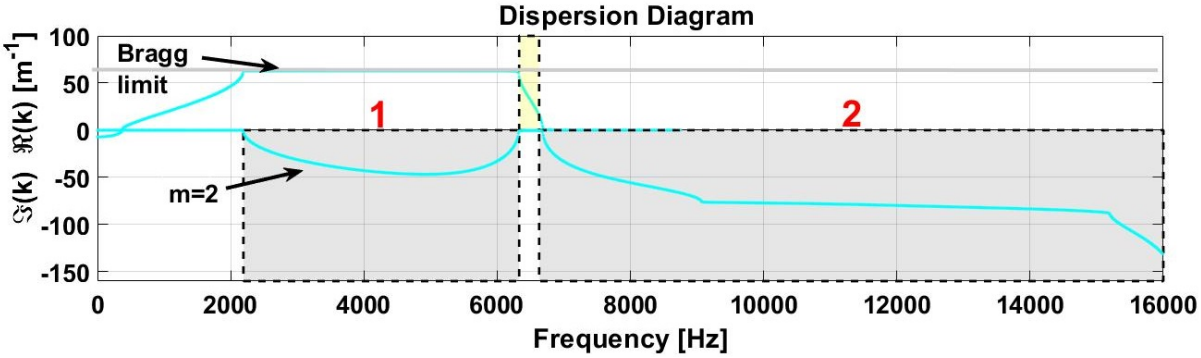

Figure 3.26: Dispersion curve only for the m =2(■) mode.

Figure 3.27 shows dispersion curves for $m = 2$ and $m = 4$. The $m = 4$ mode becomes propagating at 2.8 kHz, so the propagating part of $m = 4$ destroys the band gaps initially found, then the amount of band gaps increases to four. The first from 2.1 kHz to 2.8 kHz, the second from 3.2 kHz to 6.0 kHz, the third from 6.6 kHz to 13.7 kHz and the fourth goes from 14.0 kHz to over 16 kHz.

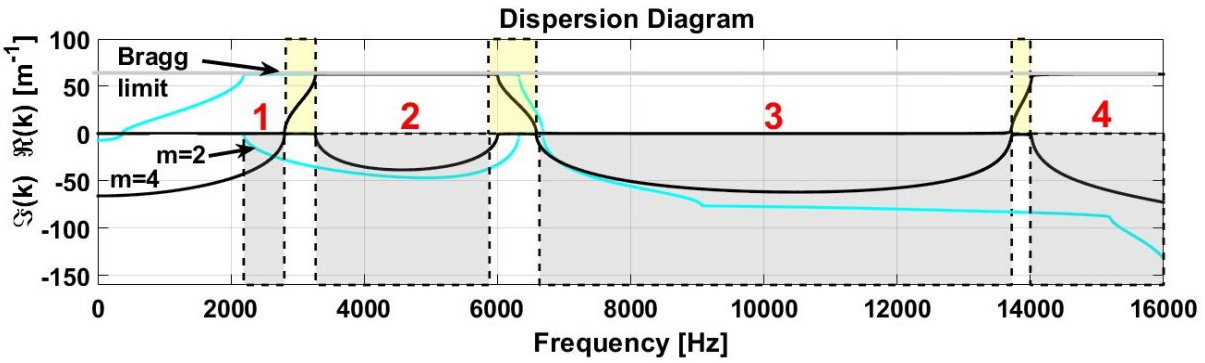

Figure 3.27: Dispersion curves for m =2(■) and 4(■) mode.

In the Figure 3.28 the $m = 6$ is added, this mode becomes propagating at 5.9 kHz and reaches the Bragg limit at 6.6 kHz, it again becomes a propagating mode at 7.4 kHz up to 8.5 kHz, splitting the existing band gap in two in this frequency range. Lastly, the $m = 6$ mode is propagated between the frequencies from 13.9 kHz to 15.3 kHz. Considering only the $m = 2$, 4 and 6 modes, five band gaps are formed. The first from 2.1 kHz to 2.8 kHz, the second from

3.2 kHz to 5.9 kHz, the third from 6.6 kHz to 7.4 kHz, the fourth from 8.5 kHz to 13.7 kHz and the fifth goes from 15.3 kHz to over 16.0 kHz.

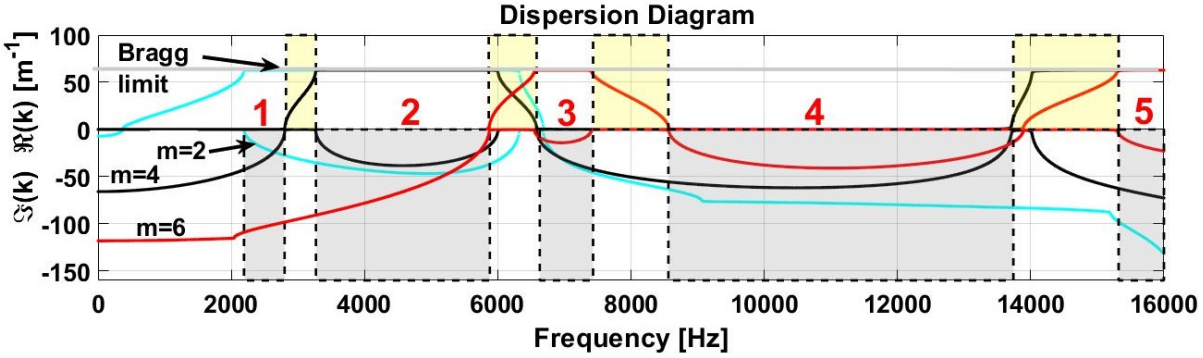

Figure 3.28: Dispersion curves for m =2(■), 4(■) and 6(■) mode.

Finally, $m = 8$ is added, Figure 3.29, this mode becomes propagating at 8.0 kHz and quickly reaches the Bragg limit in 8.1 kHz. It returns to a propagation mode at 12.9 kHz up to 14.1 kHz. The first, second and third band gaps are not affected by the mode $m = 8$ while the fourth band gap has an acting range reduced from 8.6-13.7 kHz to 8.6-12.9 kHz. After that value, neither a band gap is observed until the frequency of 16.0 kHz. Other modes of propagation appear before 16 kHz, however they do not affect the constitution of band gaps already enumerated

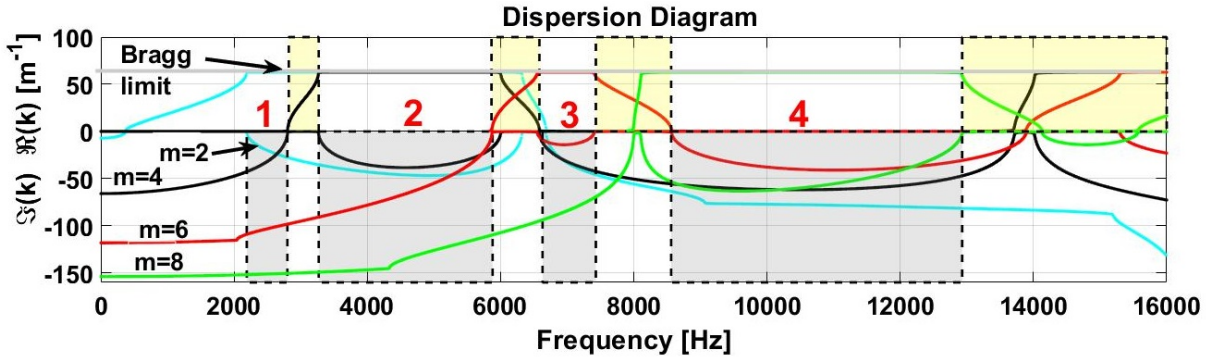

Figure 3.29: Dispersion curves for m =2(■), 4(■), 6(■) and 8(■) mode.

Figure 3.30 shows the ODS of the cylindrical shell phononic crystal studied at the frequency of 2000 Hz. At this frequency, the structure does not experience attenuation of vibration along its length.

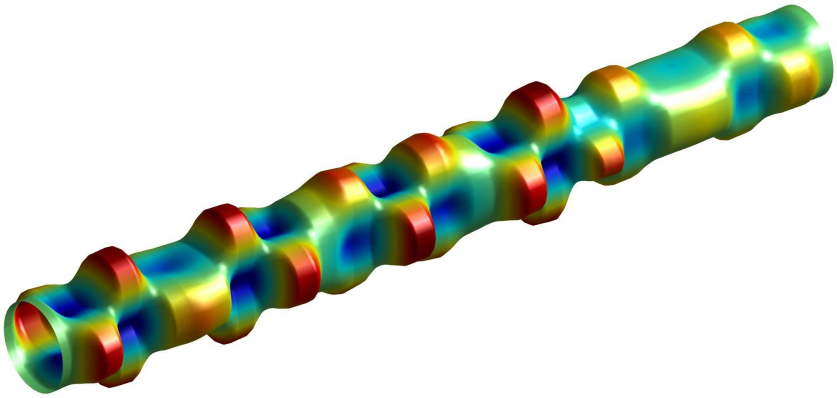

Figure 3.30: ODS of the cylindrical shell phononic crystal at the frequency 2000 Hz

Figure 3.31 shows the behavior of the cylindrical shell phononic crystal at the frequency of 2322 Hz. This frequency, the structure is found in the band gap region, but not at the deepest point of the band gap. Therefore, there is a clear attenuation of the vibration structure as it is observed points further away from the loading application places.

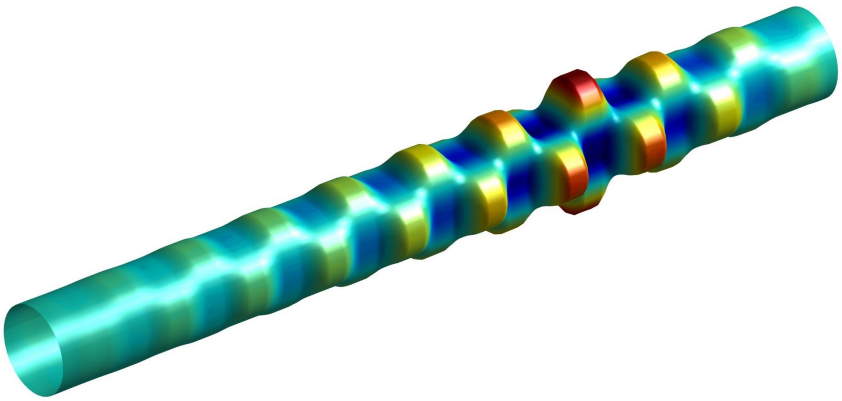

Figure 3.31: ODS of the cylindrical shell phononic crystal at the frequency 2322Hz

Figure 3.32 shows the behavior of cylindrical shell phononic crystal at the frequency of 2642 Hz. This is close to the deepest points in the band gap. Thus, displacements are only observed close to the excitation point of the structure.

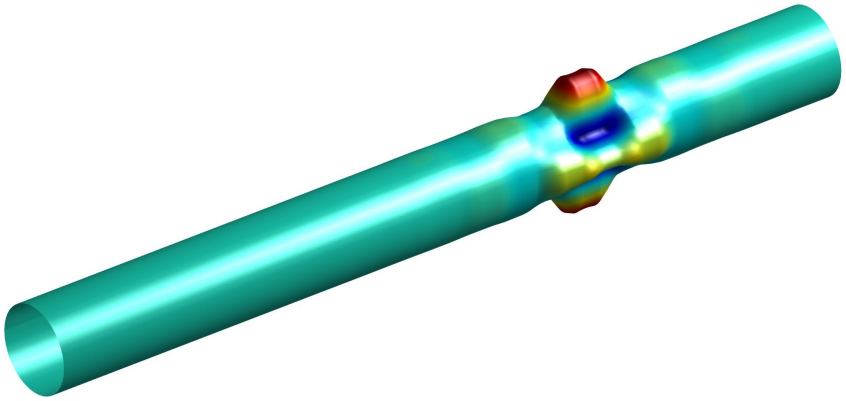

Figure 3.32: ODS of the cylindrical shell phononic crystal at the frequency 2642 Hz

Finally, Figure 3.33 shows the behavior of the cylindrical shell phononic crystal at 3200 Hz. At this frequency, the structure left the first band gap completely and is in a no region with attenuation. Thus, the structure shows a uniform vibration behavior throughout the entire cylindrical shell.

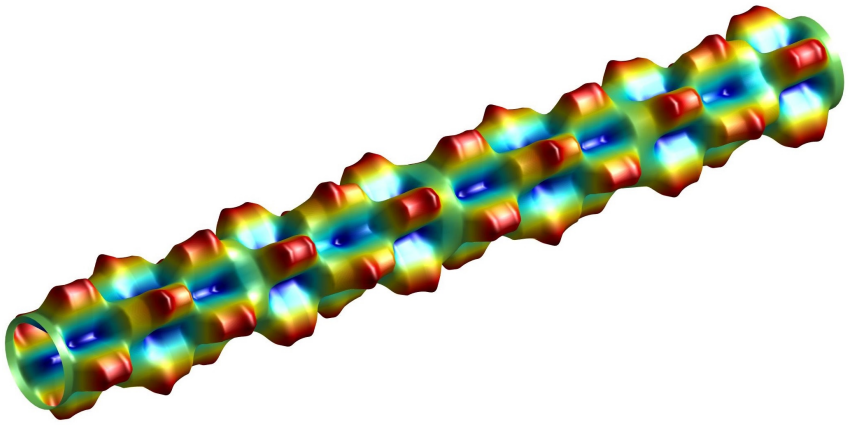

Figure 3.33: ODS of the cylindrical shell phononic crystal at the frequency 3200 Hz

4 FLUID-FILLED CYLINDRICAL SHELL SIMULATED RESULTS

In this chapter, the numerical results obtained with the computational implementation of the fluid-filled closed circular cylindrical shell models shown in Section 2.3 are evaluated. The computational implementation of the Fluid-filled circular Cylindrical Shell Spectral Element - FCSSE is verified using numerical examples. In addition, WSE is used to evaluate a fluid-filled spectral circular cylindrical phononic crystal (steel + polyacetal + steel + internal water). Simulated results are presented in the frequency domain as dispersion diagrams and displacement responses and displacement interpolated over the entire cylindrical shell.

4.1 Spectral element verification

To verify the implementation of the SE method, a circular cylindrical shell with internal fluid is evaluated, the example fluids are water and air. Then, the natural frequencies analysis using the SE method, implemented in MATLAB code. Next, dynamic responses to a single point excitation force are evaluated. Finally, an interpolation is performed between the edges of the FCSSE. thus obtaining the Operating Deflection Shapes (ODS) throughout the structure. These results are compared with those calculated by the FE method in the commercial software ANSYS.

4.1.1 Natural frequencies

In this example, a simple circular cylindrical shell of radius $a = 1.0$ m, thickness $h = 0.01$ m and length $L = 20.0$ m under Clamped-Clamped (C-C) and Free-Free (F-F) boundary conditions is calculated using the proposed SE element model and verified by the FE model. The natural frequencies are calculated over a frequency band of $DC - 50.0$ Hz. The natural frequencies are evaluated for the cylindrical shell when the fluid inside is water or air. A theoretical modal analysis using the SE method, implemented in MATLAB code, is performed. It is included a structural damping as a complex Young's modulus, $E_c = E(1 + i\eta)$. Table 4.1 shows the material and fluid properties used.

Table 4.1: Cylindrical Shell Material and Fluids Properties.

Material Properties	Stell	Water	Air
Density (ρ_S)	7850 kg/m^3	1000 kg/m^3	1.2754 kg/m^3
Sound speed (c)	-	1500 m/s	343.37 m/s
Young's modulus (E)	210 GPa	-	-
Poisson's ratio (ν)	0.30	-	-
Loss factor (η)	0.005	-	-

Since the dynamic stiffness matrix K_{Fm} (from Eq. (2.86)) is a transcendent matrix, matrix. To obtain the natural frequencies the peaks of κ_m = 1/log(|K_{Fm}|) are sought (Kolarević

et al. (2016)).

Figure 4.1 shows the plots of κ_m versus frequency with m = 1,...,5, for the cases F-F and C-C, when the internal fluid of the cylindrical shell are water and air.

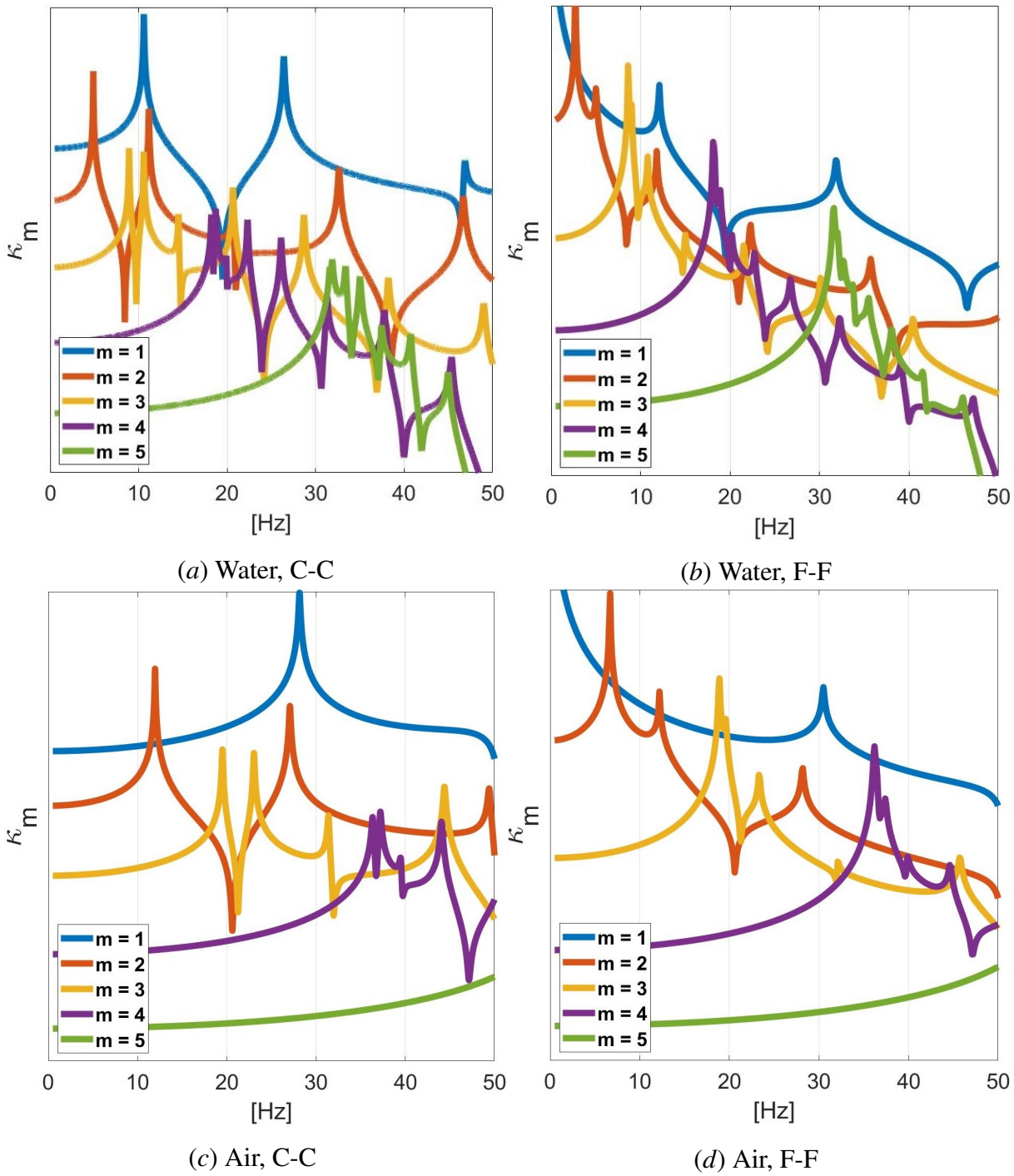

(*a*) Water, C-C

(*b*) Water, F-F

(*c*) Air, C-C

(*d*) Air, F-F

Figure 4.1: Plot κ_m versus frequency using FCSSE model with m = 1,...,5, under CC and FF boundary conditions and internal fluid water.

Each peak in Figure 4.1 represents a natural frequency and associated with a mode shape (m,n), where m and n are integer numbers that indicate the number of half waves in the directions radial and longitudinal, respectively. For the C-C and internal fluid water, Figure 4.1(a),

the first natural frequency appears at the value of 4.88 Hz and is associated with mode m = 2, so this mode of vibration is called (m, n) = (2,1). The results for the F-F case (Fig. 4.1(*b*)) are similar to the C-C case. All natural frequencies calculated on the $DC - 50.0$ frequency band for the cylindrical shell with internal fluid water are shown in Tables 4.2 and 4.3. Figure 4.1(c) and 4.1(d) shows the cases C-C and F-F, when the internal fluid of the cylindrical shell is air. For C-C boundary conditions, Figure 4.1(c), the first natural frequency appears at the value of 11.96 Hz and is associated with mode m = 2, so this mode of vibration is called (m, n) = (2,1). The results for the F-F case (Fig. 4.1(d)) are similar to the C-C case. All natural frequencies calculated on the $DC - 50.0$ frequency band for the cylindrical shell with internal fluid are shown in Tables 4.4 and 4.5.

These results of the FCSSE are compared with those calculated by the FE method in the commercial software ANSYS, using element type SHELL63 (6 DOFs/node) for the structure and element type FLUID30 for the fluid. The fluid-filled circular cylindrical shell is discretized with 4,560 structural elements and 53,936 fluid elements with a total of 56,669 nodes. Figure 4.2*(a)* shows the fluid (blue) and the structure (gray) FE mesh. Meanwhile, the proposed FCSSE model is used with only 2 elements and 3 edges, Figure 4.2*(b)*. The modal analyses were performed using C-C and F-F boundary conditions in the cylindrical shell-ends. Figure 4.2 shows the the cylindrical shell meshed by FE and SE methods.

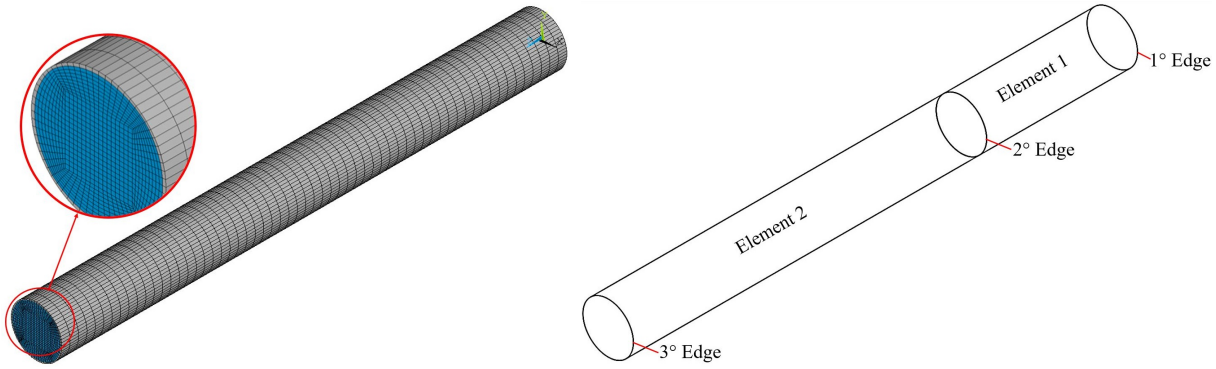

(*a*) FE Mesh (*b*) SE Mesh

Figure 4.2: Fluid-filled circular cylindrical shell: (a) FE method with a mesh detail zoom and (b) SE method.

Tables 4.2 and 4.3 show the results for the circular cylindrical shell filled with water as internal fluid. The tables also show the C-C and F-F boundary conditions including mode number, natural frequencies calculated by FE and SE and the percentage relative error. It can be seen that for both boundary conditions the natural frequency relative errors between FE and SE are very small, with the highest value of 3.53 % for C-C and 3.08 % for F-F. Of course, these values are dependent on the FE model discretization and errors even lower can be reached by using finer meshing.

Tables 4.4 and 4.5 show the results for the circular cylindrical shell filled with air as internal fluid. The tables also show, the C-C and F-F boundary conditions including mode number,

Table 4.2: Natural Frequency C-C circular cylindrical shell filled with water as internal fluid.

n	***m* = 1**			***m* = 2**			***m* = 3**			***m* = 4**			***m* = 5**		
	FE [Hz]	SE [Hz]	Error [%]	FE [Hz]	SE [Hz]	Error [%]	FE [Hz]	SE [Hz]	Error [%]	FE [Hz]	SE [Hz]	Error [%]	FE [Hz]	SE [Hz]	Error [%]
1	10.52	10.59	0.63	4.88	4.88	0.02	8.96	8.92	0.42	18.35	18.22	0.74	31.94	31.61	1.04
2	25.87	26.40	2.03	11.12	11.15	0.30	10.61	10.58	0.26	18.81	18.70	0.59	32.17	31.87	0.94
3	45.21	46.86	3.53	20.46	20.63	0.84	14.52	14.49	0.23	20.03	19.89	0.70	33.68	33.37	0.94
4	-	-	-	32.13	32.63	1.55	20.66	20.66	0.00	22.43	22.30	0.56	35.33	35.00	0.93
5	-	-	-	-	-	-	28.60	28.67	0.24	26.23	26.09	0.54	37.79	37.44	0.93
6	-	-	-	-	-	-	37.99	38.20	0.54	31.46	31.29	0.54	41.18	40.73	1.10
7	-	-	-	-	-	-	-	-	-	37.97	37.75	0.59	-	-	-

Table 4.3: Natural Frequency F-F circular cylindrical shell filled with water as internal fluid.

n	***m* = 1**			***m* = 2**			***m* = 3**			***m* = 4**			***m* = 5**		
	FE [Hz]	SE [Hz]	Error [%]	FE [Hz]	SE [Hz]	Error [%]	FE [Hz]	SE [Hz]	Error [%]	FE [Hz]	SE [Hz]	Error [%]	FE [Hz]	SE [Hz]	Error [%]
0	11.714	12.09	0.37	2.71	2.71	0.12	8.64	8.62	0.32	18.25	18.14	0.62	31.86	31.56	0.98
1	30.046	31.85	1.80	5.00	5.04	0.61	9.03	9.01	0.25	18.43	18.30	0.75	32.03	31.98	0.17
2	-	-	-	11.65	11.81	1.32	10.78	10.79	0.06	18.96	18.86	0.57	32.34	32.64	0.91
3	-	-	-	21.78	22.26	2.12	14.90	14.96	0.35	20.28	20.20	0.40	34.04	33.7	1.02
4	-	-	-	34.60	35.71	3.08	21.39	21.53	0.63	22.81	22.73	0.35	35.80	35.47	0.93
5	-	-	-	-	-	-	29.83	30.14	1.01	26.81	26.74	0.26	-	-	-
6	-	-	-	-	-	-	39.85	40.43	1.41	32.3	32.25	0.16	-	-	-

natural frequencies calculated by FE and SE and the percentage relative error. It can be seen that for both boundary conditions the natural frequency relative errors between FE and SE are very small, all errors are smaller than 1 %.

Table 4.4: Natural Frequency C-C circular cylindrical shell filled with air as internal fluid.

n	***m* = 1**			***m* = 2**			***m* = 3**			***m* = 4**		
	FE [Hz]	SE [Hz]	Error [%]	FE [Hz]	SE [Hz]	Error [%]	FE [Hz]	SE [Hz]	Error [%]	FE [Hz]	SE [Hz]	Error [%]
1	28.18	28.15	0.11	11.96	11.96	0.03	19.48	19.51	0.15	36.21	36.34	0.35
2	-	-	-	27.09	27.07	0.07	23.01	23.04	0.12	37.06	37.21	0.40
3	-	-	-	49.50	49.40	0.21	31.40	31.39	0.03	39.38	39.46	0.22
4	-	-	-	-	-	-	43.95	44.39	0.98	44.46	44.06	0.91

Table 4.5: Natural Frequency F-F circular cylindrical shell filled with air as internal fluid.

n	***m* = 1**			***m* = 2**			***m* = 3**			***m* = 4**		
	FE [Hz]	SE [Hz]	Error [%]	FE [Hz]	SE [Hz]	Error [%]	FE [Hz]	SE [Hz]	Error [%]	FE [Hz]	SE [Hz]	Error [%]
0	30.50	30.49	0.03	6.60	6.67	1.06	18.82	18.87	0.24	36.04	36.19	0.42
1	-	-	-	12.21	12.21	0.00	19.61	19.62	0.04	36.36	36.44	0.22
2	-	-	-	28.17	28.17	0.01	23.33	23.34	0.03	37.33	37.40	0.19
3	-	-	-	-	-	-	32.10	32.13	0.09	39.80	39.90	0.24
4	-	-	-	-	-	-	45.79	45.74	0.12	44.60	44.63	0.06

When comparing the results for the shell internal fluid water versus the shell internal fluid air, it is observed that for the water, more natural frequencies are absorbed than the air, that

is, by increasing the density of fluid, the appearance of natural frequencies are increasing. For example, in the case mode m = 1, C-C boundary conditions and calculated over a frequency band of $DC - 50.0$ Hz, air has only a value of 28.15 Hz, Table 4.4, while water has three natural frequencies 10.59, 20.40 and 46.86 Hz, Table 4.2.

Another analysis can be made when comparing shell internal fluid air, Table 4.4 and 4.5, versus in vacuo closed circular cylindrical shell, Tables 3.2 and 3.3, the values of natural frequencies diverge less than 1 Hz. Therefore, the results that are found when studying the shell with air are close to the shell in vacuo. Wherefore, in this thesis, the next results presented consider only water as the internal fluid of the cylindrical shell

4.1.2 Dynamic responses to a single point excitation force

Forced responses for the fluid-filled cylindrical shell modeled by SE are executed and the results are compared with those obtained by the FE model. A C-C homogeneous cylindrical shell structure with the geometry $L = 10$ m, $h = 0.02$ m, $a = 0.5$ m and the same material properties presented in the Table 4.1 is used. The fluid inside the shell is water. A radial point force of magnitude $F = 100$ N is applied at the point O, located at 3.0 m from the right-end of the shell. Total displacements are evaluated at 7.0 m from the right-end at the points A= $0°$, B= $30°$ and C= $90°$ and D= $180°$. Figure 4.3

The FE model is meshed using element type SHELL63 (6 DOFs/node) and element type FLUID30 (3 DOFs/node). The fluid-filled circular cylindrical shell is discretized with 12,800 structural elements and 128,000 fluid elements with a total of 135,273 nodes. Figure 4.3*(a)* shows the fluid (blue) and the structure (gray) FE mesh for the fluid-filled cylindrical shell, including also excitation and response points. Meanwhile, the SE mesh using with 3 elements and 4 edge, Figure 4.3*(b)*.

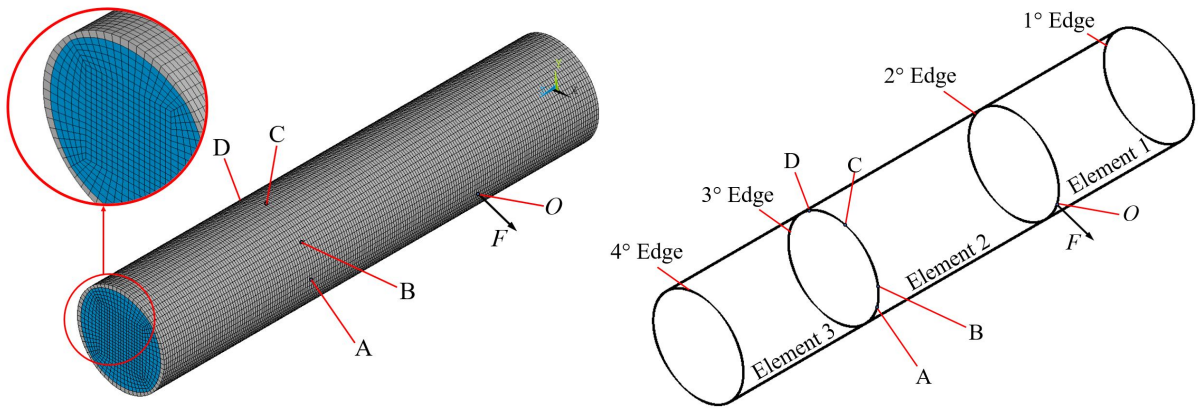

(*a*) FE Mesh (*b*) SE Mesh

Figure 4.3: Fluid-filled circular cylindrical shell, including force excitation (point O) and response (points A, B, C and D):(a) FE method with a mesh detail zoom and (b) SE method.

Figure 4.4 shows the total displacement of the C-C fluid filled cylindrical shell with ex-

citation at point *O* and responses at the points A, B, C and D, for a frequency range $DC - 50$ Hz. For all displacement response evaluated it can be observed that the SE and FE methods have good agreement. Simulations were made using the same processor Intel Core^{TM} i7-6700. The CPU time for the SE method (MATLAB) takes around 400 s and the FE method (ANSYS) 97,200 s to compute the forced responses of the fluid-filled cylindrical shell. This yields CPU time savings around 99.6 % regarding FE solution. The results made to highlight the relevance of the proposed method in terms of accuracy and CPU time saving.

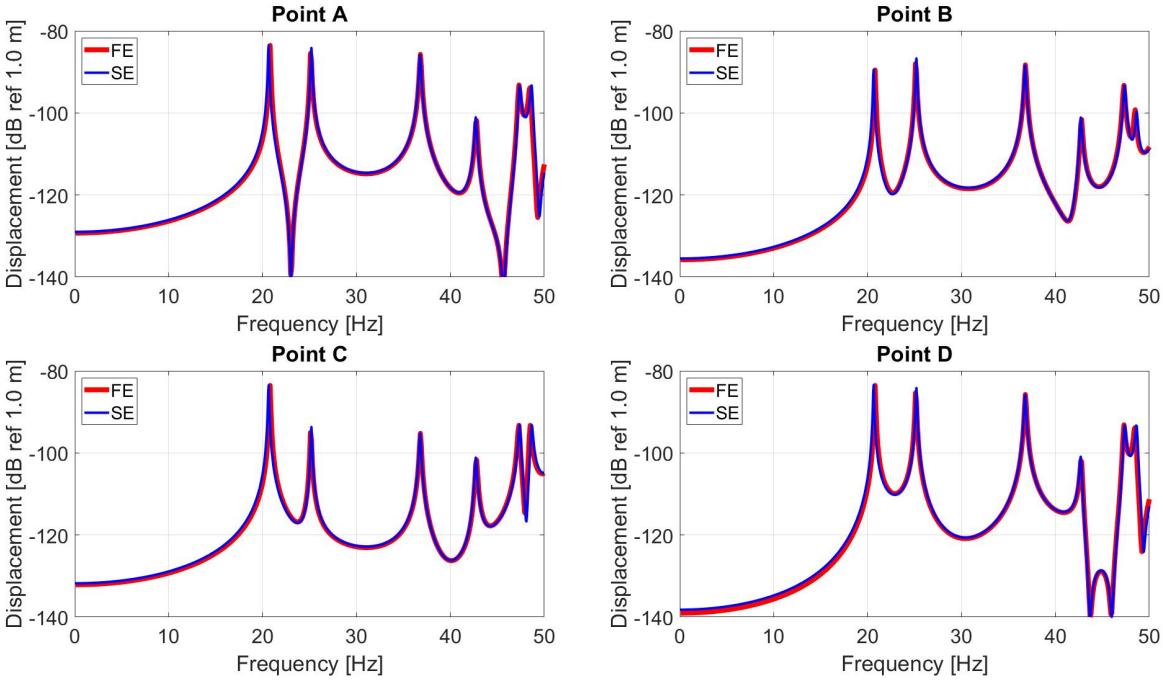

Figure 4.4: Total displacement response calculated by FE and SE methods at the points A, B, C and D and excitation at point O.

4.1.3 FCSSE interpolated results

Similar the section 3.1.5, In order to obtain the displacement results along the whole structure, an interpolation between de edges of FCSSE must be performed. By taken the displacement results calculated in the edges, and substituting them in the Eq.2.71, the integration constants $P_{i,m}$, $A_{i,m}$, $B_{i,m}$, and $C_{i,m}$ are found. Thus, the spectral amplitude of displacement components $\hat{p}(x,\varphi)$, $\hat{u}(x,\varphi)$, $\hat{v}(x,\varphi)$, and $\hat{w}(x,\varphi)$ can be calculated for any special position in the cylindrical shell between the edges.

To evaluate the interpolated results cylindrical shell of the Section 4.1.2, case excitation and response at point A, is used to calculate by FE and SE, the interpolated displacements at the angle $\varphi = 0°$, along the entire length of the structure ($L = 10$ m) (Fig. 4.5) with a discretization of $\Delta x = 0.1$ m.

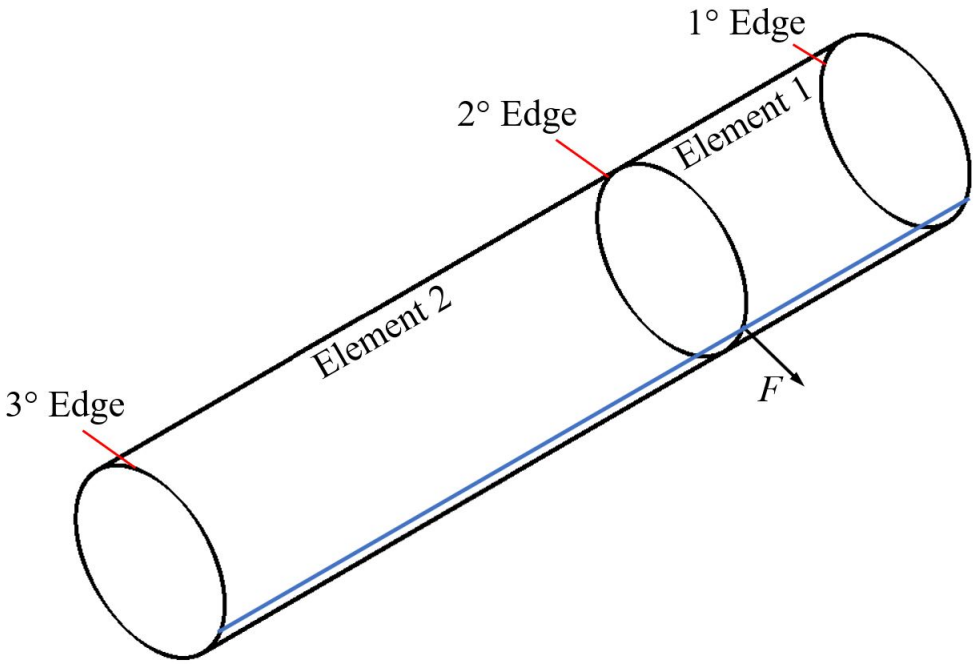

Figure 4.5: Spatial position of the interpolation line (blue line) in the cylindrical shell mode.

Figures 4.6 to 4.9 show the interpolated dimensionless displacement amplitude versus cylindrical shell length, for several frequency values with F-F and C-C boundary condition. For all results, a good agreement between FE and SE methods are observed.

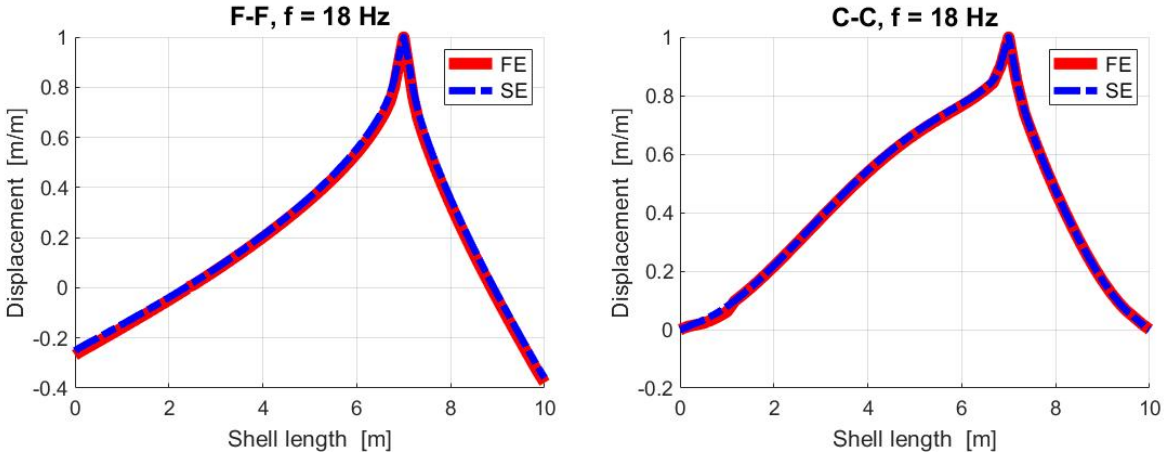

Figure 4.6: Cylindrical shell interpolated dimensionless displacement amplitude at f = 18 Hz with F-F and C-C boundary conditions.

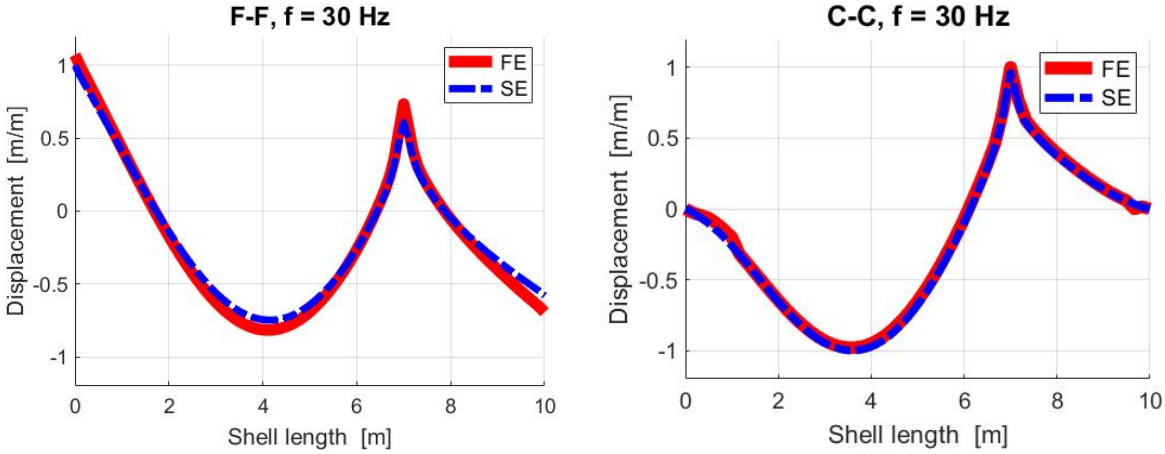

Figure 4.7: Cylindrical shell interpolated dimensionless displacement amplitude at f = 30 Hz with F-F and C-C boundary conditions.

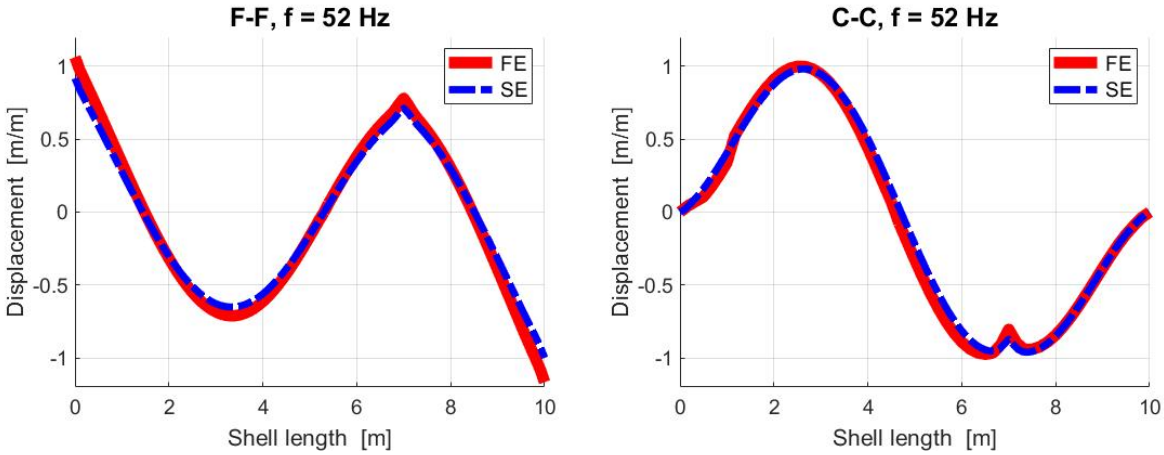

Figure 4.8: Cylindrical shell interpolated dimensionless displacement amplitude at f = 52 Hz with F-F and C-C boundary conditions.

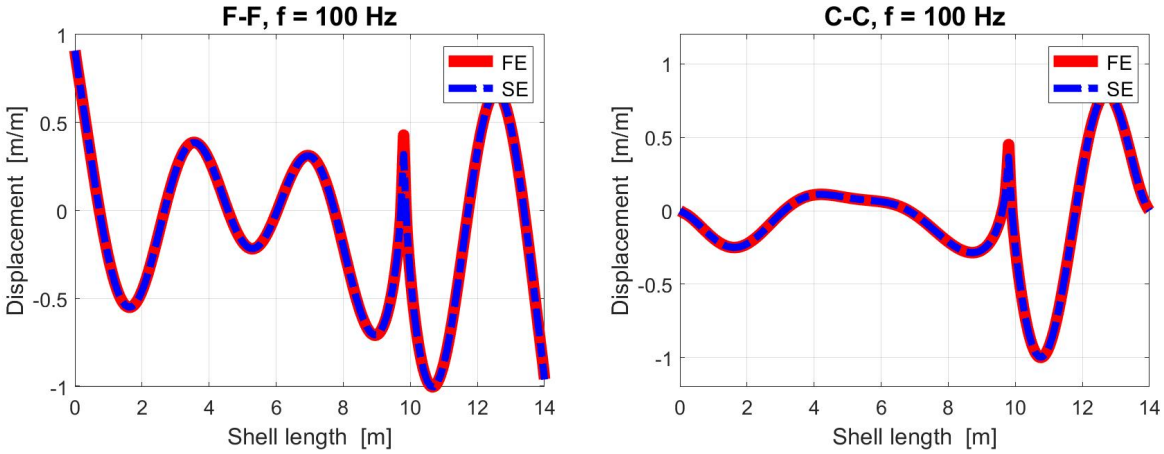

Figure 4.9: CCSSE line interpolated normalized displacement at f = 100 Hz with F-F and C-C boundary conditions.

In order to obtain the Operating Deflection Shapes (ODS) for the cylindrical shell, the procedure applied for one line ($L = 10$ m at $\varphi = 0°$ with $\Delta x = 0.1$ m discretization at x direction) is extended to several lines around the cylindrical shell circle (with discretization $\Delta x = 0.1$ m at x direction and $\Delta\varphi = \pi/20$ at the circle direction).

Figures 4.10 to 4.13 show the cylindrical shell ODS's with C-C boundary conditions calculated by FE and SE method at the frequencies f = 30, 52, 64 and 70 Hz. It can be emphasized the zero displacement at the structure ends due to the C-C boundary conditions.

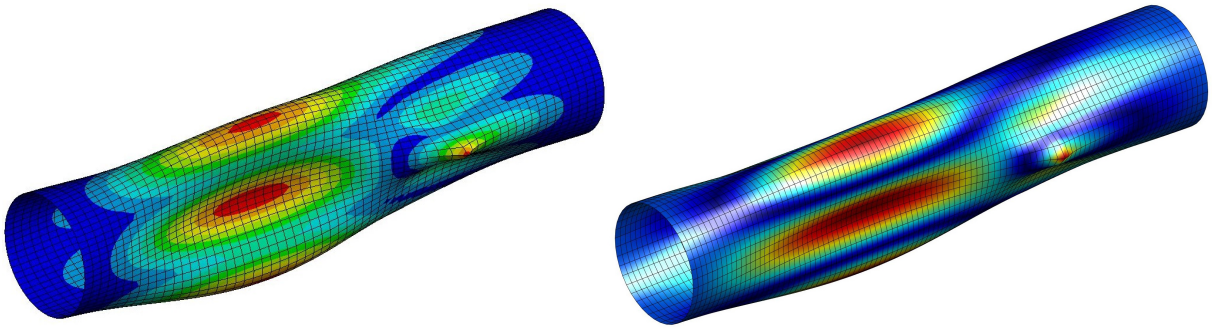

(*a*) FE model (*b*) SE model

Figure 4.10: Cylindrical shell ODS at frequency 30 Hz with C-C boundary conditions.

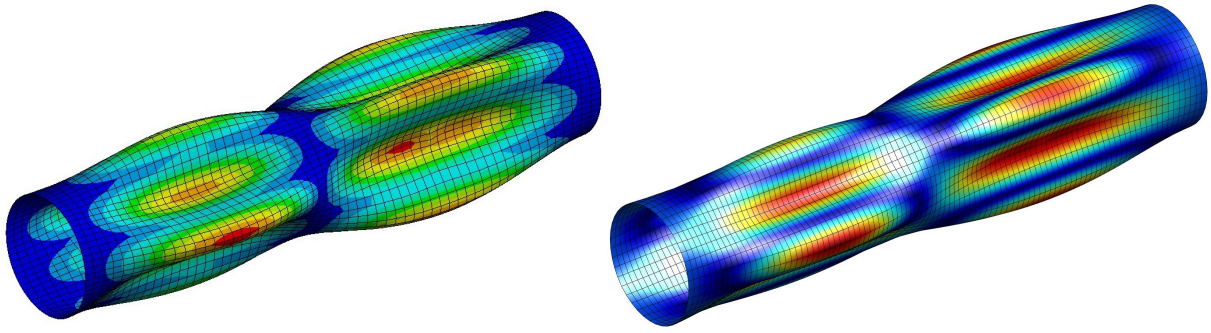

(*a*) FE model (*b*) SE model

Figure 4.11: Cylindrical shell ODS at frequency 52 Hz with C-C boundary conditions.

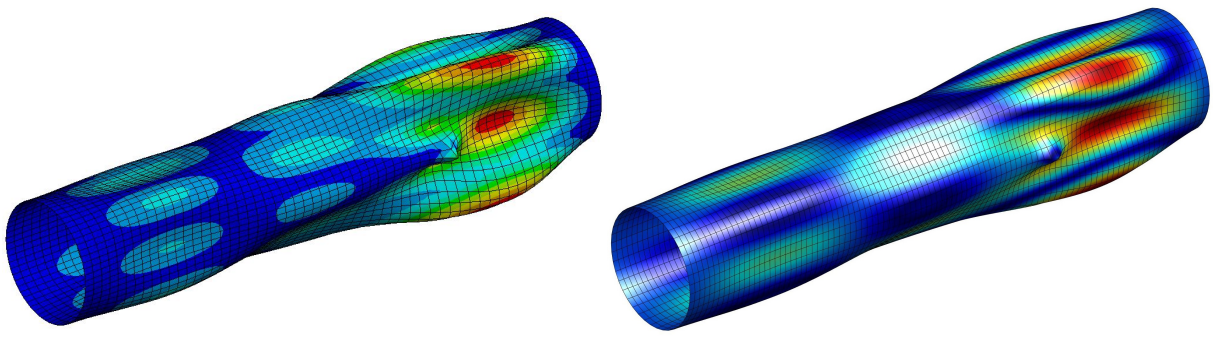

(*a*) FE model (*b*) SE model

Figure 4.12: Cylindrical shell ODS at frequency 64 Hz with C-C boundary conditions.

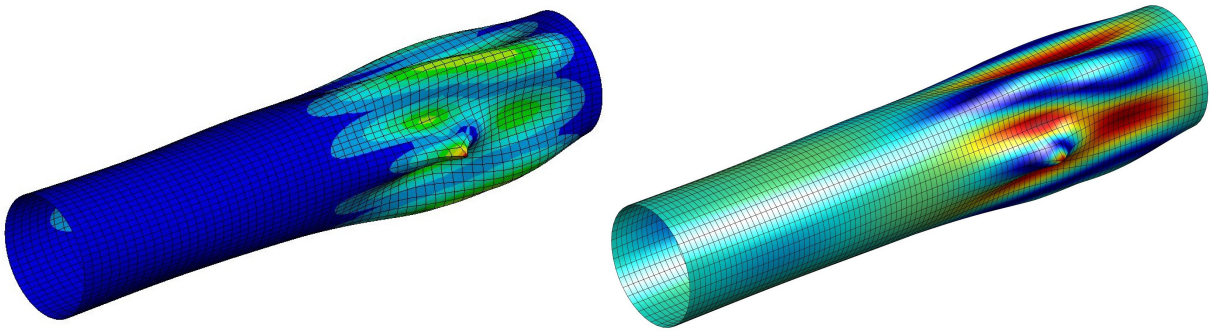

(*a*) FE model (*b*) SE model

Figure 4.13: Cylindrical shell ODS at frequency 70 Hz with C-C boundary conditions.

Figures 4.14 to 4.17 show the cylindrical shell ODS's with F-F boundary conditions calculated by FE and SE method at the frequencies f = 30, 52, 64 and 70 Hz. However, for this case, due the F-F boundary conditions, displacements at the structure ends are noticed.

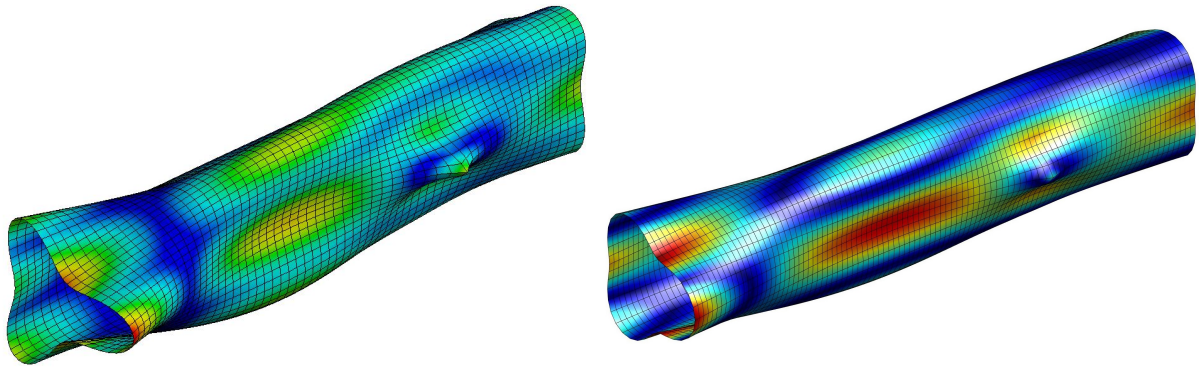

(*a*) FE model (*b*) SE model

Figure 4.14: Cylindrical shell ODS at frequency 30 Hz with F-F boundary conditions.

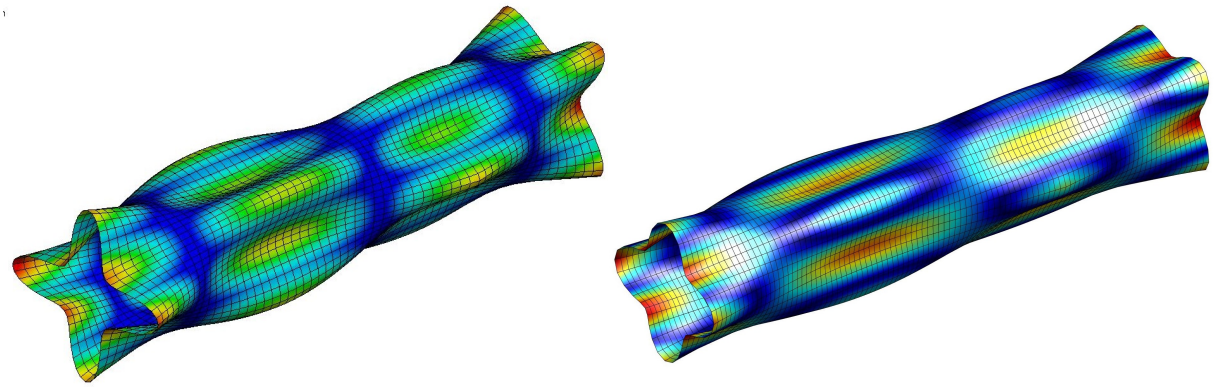

(*a*) FE model (*b*) SE model

Figure 4.15: Cylindrical shell ODS at frequency 52 Hz with F-F boundary conditions.

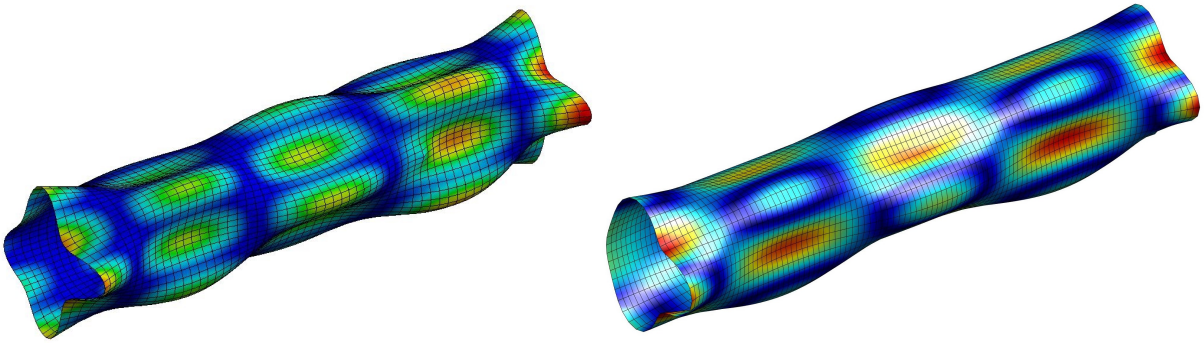

(*a*) FE model (*b*) SE model

Figure 4.16: Cylindrical shell ODS at frequency 64 Hz with F-F boundary conditions.

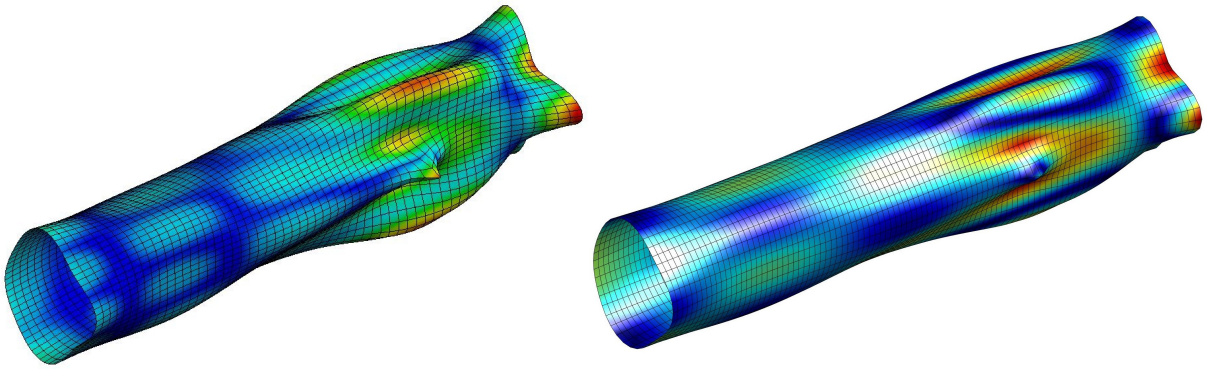

(*a*) FE model (*b*) SE model

Figure 4.17: Cylindrical shell ODS at frequency 70 Hz with F-F boundary conditions.

4.2 Wave Spectral Element verification

Another evaluation of the Wave Spectral Element - WSE approach is made using a unit-cell with $d = 0.2$ m of an homogeneous fluid-filled cylindrical shell, with the same geometry and material properties as in the case 4.1.1. Dispersion diagrams are calculated and compared with those obtained by Analytical Solution (AS) as reported by Fuller and Fahy (1982). The dispersion curves for the cylindrical shell are obtained from de Equation (2.95) by plotting a set of functions $k(\Omega)$, where $\Omega = \omega a/c_S$ is the non-dimensional frequency.

Figure 4.18 shows the dispersion diagrams calculated by WSE and AS for the $m = 1, \ldots, 4$ harmonic modes. For WSE each harmonic mode includes five branches of the wave propagation mode ($b = 1, \ldots, 5$). Meanwhile, the AS has infinite branches for each wave propagation mode. Thus, the branches that are found in the two models are compared. A discussion of these additional branches is presented in the works Fuller (1981) and Mencik and Ichchou (2007). At low frequency, both diagrams present the branch $b = 1$, which are purely real wavenumbers and corresponds to a beam type shell motion or the longitudinal elastic mode.

The branch $b = 2$ corresponds to the ring elastic mode, $m = 1$, 2 , 3 and 4, it presents cut

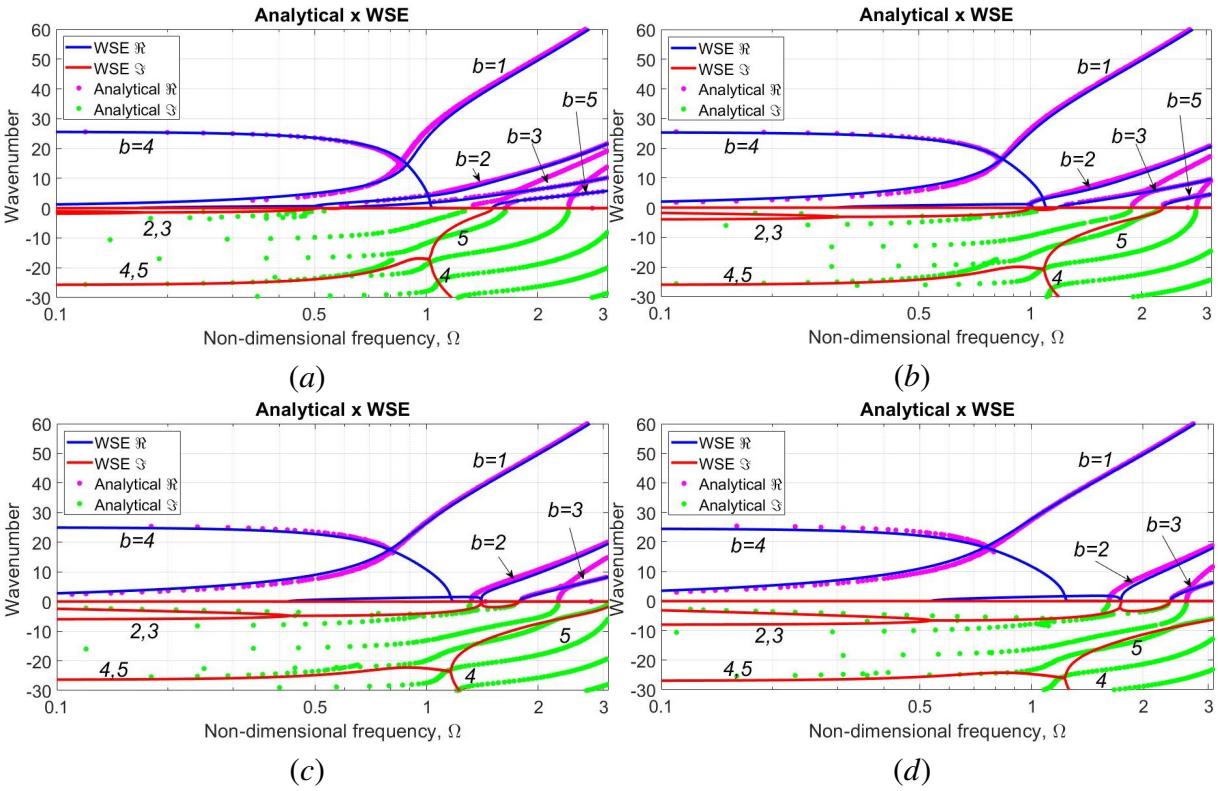

Figure 4.18: Dispersion diagram calculated by AS and WSE methods for the harmonic modes: (*a*) $m = 1$; (*b*) $m = 2$; (*c*) $m = 3$ and (*d*) $m = 4$.

on frequencies $\Omega_2 \approx 0.5$ (Figure 4.18*a*) and $\Omega_2 \approx 1.0$ (Figure 4.18*b*), $\Omega_2 \approx 1.4$ (Figure 4.18*c* and $\Omega_2 \approx 1.7$ (Figure 4.18*d*).

The branch $b = 3$ is predominantly a torsional shell motion. At low frequency it is a non-propagating mode (k is pure imaginary) with cut on frequencies, $\Omega_3 \approx 0.6$ (Figure 4.18*a*) and $\Omega_3 \approx 1.2$ (Figure 4.18*b*) and $\Omega_3 \approx 1.8$ (Figure 4.18*c*) and $\Omega_3 \approx 2.3$ (Figure 4.18*d*), and after these the waves become propagating (k is pure real).

Finally, at low frequencies the branch $b = 4$ presents complex wavenumbers where real and imaginary parts have the same absolute magnitude until before the cut on frequencies $\Omega_4 \approx 1.0$ (Figure 4.18*a*) and $\Omega_4 \approx 1.1$ (Figure 4.18*b*). $\Omega_4 \approx 1.2$ (Figure 4.18*c*) and $\Omega_4 \approx 1.3$ (Figure 4.18*d*). After these, the real part goes to zero and the imaginary part decreases as the frequency increases. Complex wave modes occur in combinations of $\pm(\Re \pm i\Im)$, and the pair that represents wave motion in the shell axial direction produces an attenuated standing wave. Then, the complex branches would represent evanescent motion.

The branch $b = 5$, at low frequency it is a non-propagating mode (k is pure imaginary) with cut on frequencies,$\Omega_3 \approx 1.5$ (Figure 4.18*a*) and $\Omega_3 \approx 2.8$ (Figure 4.18*b*) and $\Omega_3 \approx 3.1$ (Figure 4.18*c*) and $\Omega_3 \approx 4.2$ (Figure 4.18*d*), and after these the waves become propagating (k is pure real).

Figure 4.18 shows that WSE presents good approximation to the AS for some wave modes manly at low frequency bands. However, as the frequency band increase at few wave modes

WSE approaches to the AS, while at other not. At low frequencies the AS model presents many non-propagating wave modes ($\Im k \neq 0$), while these modes only become propagating as the frequency becomes higher ($\Re k \neq 0$). Also, the AS model presents much more wave modes than the WSE model, which prevents a comparison with all AS modes presented in the figure.

4.3 Phononic crystal example

An example of an fluid-filled cylindrical shell phononic crystal (PC) is evaluated including **water as internal fluid**. The WSE is applied to calculate the dispersion diagrams and the SE is used to obtain the forced responses. The unit-cell is made with three layers of two elastic materials combined as: steel(20%)-polyacetal (60%)-steel(20%) + internal water. Table 4.6 shows the PC material properties and geometric parameters. The geometric parameters and material properties are the same as shown in Section 3.3.

Table 4.6: Phononic Crystal Material Properties & Geometry

Property/Geometry	Steel	Polyacetal	Water
Density (ρ)	8030 kg/m^3	1418 kg/m^3	1000 kg/m^3
Sound speed (c)	-	-	1500 m/s
Young's modulus (E)	193 GPa	3.3 GPa	-
Poisson's ratio (ν)	0.27	0.35	-
Loss factor (η)	0.001	0.001	-
Radius (a)	0.05 m	0.05 m	-
Thickness (h)	0.0025 m	0.0025 m	-
Unit-cell length (d)	0.01 m	0.03 m	-

The total displacement response for a C-C cylindrical shell PC made with $N = 20$ unit-cells as shown in Figure 4.19, and filled with water is calculated over a frequency band of $DC - 10.0$ kHz. The PC is excited by two opposite radial point forces of magnitude $F = 100$ N at point A and the displacement response is obtained at point C.

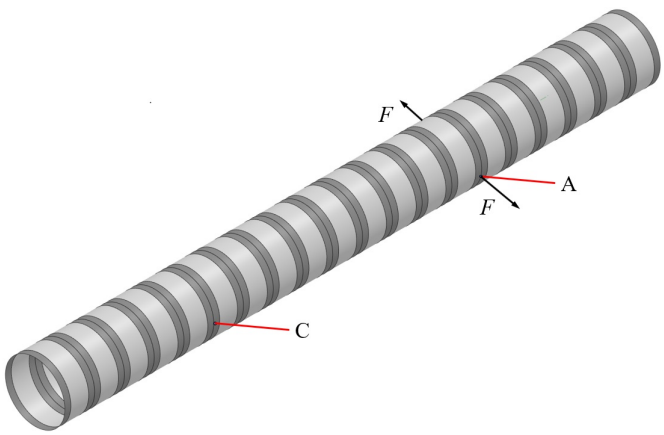

Figure 4.19: Cylindrical shell phononic crystal including $N = 20$ unit-cells and water as internal fluid, with force excitation (point A) and response (point C) positions.

The wavenumbers are calculated and the dispersion diagrams are obtained for the six wave modes $m = 2, 4, 6, 8, 10,$ and 12. The total displacement response at point C and dispersion diagrams are shown in Figure 4.20.

The displacement response at point C and the dispersion diagrams are presented in Figure 4.20. Dispersion diagrams (Figure 4.20*b*) show similar behavior as presented in Figure 3.25 (Section 3.3). In the dispersion diagrams $k(\omega)$, band gaps are identified as a frequency band where the real part of the wavenumber is the Bragg limit or zero ($\Re\{k\} = \pi/d$ = 62.83 m^{-1} or $\Re\{k\} = 0$), and the imaginary part is different from zero ($\Im\{k\} \neq 0$). Under these conditions, the waves become evanescent (non-propagating) and a band gap is identified. Otherwise, the wave is propagating and a pass band is obtained. Figure 3.25 (*bottom*) shows that at least one or two complete band gaps can be easily identified for each wave modes in the analyzed frequency band.

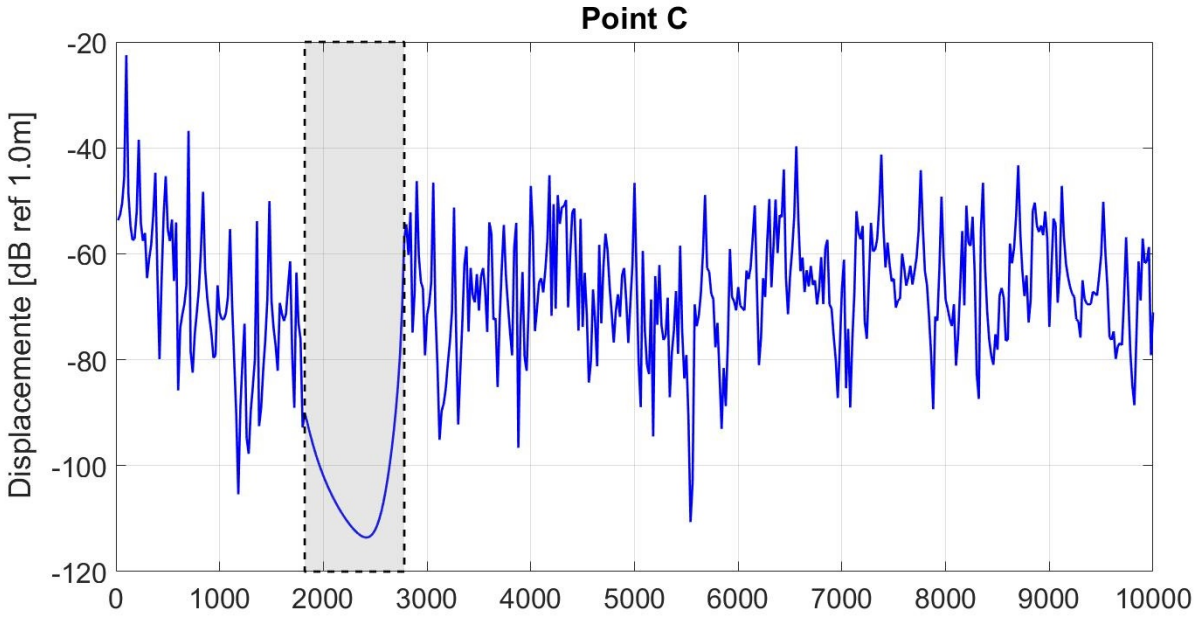

(*a*)

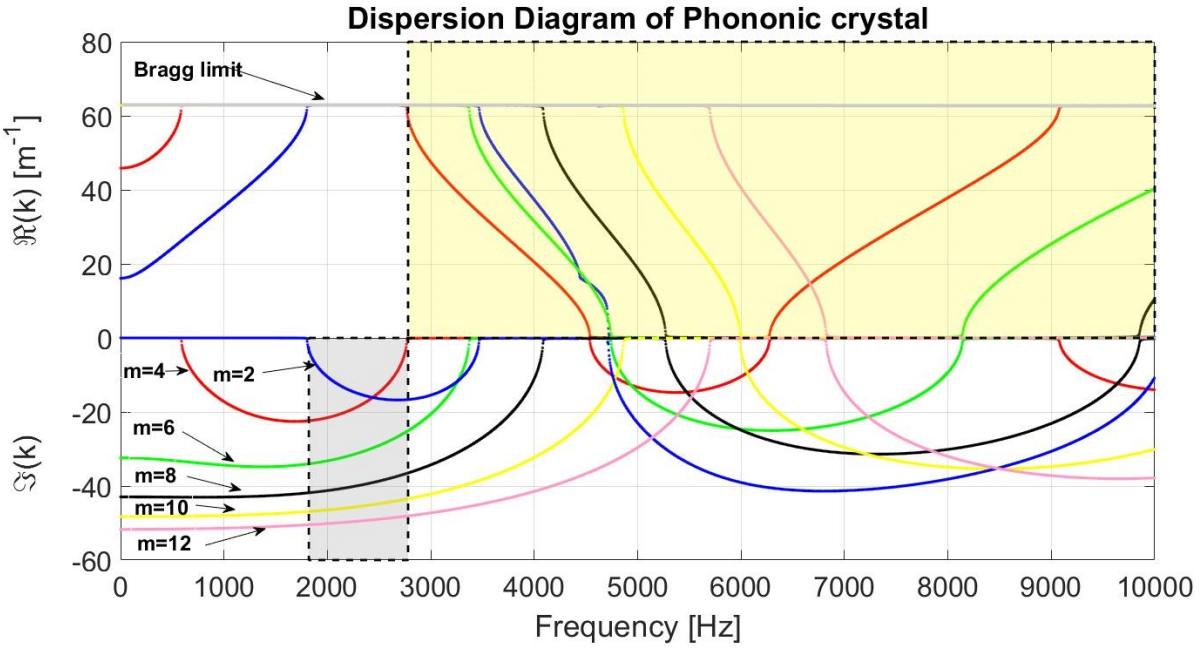

(*b*)

Figure 4.20: Fluid-filled cylindrical shell phononic crystal: *a*) Displacement response at point C to a force excitation at point A; *b*) Unit-cell dispersion diagrams for wave modes m =2(■), 4(■), 6(■),8(■),10(■) and 12(■).

However, for the analyzed frequency band only few wave modes presents a complete band gap, such as $m = 2$ (2 band gaps) and $m = 4$ (1 band gap), all other wave modes contain only one partial band gap. By using the same procedure as in Section 3.3, the dispersion diagrams for the six wave modes are evaluated and only one *effective band gap* (frequency band including only evanescent waves for all wave modes) is found in the frequency band of 1.8-2.8 kHz (gray shaded). Out of this frequency band, propagating waves are present and a pass band

(yellow shaded) is identified. Figure 4.20*a* shows the displacement response at point C, which corroborates the dispersion diagram results since it presents significant attenuation only at the same frequency band (grey shaded) as shown by the effective band gap. In this example the influence of higher modes in the calculation of the effective band gaps is more evident and can be helpful into the PC design. It can be seen in this example that for the pass band (2.8-10.0 kHz), which is the grater part of the analyzed frequency band, at least six band gaps (complete or partial) were generated, but apparently they are unable to produce significant attenuation at the PC displacement response. Of course, these results are biased by the number of modes analyzed as well as the points of excitation and response calculated, but it seems to be an important point to be raised.

Again, in order to promote the understanding, the curves are presented mode by mode revealing the mechanism of band gaps formation shown in Figures 4.21 to 4.25. Thus the Figure 4.21 shows dispersion curve only for the $m = 2$ mode, thus illustrating the appearance of band gaps, the first from 1.8 kHz to 3.4 kHz and the second from 4.7 kHz to over 16 kHz.

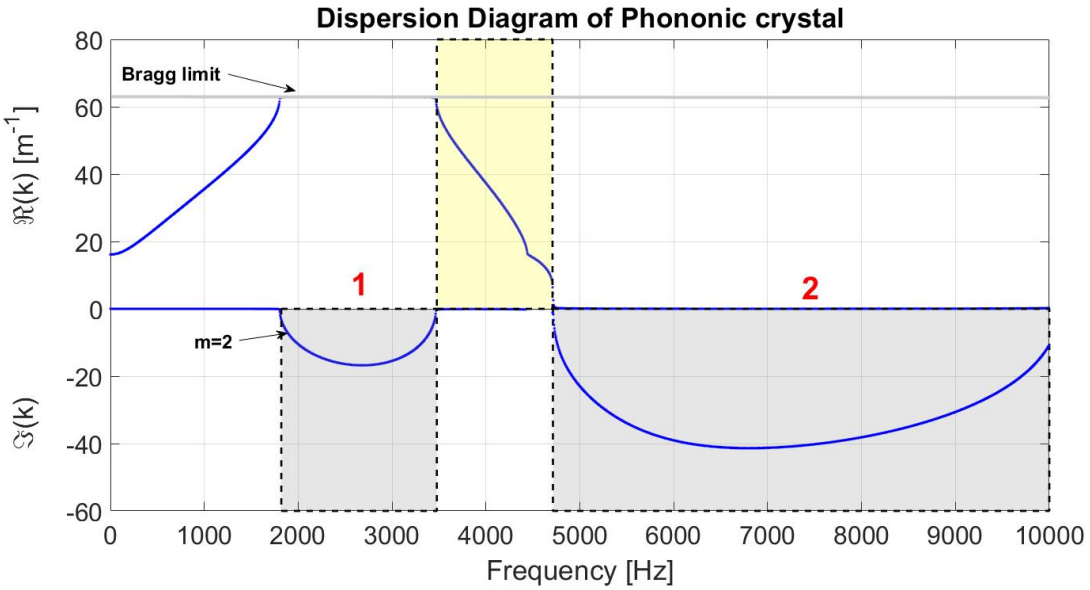

Figure 4.21: Dispersion curve only formodes m =2(■).

Figure 4.22 shows dispersion curves for $m = 2$ and $m = 4$. The propagating part of $m = 4$ destroys the band gaps initially found, then the amount of band gaps increases to three. The first from 1.8 kHz to 2.8 kHz, the second from 4.7 kHz to 6.3 kHz, and the third goes from 9.0 kHz to over 10 kHz.

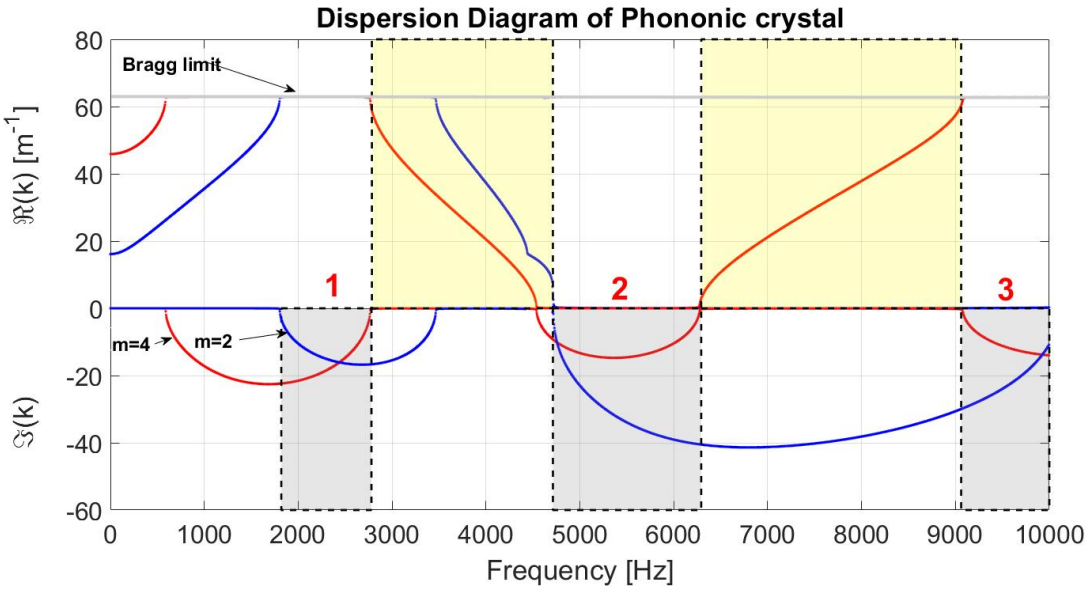

Figure 4.22: Dispersion curves for modes m =2(■) and 4(■) .

In the Figure 4.23 the $m = 6$ is added, this mode becomes propagating at 3.38 kHz and quickly reaches the Bragg limit, its a propagating mode at 3.4 kHz up to 4.7 kHz. Lastly, the $m = 6$ mode is propagated between the frequencies from 8.1 kHz to 10.0 kHz. Considering only the $m = 2, 4$ and 6 modes, two band gaps are formed. The first from 1.8 kHz to 2.7 kHz and second from 4.7 kHz to 6.3 kHz. So the $m = 6$ mode destroys the previously existing third band gaps.

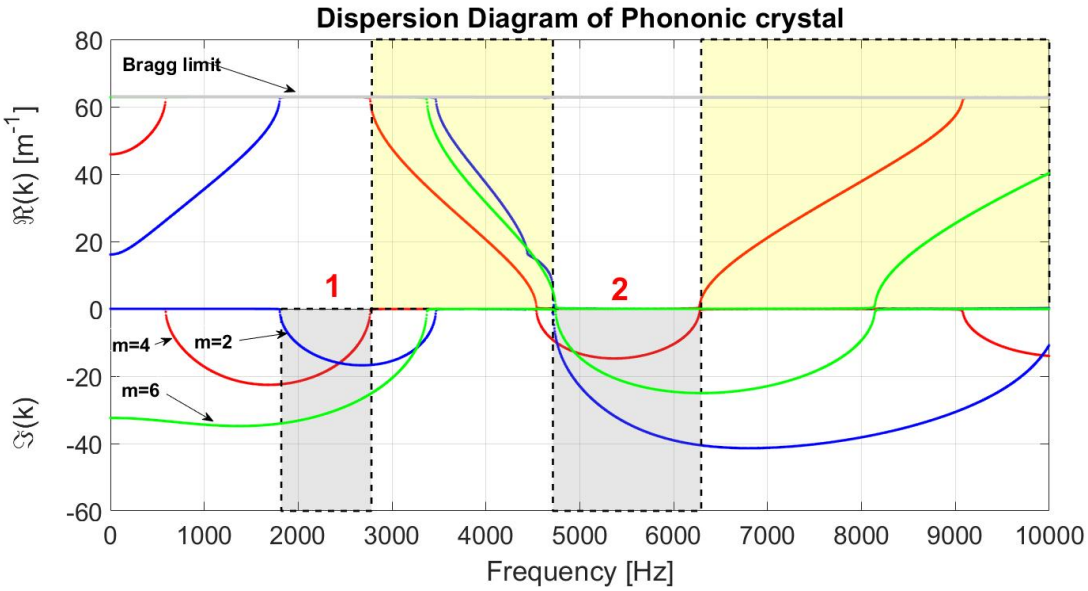

Figure 4.23: Dispersion curves for modes m =2(■), 4(■) and 6(■) .

In Figure $m = 8$ is added, Figure 4.24, this mode becomes propagating at 4.0 kHz and quickly reaches the Bragg limit. It a propagation mode at 4.0 kHz up to 5.3 kHz. The first band gaps are not affected by the mode $m = 8$ while the second band gap has a range reduced from

4.7-6.3 kHz to 5.3-6.3 kHz. After that value, neither a band gap is observed until the frequency of 10.0 kHz.

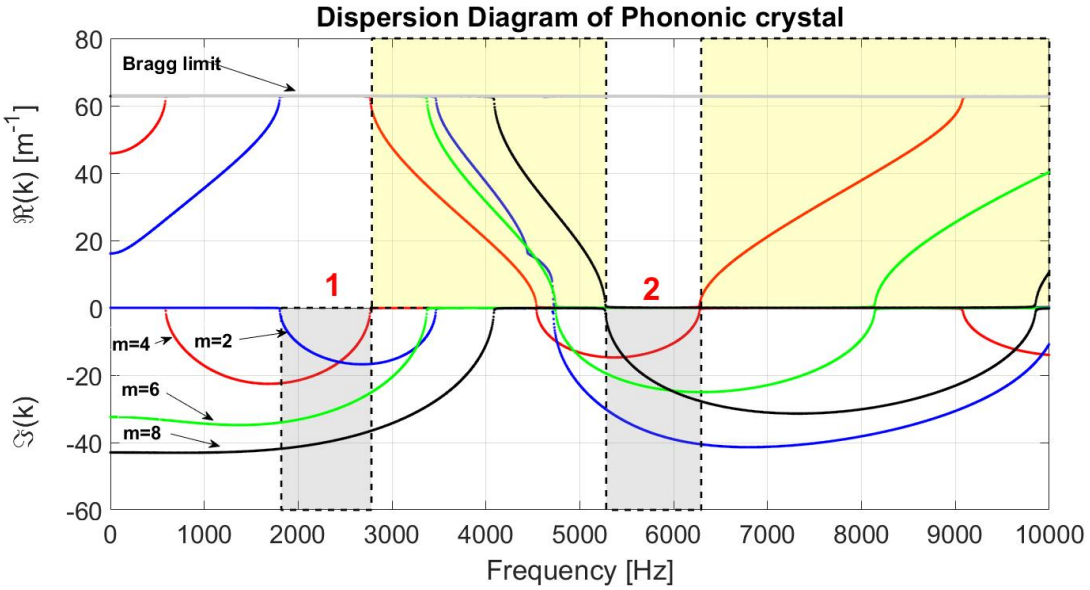

Figure 4.24: Dispersion curves for modes m =2(■), 4(■), 6(■) and 8(■)

Finally, $m = 10$ is added, Figure 4.25, this mode becomes propagating at 4.9 kHz. It is a propagation mode at 4.8 kHz up to 6.0 kHz. First band gaps are not affected by the mode $m = 10$ while the second band gap has a range reduced from 5.3-6.3 kHz to 6.0-6.3 kHz. After that value, neither a band gap is observed until the frequency of 10.0 kHz. Other modes of propagation appear before 10 kHz, however they do not affect the constitution of band gaps already enumerated.

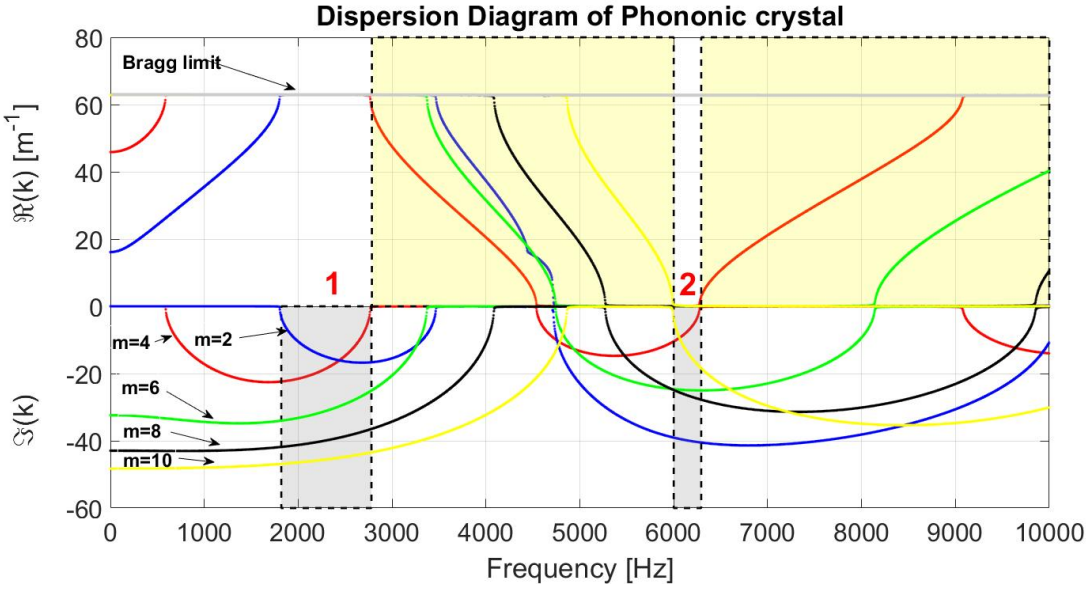

Figure 4.25: Dispersion curves for modes m =2(■), 4(■), 6(■),8(■) and 10(■) .

The second band gaps is completely destroyed with the addition of the $m = 12$ mode, see

Figure 4.20*(b)*. Therefore, for the case studied there is only one band gap.

Figure 4.26 shows the ODS of the cylindrical shell phononic crystal studied at the frequency of 1682 Hz. At this frequency, the structure does not experience attenuation of vibration along its length.

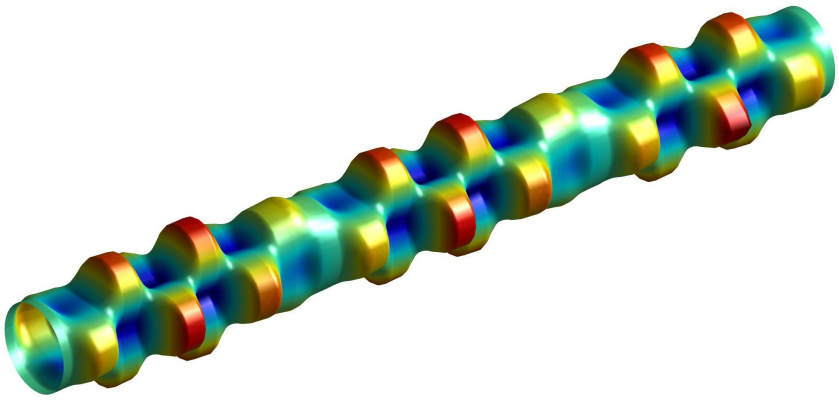

Figure 4.26: ODS of the cylindrical shell phononic crystal at the frequency 1682 Hz

Figure 4.27 shows the behavior of the cylindrical shell phononic crystal at the frequency of 1840 Hz. This frequency, the structure is found in the band gap region, but not at the deepest point of the band gap. Therefore, there is a clear attenuation of the vibration structure as it is observed points further away from the loading application places.

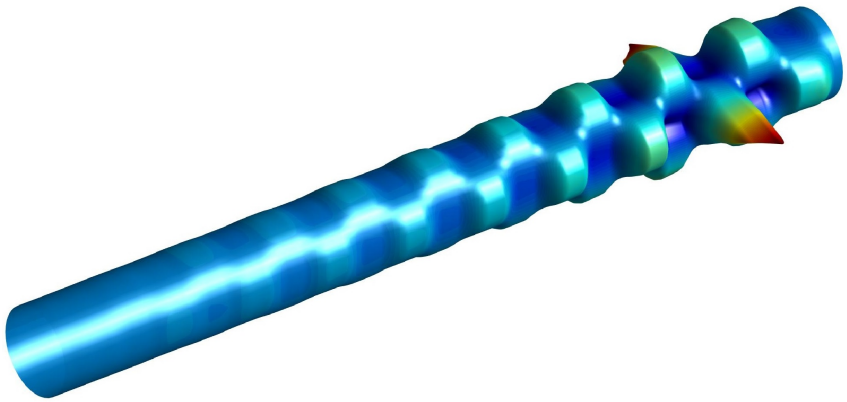

Figure 4.27: ODS of the cylindrical shell phononic crystal at the frequency 1840 Hz

Figure 4.28 shows the behavior of cylindrical shell phononic crystal at the frequency of 2400 Hz. This is close to the deepest points in the band gap. Thus, displacements are only observed close to the excitation point of the structure.

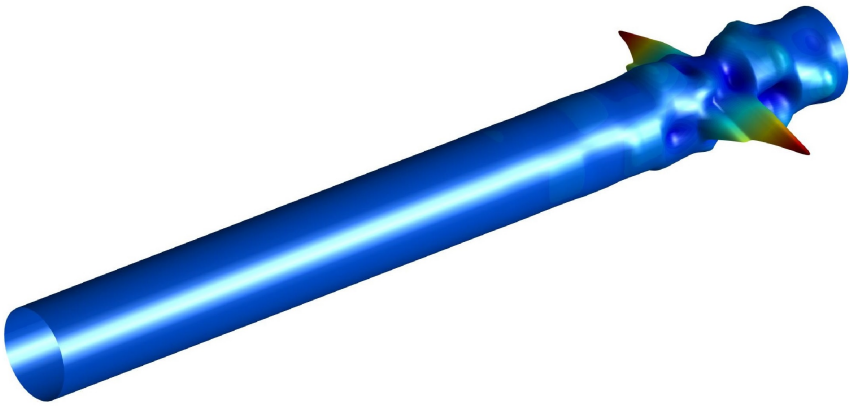

Figure 4.28: ODS of the cylindrical shell phononic crystal at the frequency 2400 Hz

Finally, Figure 4.29 shows the behavior of the cylindrical shell phononic crystal at 2900 Hz. At this frequency, the structure left the first band gap completely and is a frequency without attenuation. Thus, the structure shows a uniform vibration behavior throughout the entire cylindrical shell.

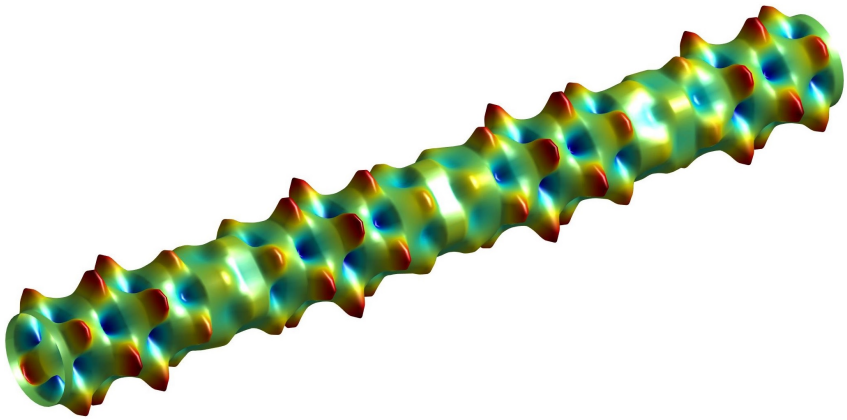

Figure 4.29: ODS of the cylindrical shell phononic crystal at the frequency 2900 Hz

5 CONCLUSION

A fluid-filled cylindrical shell spectral element was formulated and presented. Both models, in vacuo and fluid-filled closed circular cylindrical shell spectral element were theoretically reviewed, computationally implemented, and verified by the FE method using simulated examples. In addition, they were applied to the WSE method to evaluate a unit-cell of a homogeneous periodic structure and a phononic crystal made with two materials distributed in three layers, to obtain the dispersion diagrams. By connecting 20 of these unit-cells, the forced responses were obtained using the Spectral Element (SE) method.

The results of both SE models (CSSE and FCSSE) from a theoretical modal analysis and dispersion wave analysis of a homogeneous closed circular cylindrical shell spectral element are in good agreement with those calculated by the FE method (ANSYS) and analytical solution. Forced responses are also calculated by SE and present good agreement with those obtained by FE. Simulations were made using the processor Intel Core^{TM} i7-6700 and for all examples the CPU time for the SE method (MATLAB) was much shorter than that of the FE method (ANSYS).

Using the spectral element, it is possible to obtain the exact solution of the behavior of a shell at high frequencies with low computational effort. The mentioned facts are important characteristics, and can have great influence on modern dynamic behavior prediction techniques for these frequency ranges. Thus, CSSE and FCSSE are presented as an alternative for the investigation of the band gap caused by phononic crystals, because the attenuating effects on crystals are usually found at higher frequencies.

Finally, WSE is formulated for the analysis of wave propagation in a homogeneous elastic cylindrical shell. In this method, the dynamic stiffness matrix of a small slice of the cylindrical shell modeled by the SE method (CSSE or FCSSE) is used for the application of periodicity conditions in the propagation of a harmonic disturbance through the structure. The periodicity conditions result in a eigenvalue problem with a formulation that produces the equations of the force relations - displacement of the structure. Thus, the wavenumber k is used to compute at cylindrical shell phononic crystal. Dispersion diagrams are calculated and compared with those obtained by the Analytical Solution.

The WSE is applied to a unit-cell of the in vacuo and fluid-filled models of a cylindrical shell PC to obtain the dispersion diagram and identify the frequency band gaps. The band gaps may be identified for the wave modes analyzed , but correspondence with the attenuation at forced response requires the inclusion of a minimum number of wave modes in the analyzed frequency band in order to identify the *effective band gaps*. An effective band gap is the one

that contains only evanescent waves in all wave modes included in the desired frequency band. This is important because at some frequency bands there are wave modes generating evanescent waves (band gaps), while other modes produce propagating waves, which reduce the destructive interference effect (Bragg effect). As a consequence, the attenuation of the PC displacement response is reduced or the band width is shortened. Of course, the results presented in the work may be biased by the number of modes analyzed as well as the points of excitation and response calculated, but it seems to be an important point to be raised.

5.1 Future work

In the following, topics which appear as future prospects for continuation of the research developed in this thesis are listed.

- Experimentally verify the results obtained for the fluid-filled phononic crystal cylindrical shell.

- Use WSE approaches to design metamaterials equipped with a local resonator periodically distributed in a fluid-filled cylindrical shell.

- Develop a spectral element of the curved shell.

- Use CSSE and FCSSE for the investigation and monitoring of damage or cracks in a cylindrical shell.

- Use CSSE and FCSSE associated with the supercell technique to include line defects in PCs for waveguides and by confining standing waves in the defects. It could also be used to constitute resonators and filters.

- Extend the approaches proposed in this thesis to describe vibroacoustic system structures with interaction with external acoustic fields.

- Study the variability related to the physical parameters of PCs manufactured by a 3D printer.

- Formulate cylindrical shell models for structures with two-dimensional periodicities. In this thesis, only the case of structures that are periodic along one direction has been addressed.

5.2 List of publications

5.2.1 Articles in indexed journals

- GOTO, A. M.; NOBREGA, E.D.; PEREIRA, F.N.; DOS SANTOS, J.M.C. Numerical and experimental investigation of phononic crystals via wave-based higher-order rod models. **International Journal of Mechanical Sciences**, v. 181, 105776, 2020.

- PEREIRA, F.N.; DOS SANTOS, J.M.C. Phononic crystal investigation using a fluid-structure circular cylindrical shell spectral element. **Mechanical Systems and Signal Processing**, v. 148, 107100, 2021.

5.2.2 Full Papers and Abstracts in Conference Proceedings

- PEREIRA, F.N.; DOS SANTOS, J.M.C. Wave Propagation and Frequency Band Structure in Cylindrical Shells. In **Proceedings of the 24rd ABCM International Congress of Mechanical Engineering (COBEM)**, December 3-8, Curitiba, PR, Brazil, 2017.

- PEREIRA, F.N.; DOS SANTOS, J.M.C. Band Gap Investigation using Free and Forced Response with Cylindrical Shell Spectral Element. In **Proceedings of the International Conference on Structural Engineering Dynamics (ICEDyn)**, Viana do Castelo, Portugal, 24-26 June, 2019.

- GOTO, A. M.; NOBREGA, E. D.; PEREIRA, F.N.; DOS SANTOS, J.M.C. Spectral Transfer Matrix Method for Higher Order Phononic Crystal Waveguides. In **Proceedings of the International Conference on Structural Engineering Dynamics (ICEDyn)**, Viana do Castelo, Portugal, 24-26 June, 2019.

- PEREIRA, F.N.; Sousa R. W. O. ; DOS SANTOS, J.M.C. Dynamic Response Computation in Phononic Crystal Cylindrical Shells by Wave Methods. In **Proceedings of the XVIII International Symposium on Dynamic Problems of Mechanics (DINAME)**, March 10-15, Buzios, RJ, Brazil.

REFERENCES

BELI, D.; FABRO, A.T.; RUZZENE, M. and ARRUDA, J.R.F. Wave attenuation and trapping in 3d printed cantilever-in-mass metamaterials with spatially correlated variability. **Scientific reports**, v. 9, n. 1, 1–11, 2019.

CAMPOS, N.B.F. and ARRUDA, J.R.F. On the modeling of beam reinforced thin plates using the spectral element method. **Shock and Vibration**, v. 15, 425–434, 01 2008.

CASIMIR, J.; NGUYEN, M. and TAWFIQ, I. Thick shells of revolution: Derivation of the dynamic stiffness matrix of continuous elements and application to a tested cylinder. **Computers & Structures**, v. 85, n. 23, 1845–1857, 2007.

CASIMIR, J.B.; KEVORKIAN, S. and VINH, T. The dynamic stiffness matrix of two-dimensional elements: Application to kirchhoff's plate continuous elements. **Journal of Sound and Vibration**, v. 287, 571–589, 10 2005.

CASTAINGS, M.; LE CLEZIO, E. and HOSTEN, B. Modal decomposition method for modeling the interaction of lamb waves with cracks. **The Journal of the Acoustical Society of America**, v. 112, n. 6, 2567–2582, 2002.

CHEN, S.; WAMBSGANSS, M.T. and JENDRZEJCZYK, J. Added mass and damping of a vibrating rod in confined viscous fluids. **American Society of Mechanical Engineers**, pp. 325–329, 1976.

CHEN, W.; BIAN, Z. and DING, H. Three-dimensional vibration analysis of fluid-filled orthotropic fgm cylindrical shells. **International Journal of Mechanical Sciences**, v. 46, n. 1, 159–171, 2004.
URL: *https://www.sciencedirect.com/science/article/pii/S0020740303002352*

DAL POGGETTO, V.F. and SERPA, A.L. Flexural wave band gaps in a ternary periodic metamaterial plate using the plane wave expansion method. **Journal of Sound and Vibration**, v. 495, 115909, 2021.

DELANGHE, K. and SAS, P. tatistical analysis of the power injection method. **Journal of the**

Acoustical Society of America, v. 100, 291–303, 1996.

DEYMIER, P.A. **Acoustic metamaterials and phononic crystals**, v. 173. Springer Science & Business Media, 2013.

DOYLE, J.F. **Wave Propagation in Structures: Spectral Analysis using Fast Discrete Fourier Transforms**. Springer-Verlag Nova Iorque, 2nd edition, 1997. ISBN 978-0-387-94940-6.

FAHY, F. and GARDONIO, P. **Sound and Structural Vibration**. Academic Press, 2nd edition, 1985.

FARSHIDIANFAR, A. and OLIAZADEH, P. Free vibration analysis of circular cylindrical shells: comparison of different shell theories. **International Journal of Mechanics and Applications**, v. 2, n. 5, 74–80, 2012.

FULLER, C. The effects of wall discontinuities on the propagation of flexural waves in cylindrical shells. **Journal of Sound and Vibration**, v. 75, n. 2, 207–228, 1981.
URL: *https://www.sciencedirect.com/science/article/pii/0022460X81903400*

FULLER, C. and FAHY, F. Characteristics of wave propagation and energy distributions in cylindrical elastic shells filled with fluid. **Journal of Sound and Vibration**, v. 81, n. 4, 501–518, 1982.

GALÁN, J.M. and ABASCAL, R. Numerical simulation of lamb wave scattering in semi-infinite plates. **International Journal for Numerical Methods in Engineering**, v. 53, n. 5, 1145–1173, 2002.

GAUTIER, F.; GILBERT, J.; DALMONT, J.P.; BENYAHIA, L. and PICÓ, R. Korteweg's wave in a fluid filled rubber tube. **12th International Congress on Sound and Vibration 2005, ICSV 2005**, v. 3, 2278–2285, 01 2005.

GAUTIER, F.; GILBERT, J.; DALMONT, J.P. and PICÓ, R. Wave propagation in a fluid filled rubber tube: Theoretical and experimental results for korteweg's wave. **Acta Acustica United with Acustica**, v. 93, 333–344, 2007.

GONÇALVES, P.; BRENNAN, M. and CLEANTE, V. Predicting the stop-band behaviour of

finite mono-coupled periodic structures from the transmissibility of a single element. **Mechanical Systems and Signal Processing**, v. 154, 107512, 2021.

GONÇALVES, P. and BATISTA, R. Frequency response of cylindrical shells partially submerged or filled with liquid. **Journal of Sound and Vibration**, v. 113, n. 1, 59–70, 1987.

GOTO, A.M.; NÓBREGA, E.D.; PEREIRA, F.N. and DOS SANTOS, J.M.C. Numerical and experimental investigation of phononic crystals via wave-based higher-order rod models. **International Journal of Mechanical Sciences**, v. 181, 105776, 2020.

HARBAOUIA, I.; CASIMIR, J.B.; KHADIMALLAH, M.A. and CHAFRA, M. A new prestressed dynamic stiffness element for vibration analysis of thick circular cylindrical shells. **International Journal of Mechanical Sciences**, v. 140, 37–50, May 2018.

HSU, J.C. and WU, T.T. Efficient formulation for band-structure calculations of two-dimensional phononic-crystal plates. **Physical Review. B**, v. 74, n. 14, 2006.

HUSSEIN, M.I.; LEAMY, M.J. and RUZZENE, M. Dynamics of phononic materials and structures: historical origins, recent progress, and future outlook. **Applied Mechanics Reviews**, v. 66, n. 4, 38, 2014.

JEONG, K. and LEE, S.C. Hydroelastic vibration of a liquid-filled circular cylindrical shell. **Computers and Structures**, v. 66, 173–185, 01 1998.

JEONG, K.H. and LEE, S.C. Fourier series expansion method for free vibration analysis of either a partially liquid-filled or a partially liquid-surrounded circular cylindrical shell. **Computers and Structures**, v. 58, n. 5, 937–946, 1996.
URL: *https://www.sciencedirect.com/science/article/pii/0045794995001970*

KOLAREVIĆ, N.; DANILOVIĆ, M. and PETRONIJEVIĆ, M. Dynamic stiffness method in the vibration analysis of circular cylindrical shell. **Building Materials and Structures**, v. 59, n. 3, 45–61, 2016.

KOLAREVIC, N.; NEFOVSKA-DANILOVIC, M. and PETRONIJEVIć, M. Dynamic stiffness elements for free vibration analysis of rectangular mindlin plate assemblies. **Journal of Sound and Vibration**, v. 359, 84–106, 12 2015.

KUSHWAHA, M.S.; HALEVI, P.; DOBRZYNSKI, L. and DJAFARI-ROUHANI, B. Acoustic band structure of periodic elastic composites. **Physical Review Letters**, v. 71, 2022–2025, Sep 1993.

KUSHWAHA, M.S.; HALEVI, P.; MARTINEZ, G.; DOBRZYNSKI, L. and DJAFARI-ROUHANI, B. Theory of acoustic band structure of periodic elastic composites. **Physical Review B**, v. 49, n. 4, 2313, 1994.

LARBI, W. and DEÜ, J.F. A 3d state-space solution for free-vibration analysis of a radially polarized laminated piezoelectric cylinder filled with fluid. **Journal of sound and vibration**, v. 330, n. 2, 162–181, 2011.

LEE, B. and STASZEWSKI, W. Sensor location studies for damage detection with lamb waves. **Smart materials and structures**, v. 16, n. 2, 399, 2007.

LEE, U. Vibration analysis of one-dimensional structures using the spectral transfer matrix method. **Engineering Structures**, v. 22, n. 6, 681–690, 2000.
URL: *https://www.sciencedirect.com/science/article/pii/S0141029699000024*

LEE, U. **Spectral Element Method in Structural Dynamics**. 2009. ISBN 9780470823750.

LEE, U. and LEE, J. Spectral-element method of levy-type plates subjected to dynamic loads. **Journal of Engineering Mechanics**, pp. 243–247, 1999.

LEISSA, A.W. **Vibration of shells**. NASA, 1973. ISBN 19730018197.

LIU, J.; GUO, H. and WANG, T. A review of acoustic metamaterials and phononic crystals. **Crystals**, v. 10, n. 4, 305, 2020.

MEAD, D. Free wave propagation in periodically supported, infinite beams. **Journal of Sound and Vibration**, v. 11, n. 2, 181 – 197, 1970.

MEAD, D. Wave propagation in continuous periodic structures: Research contributions from southampton, 1964-1995. **Journal of Sound and Vibration**, v. 190, n. 3, 495–524, 1996.

MENCIK, J.M. and ICHCHOU, M. Multi-mode propagation and diffusion in structures through finite elements. **European Journal of Mechanics - A/Solids**, v. 24, n. 5, 877 – 898, 2005.

MENCIK, J.M. and ICHCHOU, M. Wave finite elements in guided elastodynamics with internal fluid. **International Journal of Solids and Structures**, v. 44, 2148–2167, 04 2007.

MENCIK, J.M. and ICHCHOU, M. A substructuring technique for finite element wave propagation in multi-layered systems. **Computer Methods in Applied Mechanics and Engineering**, v. 197, n. 6-8, 505–523, 2008.

MIRANDA JR, E.J.P.D. and DOS SANTOS, J.M.C.D. Band structure in carbon nanostructure phononic crystals. **Materials Research**, v. 20, 555–571, 2017.

MUNJAL, M. Response of a multi-layered infinite plate to an oblique plane wave by means of transfer matrices. **Journal of Sound and Vibration**, v. 162, n. 2, 333–343, 1993.

NASCIMENTO, R.F. **Propagação de ondas utilizando modelos de elementos finitos em guias de onda estruturais**. 2009. PhD (Thesis). Universidade Estadual de Campinas, Faculdade de Engenharia Mecânica.

NEFOVSKA-DANILOVIC, M. and PETRONIJEVIć, M. In-plane free vibration and response analysis of isotropic rectangular plates using the dynamic stiffness method. **Computers and Structures**, v. 152, 05 2015.

NOBREGA, E.D.; GAUTIER, F.; PELAT, A. and DOS SANTOS, J.M.C. Vibration bandgaps for elastic metamaterial rods using wave finite element method. **Mechanical Systems and Signal Processing**, v. 79, 192–202, 2016.

PEREIRA FLAVIO, .N. and DOS SANTOS, J. Phononic crystal investigation using a fluid-structure circular cylindrical shell spectral element. **Mechanical Systems and Signal Processing**, v. 148, 107100, 2021.

PEREIRA FLAVIO, .N. and DOS SANTOS, J.M.C. Wave propagation and frequency band structure in cylindrical shells. **24th International Congress of Mechanical Engineering - COBEM 2017**, pp. 192–202, 2017. December 3-8, Curitiba, PR, Brazil.

QATU, M. Recent research advances in the dynamic behavior of shells: 1989-2000, part 2: Homogeneous shells. **Applied Mechanics Reviews**, v. 55, 09 2002.

RODRIGUES, G.K.; SILVA, M.M.D. and DE OLIVEIRA, L.P. Modular modeling approach for fdm printed structures and piezo disks for metamaterial design. **Latin American Journal of Solids and Structures**, v. 16, n. 7, 2019.

ROSA, M.I.; PAL, R.K.; ARRUDA, J.R. and RUZZENE, M. Edge states and topological pumping in spatially modulated elastic lattices. **Physical review letters**, v. 123, n. 3, 034301, 2019.

SALES, T.D.P.; RADE, D.A. and INMAN, D.J. A morphing metastructure concept combining shape memory alloy wires and permanent magnets for multistable behavior. **Journal of the Brazilian Society of Mechanical Sciences and Engineering**, v. 42, n. 3, 1–18, 2020.

SANTOS, E.; PEREIRA, V.; ARRUDA, J. and DOS SANTOS, J. Structural damage detection using energy flow models. **Shock and Vibration**, v. 15, n. 3, 4, 217–230, 2008.

SHI, S.; CHEN, C. and PRATHER, D.W. Plane-wave expansion method for calculating band structure of photonic crystal slabs with perfectly matched layers. **JOSA A**, v. 21, n. 9, 1769–1775, 2004.

SIGALAS, M. and ECONOMOU, E. Elastic and acoustic wave band structure. **Journal of Sound and Vibration**, v. 158, n. 2, 377–382, 1992.

SIGALAS, M. and GARCıA, N. Theoretical study of three dimensional elastic band gaps with the finite-difference time-domain method. **Journal of Applied Physics**, v. 87, n. 6, 3122–3125, 2000.

SIGALAS, M. and SOUKOULIS, C. Elastic-wave propagation through disordered and/or absorptive layered systems. **Physical Review B**, v. 51, n. 5, 2780, 1995.

SILVA, Priscilla Brandão. **Dynamic analysis of periodic structures via wave-based numerical approaches and substructuring techniques**. August 2015. PhD (Thesis). Universidade Estadual de Campinas, Faculdade de Engenharia Mecânica.

SILVA, P.B. and ARRUDA, J.R.F. Wave spectral finite element analysis of two-dimensional

waveguides. **Proceedings of the 11th International Conference on Computational Structures Technology - Stirlingshire, Scotland**, pp. 1–18, 2012.

SINHA, B.K.; PLONA, T.J.; KOSTEK, S. and CHANG, S.K. Axisymmetric wave propagation in fluid-loaded cylindrical shells. i: Theory. **The Journal of the Acoustical Society of America**, v. 92, n. 2, 1132–1143, 1992.

SOUSA, R.W.O.; MENCIK, J.M. and DOS SANTOS, J.M.C. Band gaps in plates and cylindrical shells with 1d periodic elastic properties. **24th International Congress of Mechanical Engineering - COBEM 2017**, v. 190, 495–524, 2017. December 3-8, Curitiba, PR, Brazil.

THINH, T.I. and NGUYEN, M.C. Dynamic Stiffness Method for free vibration of composite cylindrical shells containing fluid. **Applied Mathematical Modelling**, v. 40, n. 21-22, 9286–9301, nov 2016.
URL: *https://linkinghub.elsevier.com/retrieve/pii/S0307904X16303262*

WU, F.; LIU, Z. and LIU, Y. Acoustic band gaps in 2d liquid phononic crystals of rectangular structure. **Journal of Physics D: Applied Physics**, v. 35, n. 2, 162, 2002.

ZHANG, X. Frequency analysis of submerged cylindrical shells with the wave propagation approach. **International Journal of Mechanical Sciences**, v. 44, 1259–1273, 07 2002.

ZIENKIEWICZ, O.C. **The finite element method**. McGraw-Hill, 1977.